Cape Peninsula University of Technology

ENERGY HARVESTING IN LORAWAN FOR SPACE COMMUNICATION

by

YOLANDA NXUMALO

221589902

Course-based degree with 50% dissertation submitted in fulfilment of the requirements for the degree

MASTER OF ENGINEERING: SATELLITE SYSTEMS AND APPLICATIONS

In the Faculty of Engineering & the Built Environment

at the Cape Peninsula University of Technology

Supervisor: Dr Vipin Balyan

Co-supervisor: Dr Gunjan Gupta

Bellville

Date submitted: 06 March 2025

DECLARATION

I, Yolanda Dolly Nxumalo, declare that the contents of this thesis/dissertation represent my own unaided work, and that the thesis/dissertation has not previously been submitted for academic examination towards any qualification. Furthermore, it represents my own opinions and not necessarily those of the Cape Peninsula University of Technology.

Signed: 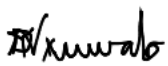 **Date: 03/08/2024**

ABSTRACT

The application of LoRa in Internet-of-Things (IoT) and remote sensing improves data collection, connection, and monitoring over wide geographic areas. Its low-power, long-range communication characteristics have resulted in its widespread adoption in industries including asset tracking, environmental monitoring, agriculture, and healthcare, especially in remote and infrastructure-constrained regions. Applications include soil moisture monitoring, wildlife tracking, and precision agriculture. However, terrestrial LoRa communication has coverage limitations due to line-of-sight constraints wherein sparse population density or complex terrain might block or reflect the signal. In addition, the devices require recurrent recharging or battery replacement which poses significant operational challenges and increases costs. To address these challenges, satellite-based LoRa communication emerges as a potential solution for global coverage. However, robust power management techniques are required due to the power requirements of direct-to-satellite communication and the challenging environmental conditions that are frequently encountered in remote regions. This research introduces a novel Ambient Energy Management (AEM) system designed for energy harvesting to power LoRa Internet of Things (IoT) devices operating in a Direct-to-Satellite (DtS) communication environment. This study explores how duty cycle, signal design, and energy harvesting techniques interact while tackling the difficulties of energy optimization in this setting. The objective of the research is to increase energy efficiency, prolong system lifespan, and broaden the possible uses of LoRa-based IoT systems while complying with regional regulatory standards, including those described by ICASA (Independent Communication Authority of South). This study contributes to the advancement of energy-autonomous IoT systems by introducing novel algorithms and insights into the management of harvested energy for satellite communication.

ACKNOWLEDGEMENTS

I wish to thank:

- First and foremost, I want to appreciate my beloved grandfather, Bafana Nxumalo for dedicating his life in uplifting the lives and futures of his daughters and subsequently that of mine as his grandchild. Ensuring that I have a fighting chance in this world long after he is gone.
- I would like to give thanks to my supervisor for providing direction and motivation thus far towards my thesis
- I want to express my honour to Dr Elin Davies, my mentor for making this research possible by introducing me to satellite global coverage communication tailored for remote regions of the world during our joint DADS (Digital-And-Drone-Solutions) project.

TABLE OF CONTENTS

LIST OF FIGURES

LIST OF TABLES

LIST OF EQUATIONS

ABBREVIATIONS AND ACRONYMS

AP	Access Points
ADR	Adaptive Data Rate
AEM	Ambient Energy Management
BCE	Before The Common Era
BER	Bit-Error-Rate
BLE	Bluetooth Low Energy
BIPV	Building Integrated Photovoltaics
BW	Bandwidth
CSS	Chirp Spread Spectrum
CDM	Code Division Multiplexing
SIP	Cross-Ministerial Strategic Innovation Promotion
dB	Decibal
dBi	decibel-relative-to-isotrope
DC	Direct Current
DL	Downlink
DtS	Direct-to-Satellite
ELDO	European Launcher Development Organisation
ESA	European Space Agency
ESRO	European Space Research Organisation
FDD	Frequency Division Duplex:
FHSS	Frequency Hopping Spread Spectrum
FUOTA	Firmware Update Over-The-Air
GEO	Geostationary Orbit
GPS	Global Positioning System
GSMA	Global System For Mobile Communications
GSO	Geosynchronous Orbit
HEO	Highly Elliptical Orbit
Hz	Hertz
ICASA	Independent Communications Authority of South Africa
IEC	International Electrotechnical Commission
ISM	Industrial, Scientific and Medical
ISO	International Organization For Standardization
ITU	International Telecommunication Union
ITU-R	International Telecommunication Union Radio
IoT	Internet-of-Things
ISS	International Space Station
KPI	Key Performance Indicators
LEO	Low Earth Orbit
LPT	Laser Power Transfer
LPWAN	Low-Power Wide Area Networks
LTE-M	Long-Term Evolution - Machine Type Communication
MGS	Micro Generator System
MIT	Massachusetts Institute Of Technology

MCU	Microcontroller Unit
MEO	Medium Earth Orbit
ms	Milliseconds
METI	Ministry Of Economy and Trade and Industry
NASA	National Aeronautics and Space Administration
NGO	Non-Governmental Organisation
NP-IoT	Narrow Band Internet of Things
OBW	Occupied Bandwidth
PAN	Private Area Network
PDR	Packet Delivery Rate
PSD	Power Spectral Density
PV	Photovoltaic
RF	Radio Frequency
SBD	Schottky Barrier Diode
SF	Spreading Factor
SLA	Service Level Equipment
SIR	Signal-to-Interference Ratio
SNR_dB	Signal-to-Ratio Decibal
SPS	Solar Power Satellite
SDD	Space Division Duplex
SSO	Sun-Synchronous Orbit
TDD	Time Division Duplex
TEG	Thermoelectric Generator
TOA	Time On Air
TWT	Traveling-Wave-Tube
UHF RFID	Ultra High Frequency Radio Frequency Identification:
W	Watts
WISP	Wireless Identification and Sensing Platform
WPAN	Wireless Personal Area Network
WPT	Wireless Power Transfer

Chapter 1: Research Proposal

1.1. Statement of Research Problem

The energy generated by energy harvesters and the energy needed by WSN (wireless sensor nodes) are incongruent. Thus, there is a need to address this imbalance by lowering WSN power consumption and increasing the power output that can be collected and/or extracted to the WSN to obtain optimum performance of battery powered Internet-of-Things (IoT) devices.

1.2. Background to the Research Problem

Batteries are the major source of power for large number of IoT (Internet-of-Things) (networks of sensor nodes) devices deployed worldwide. However, dependence on batteries is not a feasible solution in the long-term for IoT because batteries are large, have a short lifespan, and contain dangerous chemicals that harm the environment. On the other hand, batteryless/wireless devices rely on enduring capacitors which are charged by energy harvesters. Because capacitors have a limited energy storage capacity, they exhibit an interrupted on–off behaviour (Carmen Delgado, 2021). Long-power wide area networks (LPWAN) have been popularly adopted due to their ability to maintain an extended radio range for exceedingly little energy utilization for instance LoRaWAN (Carmen Delgado, 2021; Hafiz Husnain Raza Sherazi, 2021). However, commonly produced wireless sensor nodes (WSN) are power demanding, thus energy harvested by energy harvesters is insufficient to power the WSNs to meet its intended functions. Which illustrates the discrepancy. Due to this imbalance, it is necessary to reduce WSN power consumption while enhancing the power capacity that the WSN can gather and/or extract (Tingwen Ruan, 2017).

1.3. Literature Review

Everyday life has been enhanced by transitioning common items to become internet-connected information sources that are capable of sensing, actuating, locating and communicating with one another as part of tens of billions of IoT network devices. These devices typically include, a radio chip, a battery, a microcontroller unit (MCU), and one or many sensors and/or actuators (Carmen Delgado, 2021).

1.3.1. LoRaWAN

This section briefly discusses and compares different RF-established networks for IoTs, how LoRaWAN and UHF RFID (Ultra high frequency Radio frequency

identification) affect each other and how they can co-exist without RF-interference, analyse multiband antennas to utilise with LoRa Edge and finally discuss and compare LoRaWAN classes.

RF-Established Networks for IoT

The two main RF categories are WPAN (Wireless Personal Area Network) and the former is short range technologies and can either have a low or high bitrate that consumes low or high amounts of power, such as Bluetooth, Wi-Fi, Zigbee and Z-Waze. The latter is for long range technologies with a minimal bitrate and minimal power application (SemTech, 2020).

Bluetooth has several modes, the most significant of which is BLE (Bluetooth Low Energy), which operates at a frequency of 2.4GHz but with limited data transfer and prevents interference by using the FHSS (Frequency Hopping Spread Spectrum) modulation mechanism. The BLE implementation in Bluetooth 4 transmits data at a rate of 1Mbps, while Bluetooth 5 transmits data at a rate of 2Mbps. When messages are transmitted between nodes in Bluetooth Mesh, the BLE range increases; nevertheless, for wide area connection, many nodes are necessary (SemTech, 2020).

BLE system works well for tasks that need little power, little latency, a high level of service, and a limited range when using Bluetooth Mesh. They do, however, perform far worse in long-range applications (SemTech, 2020).

On the other hand, Zigbee and Z-Wave are designed to utilize very limited energy as possible and (Low data rates imply lower frequency) their low frequencies permit signals to pass through walls and other barriers with ease and are less prone to interference. Because their operational range is limited the total range of the network can be increased by meshing numerous devices. Zigbee supports both sub 1000MHz and 2.4GHz and 900MHz is the frequency of Z-Wave (SemTech, 2020).

Light switches and temperature sensors in the house are good candidates for Zigbee and Z-Wave since they demand advanced level of service while they only utilize little data. Generally, they are suited for functions that require minimal power consumption, advanced level of service, little latency, and an adaptable range with many devices but less suitable for applications requiring large volumes of bitrate and long range (except if each device mesh covers one entire region) (SemTech, 2020).

To satisfy the expectations of IoT deployments, LPWANs, a new class of RF based communication standards, combine high energy efficiency with long-range communications. (U. Raza, 2017). They can traverse barriers such as buildings and

span a broad spectrum of frequencies, both licensed and unlicensed. Cellular, Sigfox and LoRa, LoRa and LoRaWAN are the most widely adopted LPWANs (SemTech, 2020) and are discussed below.

Cellular systems originated to meet high bandwidth connectivity like phone conversations that allow for increased bandwidth and transmit bigger volumes of data, they employ licensed frequency bands, which are normally in the 0.5GHz to 4GHz range, while 5G systems might utilize frequencies as high as 100GHz. Since increased frequencies offer narrower capabilities, there are currently benchmarks in place for cellular systems focused on IoT connections to operate at shorter wavelengths to reach broader spectrum (SemTech, 2020).

For IoT functions, NB-IoT (Narrow Band Internet of Things) and LTE-M (Long-Term Evolution – Machine Type Communication) are the two main cellular standards to consider. Both are classified as 5G technology. The NB-IoT type employs extremely small frequency channel widths with longer range and consumes less power in comparison to LTE-M which has a faster data throughput with lower latency. In contrast to NB-IoT, LTE-M additionally supports device mobility, permitting a device to switch to a different cell tower if it moves during data transmission (SemTech, 2020). In comparison to other conventional LPWANs cellular networks have faster data rates which permits larger packet delivery. Cellular solutions utilize licensed frequencies, which reduce interference and allow messages to be transmitted as frequently as needed. As a result, cellular systems have an increased standard of service with minimal latency. There are suitable for immediate response for example locking an entrance over a large distance immediately when an intruder is detected (SemTech, 2020).

Typically, mobile network companies own cellular networks. Depending on the coverage of the target location, using cellular for IoT solution allows the use of an existing infrastructure. However, since the cellular IoT requirements are still in their early stages, network operators are currently putting infrastructure in place to accommodate them. Local network providers with limited coverage may implement either NB-IoT or LTE-M unlikely both (SemTech, 2020).

Cellular networks are more expensive than unlicensed solutions because they require a network provider subscription. A current map of mobile IoT installations is maintained by GSMA (Global System for Mobile Communications) to locate providers in a specific area. Electric metering is an application that would benefit from a cellular IoT

deployment. Payload length and high data rate, low latency and high quality of services are its advantages (SemTech, 2020).

LoRa and Sigfox, two additional popular LPWAN technologies, employ unregulated radio frequencies from 0.433GHz to 0.928GHz to send limited messages across vast ranges. In contrast to cellular networks, LoRa and Sigfox networks are founded on a star network architecture, which guarantees that any gateway within range can receive and transmit a broadcast message to the Cloud. This improves the chances of a signal from a device that is out of the limitation range of numerous gateways, to be picked up. Its primary characteristics are low power and low range (SemTech, 2020).

The first contemporary LPWAN, as it is currently defined was Sigfox that was created in 2010. Sigfox transmits 100Hz wide messages using ultra-narrowband attenuation on unlicensed channels between 862MHz and 928MHz. This implies that within their operational range, Sigfox devices communicate on a stochastic channel, which lowers the possibility of interference from background noise. Because of the limited spectrum employed, Sigfox has the widest range of all the solutions we're looking at, but at the cost of a poor data throughput. As a result, the amount of data sent every message must be limited to fewer than 12 bytes per message (SemTech, 2020).

Sigfox only permits for the uplinking of six messages per hour from a node to the cloud server and the downlinking of four messages per day from the cloud server to a node. Because of such constraints, Sigfox should be used for functions that require communication of a few basic variables per day with minimal power requirements. Until recently, subscription to Sigfox's public network was expected from prospective users to utilize it. On the other hand, Sigfox is actively developing PAN (Private Area Network) technology, which is set to enable private network instance for a host. Sigfox's advantage is providing all LPWAN options with the longest range (SemTech, 2020).

LoRa employs unlicensed airwaves ranging from 433MHz to 928MHz that are location dependent, and a patented Chirp Spread Spectrum (CSS) modulation system which transmits data utilizing a small band of (0.125, 0.25, and 0.5MHz) distributed through a broader channel bandwidth, resulting in low noise levels and interference resistance. To reach longer distances at the trade-off power, the modulation strategy can be varied by adjusting the Spreading Factor. LoRaWAN is an open-source networking protocol (based on LoRa) that specifies how devices connect with gateways. LoRa has a longer range than Cellular, but not as long as compared to Sigfox. The packet size constraints, on the other hand, are variable, and with the

appropriate configuration far more data per packet can be transmitted than with Sigfox (SemTech, 2020).

A LoRa message's maximum packet size is determined by the data rate and region. Varied data speeds can be obtained by adjusting the bandwidth and spreading factor. Because the frequency is higher, an increased data rate indicates narrow coverage. One maximum message size to be sent can be controlled based on user case ranging from 11 to 242 bytes.

A variety of public LoRaWAN network operators are available. Setting up one's private system utilizing private gateways and software is also doable. Which enables connectivity anywhere there is access to a site where a gateway may be installed. A private LoRaWAN network allows users to retain all data within its own domain. Unlike any of the other technological solutions discussed thus far, the ability to build up one's own network allows the user total command of their network, data, and prices. LoRa operates on different classifications which will be discussed later in this section.

Advantages of LoRaWAN include the ability to control the maximum packet size that can be larger than that of Sigfox and being able to send data over longer distances. One low-cost private network may be set up quickly. Flexible, with a mix of devices operating together with varying power and latency requirements (SemTech, 2020).

Table 1.1: LPWAN technologies comparison *(SemTech, 2020)*

	NB-IoT	**LTE-M**	**LoRa**	**Sigfox**
Coverage	Average	Average	extensive	Most extensive
Sensitivity	Strong	Strongest	Weak	Weakest
Mobility	No	Yes	Yes	Yes
Data rate	Super	Superior	Weak	Weakest

For the star-of-stars architecture the gateway transports communication across the end-device and the main network server. Gateways use conventional IP connections to connect to the network server. They simply convert RF transmissions to Ip datagrams and the other way around. The wireless connectivity makes use of LoRa's physical layer's long-range capabilities, permitting for a single-hop link connecting end-devices with the multiple gateways. Bidirectional communication is possible with LoRa-

based end-devices. Multicast addressing groups are also supported, allowing for more effective use of the spectrum for specialized activities (Semtech, 2020).

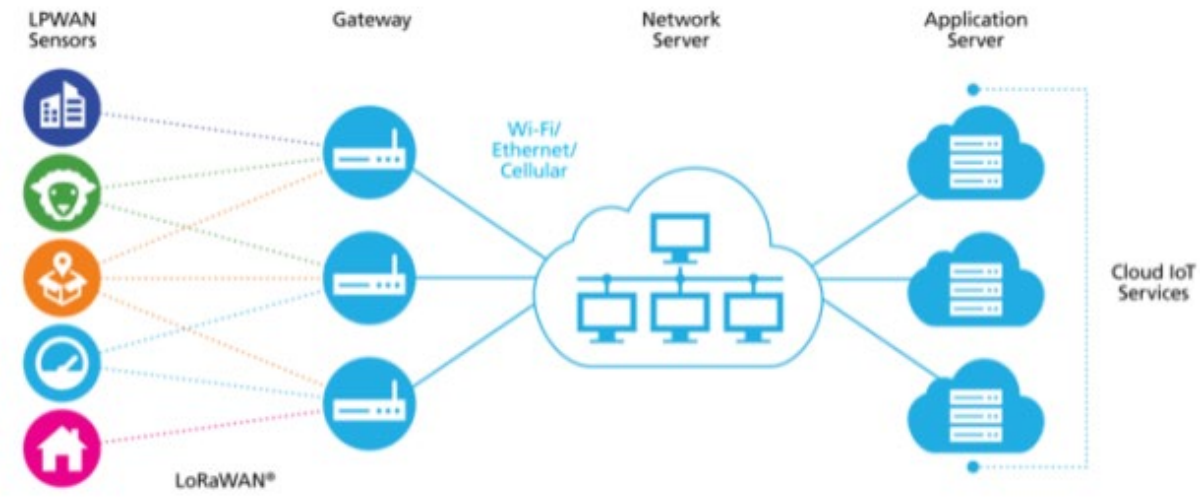

Figure 1.1: **LoRaWAN end-to-end secured payload**

(Semtech, 2020)

The physical layer of LoRaWAN is based upon LoRa/FSK communication connecting end-devices and gateways, that utilises sub-GHz ISM bands. When powerful interferers coexist, occupying identical spectrum and location, certain penalties can still be detected, despite being resilient to co-channel and neighbouring channel interferences (Semtech, 2020).

The transmission of LoRa packets can be disrupted by a collocated RFID reader producing 4 Watts ERP and occupying identical location and frequency spectrum in the following conditions. Harm to the signal-to-interference-and-noise ratio (SINR) might occur should the RFID reader porter and the LoRa signal share identical channel frequencies. The signal-to-interference ratio (SIR) of one common LoRa-based chipset should be between -5 and -19.5 dB. Filtering cannot be used to improve the interference rejection when this occurs. Connecting LoRa porters with Reader signals may result in interference, this is most likely caused by the power dissipation across the RFID Reader on-to and towards the LoRa channels (Semtech, 2020). Furthermore, the powerful signal will have an influence on the LoRa-based receiver's AGC mechanism. Intermodulation products of the 3rd- and 5th order may experience disturbances because of the intermittence pertaining to its front-end. Given the huge

number of interfering sources co-located and the ERP of the interfering signal, the potential impact is significant (Semtech, 2020).

A LoRa-established end-device and gateway generate minimal power and RFID readers have a high density as a result impact of LoRaWAN broadcasts on an RFID system is insignificant (Semtech, 2020).

LoRaWAN offers adaptive capabilities that allow it to co-exist with technologies which emit frequency-selective interference, like UHF-RFID (Semtech, 2020).

LoRa attenuation offers significant co-channel and adjoining-channel elimination:

- According to the SX1262 datasheet, the spreading factor (SF) determines the 5-19 dB range of the single porter interference for co-channel elimination and 60-72 dB range for adjoining-channel elimination.
- According to the LoRaWAN MAC protocol, an adjustable channel plan generated by the Adaptive Data Rate (ADR) command is required. Such a property enables the network server to deactivate channels which were noted to contain increased amount of obstruction to improve general packet communication standard.
- All UHF RFID readers are commanded by the system with programmable channel layout. Other cutting-edge solutions permit a change of the RFID channel plan while they are running whilst avoiding the loss of data.
- Because end-nodes (RFID tag) are passive devices, the channel plan is not stored. Thus, it's possible to tailor these tags with whichever channel scheme employed by the reader.

1.3.2. Energy Harvesting

Energy harvesting technique is about capturing environment's energy, usually with the use of renewable energy sources. Harvested energies include those that are carried in electromagnetic waves of various lengths - from conventional radio frequencies utilized for communication to solar, thermal gradients, kinetic and potential energy, and so on. In general, there are two sorts of sources of accumulated energy. The first is the inherent energy present in the environment in which the harvester functions (like Sun providing power to photovoltaic cells) (Graczyk, 2017). The second source of waste energy is that which is emitted by other functioning equipment (e.g., electric motor providing power to thermal or kinetic harvester). When energy is collected, it is commonly transformed to electricity and stored. Depending on the technology utilized, the power generated by transportable, autonomous harvester systems ranges from

tens of microwatts through tens of milliwatts. As a result, devices powered by energy collecting devices must be minimal in terms of power consumption. Thus, the functionality of such systems must be constrained, especially as they are likely to operate in charge (energy build-up over a few minutes or tens of minutes) and respond autonomously (perform the measurement and processing quickly and effectively). State-of-the-art research, aided by increased industry interest in energy harvesting, as well as recently announced novel products, demonstrate that the approaches presented are a feasible power source for sensors, sensor networks, and personal gadgets (Graczyk, 2017) and have also made battery-less devices possible.

The activities and present research in this subject are focused on small, extremely low-power devices that capture energy on a small budget (which is suitable for them). Sensor autonomy (wireless communication), safety (no power lines), and no or little maintenance are all goals of these technologies, such as, technological advances in the automotive industry (tire pressure monitors, using the piezoelectric effect), aerospace industry (fuselage sensor network in aircraft, using the thermoelectric effect), manufacturing automation industry (various sensor networks, using the thermoelectric, piezoelectric, electrostatic, and photovoltaic effects), personal devices (wrist watches, vital signs monitors, remote controls, utilizing piezoelectric and the thermoelectric effect), and personal devices (wrist watches, vital signs monitors, remote controls, using piezoelectric and the thermoelectric effect) (Graczyk, 2017) and battery-less devices.

One of the major challenges in realizing the idea of a global IoT (Internet-of-Things) has been battery lifespan restrictions. Devices are sometimes positioned in difficult-to-reach regions, making battery maintenance or replacement expensive and risky. There are cases that require compact devices, yet a battery is very large. Batteries are known to be costly, large, and toxic; they are temperature sensitive, temporary, and hence inappropriate for feasible IoT (Sorbet, 2017). Furthermore, when combined with high current peaks, batteries degrade faster. An IoT device often spends the significant amounts of its life sleeping unless required to waken to execute its functions, that typically involve data communication. Such actions need significant power compared to sleep mode. Resulting in charge surges being common in IoT devices during transmission and reception (Carmen Delgado, 2021). As a result, batteries will deteriorate more quickly than anticipated. Furthermore, battery replacement and maintenance raise the operational expenses of IoT deployments, limiting their prospective influence regarding expanding the device amount, distribution within difficult-to-reach sites, in addition to network endurance, as batteries die out

eventually, and recharging capability diminishes. Batteryless IoT devices are a viable answer to the IoT's battery dilemma. They are smaller, last longer, are better for the environment, and their maintenance is cost-effective. They are therefore especially well-suited for tasks within remote locations and large-scale deployments (Carmen Delgado, 2021).

First, battery maintenance is difficult, risky, and expensive for devices embedded in materials or distributed at distant (example, desert region), risky (example, underground tunnels), or other remote sites. Many of these gadgets can't be accessible for battery change without causing damage to the materials in which they're housed. Furthermore, if chemical batteries are implanted into live tissue, they may cause harm (e.g., brain chips). In addition, while widely distributed devices are reachable, battery maintenance is extremely time consuming, difficult, and expensive due to the volume of the deployment. This is useful for fine-grained environmental monitoring (for example, air humidity) within urban areas, as well as monitoring items in vast logistical warehouses. Furthermore, although battery replacement is economically possible in some circumstances, it may not be desirable for certain factors, including user convenience or the need for servicing time. Of instance, it might not be feasible to expect the wearer of a wearable device for the elderly to mechanically charge or replace batteries. In some circumstances, devices could also have a requisite lifespan without maintenance (Carmen Delgado, 2021).

A batteryless device, unlike its battery-powered counterpart, should gather power off its surroundings then save within its tiny capacitors. Because they may survive a far higher number of usable capacities unlike rechargeable batteries, these capacitors can potentially last well over 10 years (P. Spanik, 2014). Furthermore, they are less expensive to manufacture and recycle, making them friendlier for the environment. However, there are certain drawbacks to this new paradigm: energy harvesting being inconsistent, there is a finite rate of energy retention, power interruptions are inevitable, and performance is intermittent. (Sorbet, 2017). The location (i.e., the power supply's availability) and function specifications (example, power and rate of implication) both influence which sort of harvester source should be chosen. Photovoltaic has a energy capacity of 100 mW/cm^2, but RF-based collectors have a power density of 10 $\mu W/cm^2$ (al., 2014). Various commercial batteryless alternatives are already available on the market. While commercial solutions with communications are currently restricted, there are various batteryless IoT prototypes with communications. The industrial products and proof of concepts are grouped in Table 1.2 according to the power source they

use, with the most important characteristics being highlighted (Carmen Delgado, 2021).

Table 1.2: Energy harvesting prototypes and commercials *(Carmen Delgado, 2021)*

Mechanism	Proof of concept/Product	Energy source	Communication	Function
EnOceon, Takahashi *et al* (K. Takahashi, 2019)	Proof of concept	Electromechanical	928MHz	Smart footwear which transmits radio frequency tags while you're moving
Fraternali (F. Fraternali, 2018)	Proof of concept	Solar	Bluetooth Low Energy	Detection capacity
Dekimpe *et al* (R. Dekimpe, 2019)	Proof of concept	Radio Frequency	Bluetooth Low Energy	Smart footwear for monitoring people with dementia
Loubet *et al* (G. Loubet, 2019)	Proof of concept	Radio Frequency	LoRaWAN	Construction intelligence and fault diagnosis
Orfei *et al* (F. Orfei, 2016)	Proof of concept	Electromechanical	LongRangeWideArea	Smart monitoring utilizing structural pulses
Dalpiaz *et al* (G. Dalpiaz, 2018)	Proof of concept	Electromagnetic	LongRangeWideArea	Smart strain monitor
Smart switch (EnOceon, 2022)	Product	Electromechanical	868MHz	Smart shutter automation
Smart boot (SolePower, n.d.)	Product	Electromechanical	WiFi/Cellular	Smart military footwear monitoring
Instep (InStep Nano Power, 2016)	Product	Electromechanical	Bluetooth Low Energy	Smart footwear motion monitoring
Bionic power walk (Bionic Power, n.d.)	Product	Electromechanical	–	Wearable military motion monitor
Sequent watch (Sequent, 2022)	Product	Electromechanical	Bluetooth Low Energy	Monitoring of movement and vital signs
Lunar watch (Wearable, 2022)	Product	Solar	Bluetooth Low Energy	Monitoring steps and sleeping
Matrix power watch (Matrix, 2022)	Product	Thermoelectric	Bluetooth Low Energy	Monitoring steps and sleeping

1.4. Objective of the Project

Determine a feasible ambient energy harvesting management system that is compatible for IoT LoRa node devices that communicate directly to LoRaWAN satellites.

1.5. Research Design and Methodology

This section describes the research procedure to be adopted for developing the energy harvesting in LoRaWAN for space communication protocol which includes a system diagram and description of how it works.

Literature review

Research LoRa and LoRaWAN configuration and how its node applications work, then research energy harvesting and how it's used for IoT devices then finally research space communication with a specific focus on Direct-to-Satellite (DtS) communication for LoRaWAN IoT.

Communication design protocol

a. Sensors powered by energy harvesting send signals directly to the passing satellite.
b. The signals use LoRaWAN network protocol that has been deliberately developed to preserve power consumption.
c. The satellites are LEO orbiting CubeSats that save messages for a brief period up until they go over a network of ground stations.
e. Messages received from the CubeSats are transmitted spontaneously from the ground station to a cloud platform.
f. Data is accessed from a web-based program.

Design analyses

The research development focus is on improving the efficiency of the AEM (Ambient Energy Management) of the energy harvesting system. MATLAB LoRa toolbox will be used for simulation and analyses of the design. Outcome of the design analysis is a novel protocol for energy harvesting DtS IoT system.

Testing

LoRaWAN nodes device communication will be adopted and tested, the required data link to successfully send signals to the satellite then the power required to operate the device will be determined for a feasible energy harvesting design. MATLAB LoRa toolbox will be used to simulate data link communication.

Findings

Analyse and compare simulations results, draw conclusions, and give recommendations for future research.

1.6. Budget

Table 1.3: Budget cost for research project

Requirement	Cost
MATLAB software license	Payment covered by CPUT
Funding for one journal paper	R4000
Printing ink and paper	R1000
Total	**R5000**

1.7. Project Plan

Table 1.4: Project timetable

Start	End	Days	Task
3-Mar-22	10-Jun-22	100	Literature review
3-Mar-22	5-Jul-22	125	Research proposal
6-Jul-22	20-Oct-22	107	Research proposal corrections
5-Aug-22	12-Nov-22	100	Research Methodology design
12-Nov-22	21-Dec-22	40	Simulation and Analysis
20-Oct-22	26-Feb-23	130	Thesis writing and corrections
27-Feb-23	27-Feb-23	1	Thesis submission

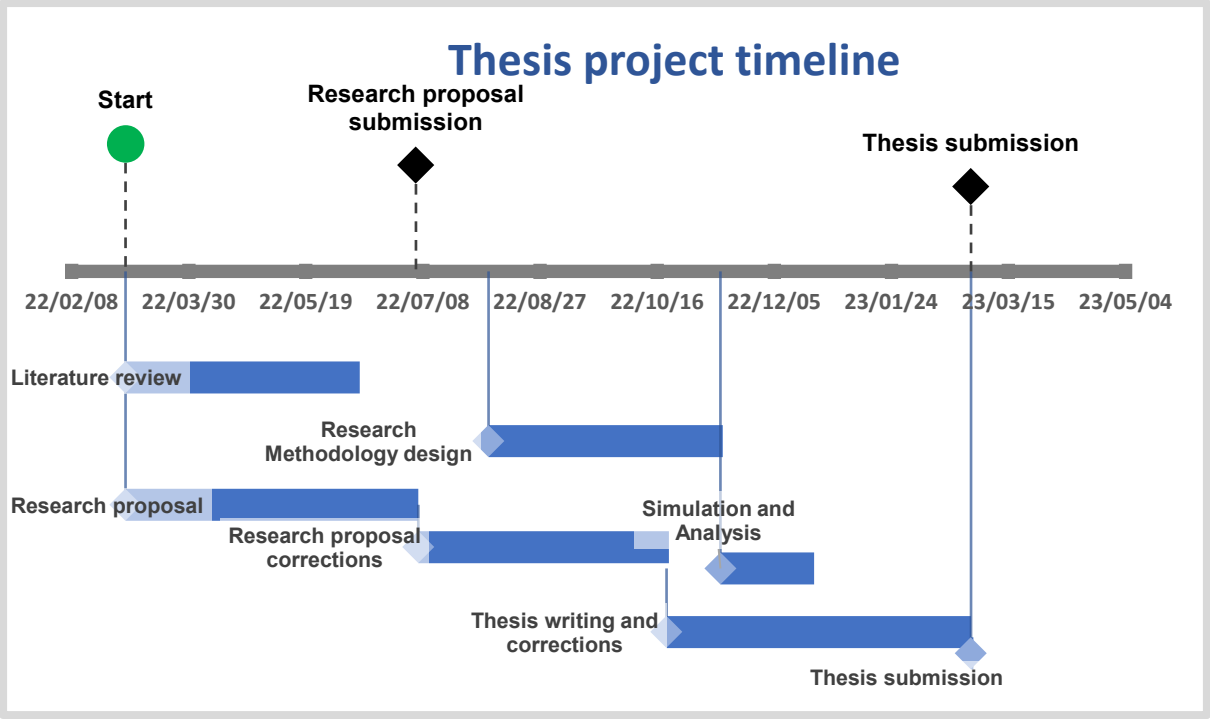

Figure 1.2: Thesis deliverable timeline

1.8. Delineation of the Research

- The electromagnetic waves used as a source of power are restricted to; optical, solar and radio frequency.
- Only the LoRa configuration is used for satellite communication
- Satellite communication analyses is limited to DtS for CubeSats orbiting in LEO

1.9. Significance of the Research

Contribution to the research and development of batteryless IoT devices that can send and receive communication from anywhere in the world. This is significant for search and rescue missions, communication for remote towns and villages, GIS (Geographic Information Systems) projects and everyday general communication.

Direct-to-Satellite (DtS) IoT communication advances the research and development solution to South Africa's GDP (Gross Domestic Product) loss due to theft of cell phone batteries from communication towers. The replacement of Telecommunication towers by DtS communication eliminates the need for cell phone towers, thieves cannot reach satellites in space unlike telecommunication towers.

In addition, to reducing the cost for start-ups and research and development projects that require DtS communication. Improving efficiency of energy harvesting technique can improve on-board processing for satellites in space.

1.10. Expected Outcomes, Results and Contributions of the Research

An improved efficiency for AEM for energy harvesting systems for DtS IoT devices that use LoRa protocol. Consequentially improve wireless power transfer and communication anywhere in the world.

Thesis Outlook

Chapter 2: LoRaWAN Technology

Delves into the intricacies of LoRaWAN technology, exploring its transmission functions, applications in conjunction with RFID, operating bands, network investments, and communication system design.

Chapter 3: Energy Harvesting Techniques

Chapter 3 examines various energy harvesting methods, focusing on kinetic energy and electromagnetic radiation, including solar energy and radio frequency.

Chapter 4: Space Communication and LoRaWAN

This chapter traces the evolution of space communication, beginning with Sir Arthur C. Clarke's visionary concept of geostationary satellites. It explores the impact of technological advancements on the space race, the establishment of space agencies, and the development of broadcasting satellites and space orbits. Additionally, the chapter investigates the potential of integrating LoRaWAN with satellite communication.

Chapter 5: Software Development Methodology

Chapter 5 outlines the methodological approach employed to develop a software-based solution for optimizing energy harvesting in LoRaWAN networks, tailored specifically for space-based communication. The chapter emphasizes software development techniques and tools used in the project.

Chapter 6: Experimental Results and Analysis

This chapter presents a detailed analysis of the experimental results obtained from the developed software solution. It evaluates the performance of the solution in terms of energy efficiency, network coverage, and data reliability.

Chapter 7: Conclusion

The final chapter summarizes the key findings of the research, discusses the implications of the results, and provides recommendations for future work. It concludes by highlighting the contributions of the research to the field of space communication and energy-efficient IoT networks.

Chapter 2: LoRaWAN

2.1. Uplink and Downlink Functions

Most LoRaWAN-established functions have been designed to broadcasting uplinks. With feedback enabled, downlinking is primarily utilized for provision and controlling the network. In most cases, the network can detect unsuccessful downlink transmissions (for e.g., an unsuccessful add acceptance message or a botched ADR instruction), and downlinks retransmission is then efficiently programmed (Semtech, 2020).

2.2. RFID and LoRaWAN Applications

RFID and LoRaWAN are better suited for diverse functions for settings like a major factory. RFID, for instance, can be best applicable to data collecting at choke points, such as scanning a vehicle at a loading port. LoRaWAN, on the other hand, is ideal for providing ubiquitous coverage indoor and outdoor, allowing the user to monitor and locate an element in a yard or warehouse (Semtech, 2020). LoRaWAN can also serve additional sensing and monitoring functions. The two systems may thus operate within identical areas and frequency spectrum to improv the demands of users (Semtech, 2020).

2.3 Operating Bands and Network Investments

LoRa's operating bands, predominantly between 863 and 928MHz, are used for unregulated RF-based devices such as remote-controlled home appliances. Investments made by conventional cellular systems operators to instal stations countrywide, gateways that have a density ranging from 1 gateway per 1000 km^2 (installed in the countryside) to 1 gateway per 5 km^2 (installed in congested cities), with intentions of densifying networks to increase traffic capture (SemTech, n.d.).

2.4 Communication System Design

Whenever building a communication system, porters employ classic transmission models and technologies to simulate coverage, using calculated estimations like:

- The gates' height (base stations)
- The gateway's responsiveness and radiated power
- The efficiency of the emitting power of linked node
- The node’s radiation sensitivity

The two top listed items are managed closely: a gateway is an industrially standardized hardware that may be prized anywhere between a few 100 to a few 1000 rands, and they have cutting-edge antennas affixed to a stationary position above the building. Although flawed, the many years of testing and refining the cellular and pagers has benefited the transmission prototypes (SemTech, n.d.).

To ensure coverage, porters make assumptions regarding the actual radiated power of linked devices going to the network. The effective radiated power (e.r.p.) in Europe has been officially restricted to 25 milliwatts, where telecom carriers shall ensure a specific coverage of a region presuming real power flowing from the devices is 25 milliwatts. The Service Level Agreement (SLA) and coverage map become meaningless without a good (device and) antenna design. Therefore, getting the LoRa antenna design right the first time is critical (SemTech, n.d.).

The performance of the GNSS antenna aboard Semtech's LoRa Edge devices is equally critical for the aided GNSS scanner. The sensitivity of our aided GNSS scanner is around 141dBm. The US military promises that the GPS signal will be larger than 130dBm in any location on the earth (https://www.gps.gov/technical/icwg/IS-GPS-200L.pdf). Because trackers developed for IoT are space restricted, rarely perfectly aligned, as well as often lacking circular-polarized antennas that face to the sky, the efficiency of GNSS antenna is critical (SemTech, n.d.).

Wi-Fi spectrum efficiency is less important over populous locations because multiple Wi-Fi access points (AP) can easily be accessed frequently. Having a well-designed antenna, on the other hand, guarantees that as many entry points as feasible are seen.

Ignion's TRIO mXTEND™ (NN03-310), which is the owner of the innovative Virtual Antenna™ technology. No other antenna in the industry that can control three different radios simultaneously (LoRa, multiband GNSS, and Wi-Fi/Bluetooth) within a single antenna device. It's suitable for usage with the LR1110 because of its small, off-the-shelf, multiband, high-efficiency, and adjustable characteristics (SemTech, n.d.) minimizing integration complexity.

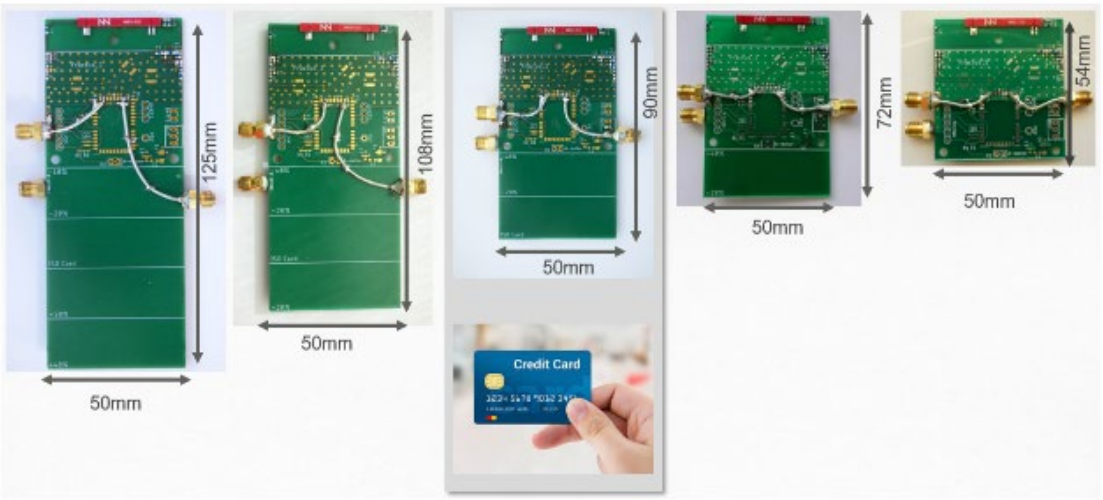

Figure 2.1: **TRIO mXTEND adjustable-length board**

(SemTech, n.d.)

For the reference PCB size, TRIO mXTEND gives great performance in these three bands (90mm x 50mm). Generally, LoRa channel efficiency increases with PCB size.

As the PCB shrinks, performance degrades, as it does with other traditional antenna systems used in low frequency range when the board size is much smaller than the wavelength. The TRIO mXTEND has the benefit that detuning induced through PCB dimension difference is sometimes rectified through corresponding network modification, not requiring antenna customisation. With traditional antenna designs, where the working frequencies are dictated by the antenna shape, this change is more difficult to do.

In all circumstances, the emitting order is omnidirectional and that's advantageous to devices that are constantly moving and whose incoming wave direction is uncertain. The materials in the immediate surroundings have two effects on the radiation: detune the antenna and absorb power. The TRIO mXTEND has a resistant to detuning caused by the presence of nearby materials. Metallic settings have the greatest influence on detuning, proceeded with physical contact. When detuning happens, it is possible to adjust the matching network to compensate (SemTech, n.d.).

When the distance from nearby material is greater, the higher the performance. Place the gadget as close as possible to the metallized segment's edge, with a threshold distance of 25 mm, in the most crucial situation, the metal scenario. If the antenna

region protrudes the metallic section, even higher performance is predicted (SemTech, n.d.).

LoRaWAN is built upon LoRa and radio transmission following the LPWAN code, utilises unlicensed subGHz spectrum allowing for far-distance communications (upwards of 10 km countryside regions) with minimal power requirements (R. Sanchez-Iborra, 2018; Lorawan, n.d.). End devices in LoRaWAN network have three operational modes: A – C. The class's device determines how much energy is saved and when downlinking may occur, however, all classes permit uplinking anytime. Energy is saved by the device when the battery is long-lasting (Yonatan Shiferaw, n.d.; Semtech Corporation, 2019). Figures 2.2 and 2.3 illustrate the uplink and downlink transmissions respectively and figure 2.4 is a representation of energy consumption by class device (not drawn to scale), view following image.

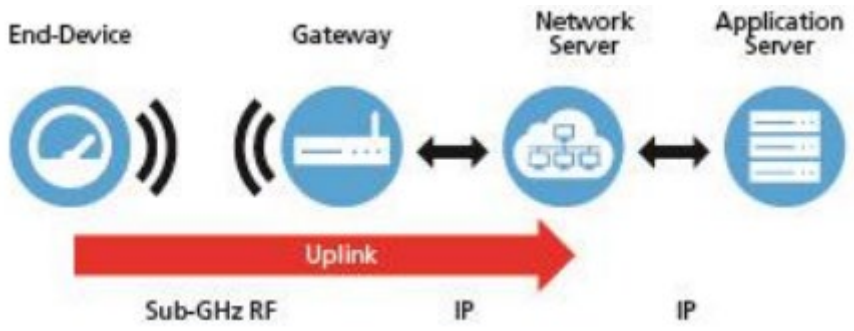

Figure 2.2: **LoRaWAN uplink transmission**

(Semtech Corporation, 2019)

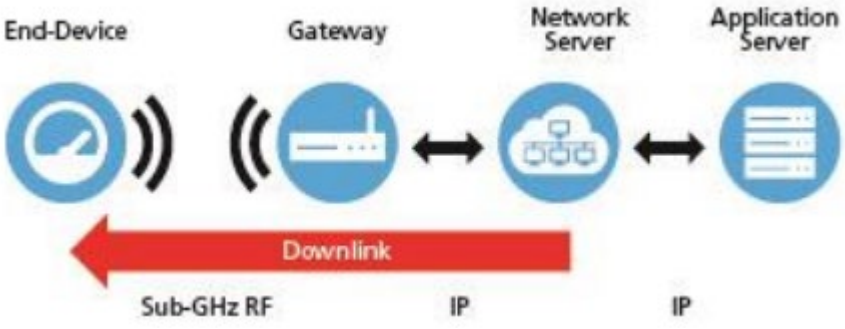

Figure 2.3: **LoRaWAN downlink transmission**

(Semtech Corporation, 2019)

Class A ("Aloha") communications must be supported by all endpoint device, of which most of them are on sleep mode. The change in a sensor read or the trigger of a timer is what connects the end-device to the network server since LoRaWAN isn't a "fitted" code. Anytime they choose, they can awaken and connect to the server. Subsequent to sending an uplink, the device "listens" for a network message one and two seconds later (receiving windows) prior to sleeping again. Class A batteries use the least amount of energy and have the longest battery life (Semtech Corporation, 2019).

Class B end devices, on the other hand, create a receive window to check for a downlink when woken up based on a customizable, system-designed timetable, instead of being on stand-by for its triggers to detect differences within its atmosphere. The network's periodic beacon signal permits endpoints to coincide with their central timers with the network server (Semtech Corporation, 2019) making that mode better suitable for battery-powered or energy-harvesting devices, which are common in IoT end-devices (Yonatan Shiferaw, n.d.).

Finally, Class C ("Continuous") end devices are never asleep. Unless transferring data responding to a endpoint trigger, they're continuously listening for downlink signals from the network. They are the most energy consuming devices typically requiring continuous supply of power than batteries (Semtech Corporation, 2019).

An Aloha-style network is used by the LoRaWAN protocol. End devices in this form of network are free to communicate whatever they choose. The up-linked message is what initiates the receiving window (Rx) of the endpoint to permit delayed downlink messages by the network server. It's an architecture optimised for functions requiring transferring downlinks following an uplink otherwise a downlink may be arranged in advance.
Mode A endpoint initiates a brief reception window after an uplink (Rx1). Rx1's start time begins a defined phase after broadcasting the uplink for the endpoint whose delay is typically 1s long, although adjustable. A follow-up receive window – Rx2 – is opened, which usually begins 2s later, should a downlink not be admitted within the first window.

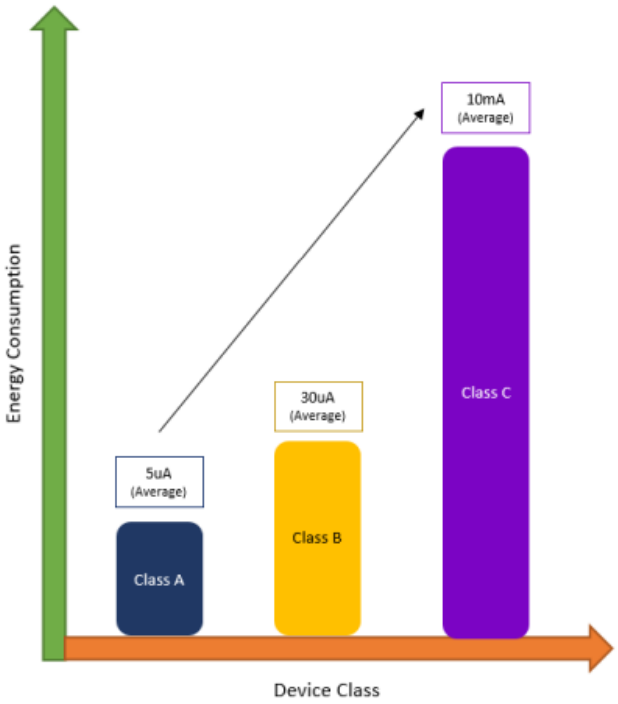

Figure 2.4: Energy consumption by end-device class

(Semtech Corporation, 2019)

Figure 2.5: Received window: nothing is received

(Semtech Corporation, 2019)

Figure 2.6: Received window: Rx 1 window received packet

(Semtech Corporation, 2019)

Figure 2.7: **Received window: Rx 2 window received packet**

(Semtech Corporation, 2019)

Rx1's default delay (RECEIVE DELAY1) being a system specification according to LoRa Alliance LoRaWAN Regional Parameters. Using MAC command RxTimingSetupReq, network operator can change the default delay. The default is generally 1s. Prior to initiating Rx2 the endpoint pauses 1s following the end of Rx1.

The LoRaWAN Regional Parameters document defines the conventional connection linking the frequencies of Rx1 downlink, the uplink and the and data rate. Its data speed is determined by the speed utilized in support of uplink transmission. This network operator can change the default parameters remotely by using the appropriate LoRAWAN MAC instructions.

A MAC command can be used to set the frequency and data rate for Rx2. The defaults are determined by the region. Each receive window must last at least if the radio transceiver on the end device needs to properly identify a downlink preamble. If a downlink preamble is detected during this time, the receiving radio allows access till it downlink data is decoded. To conserve energy, a device won't initiate Rx2 should the downlink be recognized and decoded during Rx1 and determined appropriate for the endpoint which accepted it (after it’s address and Message Integrity Check (MIC)). The endpoint goes on to Rx2 as intended if it doesn't get a downlink message during Rx1. Even if an endpoint has nothing to accept, it initiates it’s receive windows with SF7 data rate, that’s 5.1 milliseconds minimum. It takes 164 ms at SF12 data rate to reach its maximum. If the device receives a downlink, the message will be demodulated in fewer than 100 milliseconds at SF7. It can take more than two seconds at SF12.

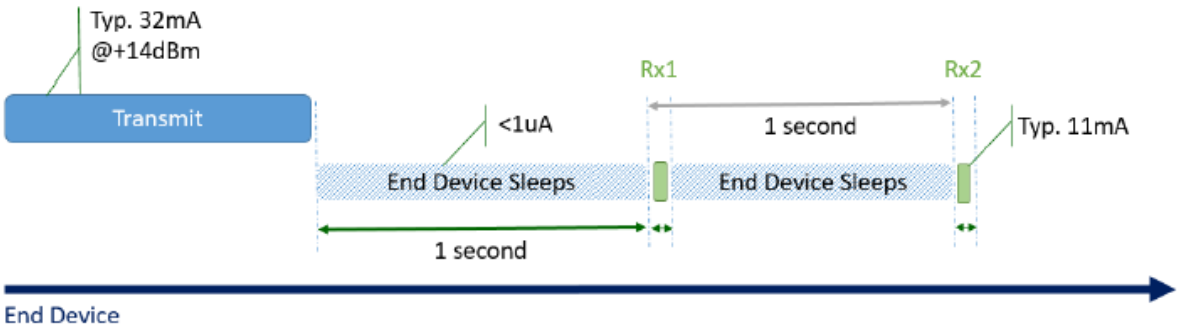

Figure 2.8: **SX126x radios transmission uplinks, downlinks, and wake-up times**

(Semtech Corporation, 2019)

The LoRaWAN system infrastructure illustrated in Fig 2.9. It's main distinction to other approaches would be that end devices are connected to the network directly rather than being completely connected with one gateway. Endpoints instead transmit with every gateway in radius. Every receiving gateway delivers a data packet to the network server, which de-replicates it then transfers one form to the database server (Semtech Corporation, 2019).

This topology has a few advantages:

- Intricate system devising is not compulsory. It's possible for gateways to be introduced whenever and from any location.
- Every uplink received by the gateways is a duplicate data packet, making accurate message delivery is more reliable. Uplink spatial diversity is the term for this.
- It is not necessary to allocate new frequencies when gate numbers change or to plan for distinct frequencies on every gateway. Every gateway is continually monitoring on every network frequency.
- Because every gateway may accept messages from any device, mobile devices can run at little power. This implies that, unlike cellular networks, the LoRaWAN network is unaffected by the device's movement and merely gets uplinks from the gateways closest to the device's present position.

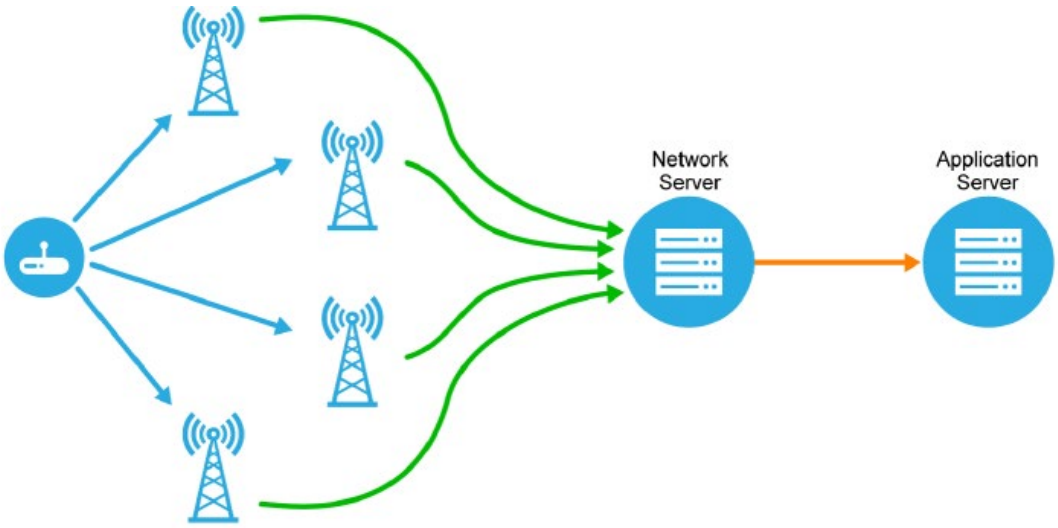

Figure 2.9: Topology of LoRaWAN network

(Semtech Corporation, 2019)

Unconfirmed or confirmed messages from and to end devices to network and application servers are enabled. Using adjacent gateways, a smoke detector, for example, regularly sends unacknowledged uplinks to a host system to verify that it is functioning. The cloud provider receives data from the gateways and transmits it to the host system; however, the host is not required to acknowledge an unconfirmed message (Semtech Corporation, 2019). The endpoint expects the host system validation of the message as received when delivering a confirmed message. Let's take another look at the smoke alarm. A smoke detector will send notifications when it senses something, and these notifications must be validated before the alarm is acknowledged. The smoke detector receives the signals from the affirmation that the warning has been addressed. Since network downlinks are a limited resource, they must be utilized responsibly. Only highly critical sensor data should be sent via confirmed messages (Semtech Corporation, 2019).

A smoke detector transmits encrypted, unconfirmed messages to two gateways, as shown in Figure 9. The communications are encrypted before being sent to the network server via the gateways. The host system decrypts the metadata, thereafter, transferring data packet to the application server takes place, that then decrypts the data (Semtech Corporation, 2019). The smoke detector, which is shown in orange, is sounding an alarm. The alert continues to broadcast because the acknowledgment has not been received in the first two cases, even though these are confirmed messages. Following the third alert transmission (illustration following page) the device

and the most effective gateway finally receive an acknowledgement from database server via host system. (Semtech Corporation, 2019).

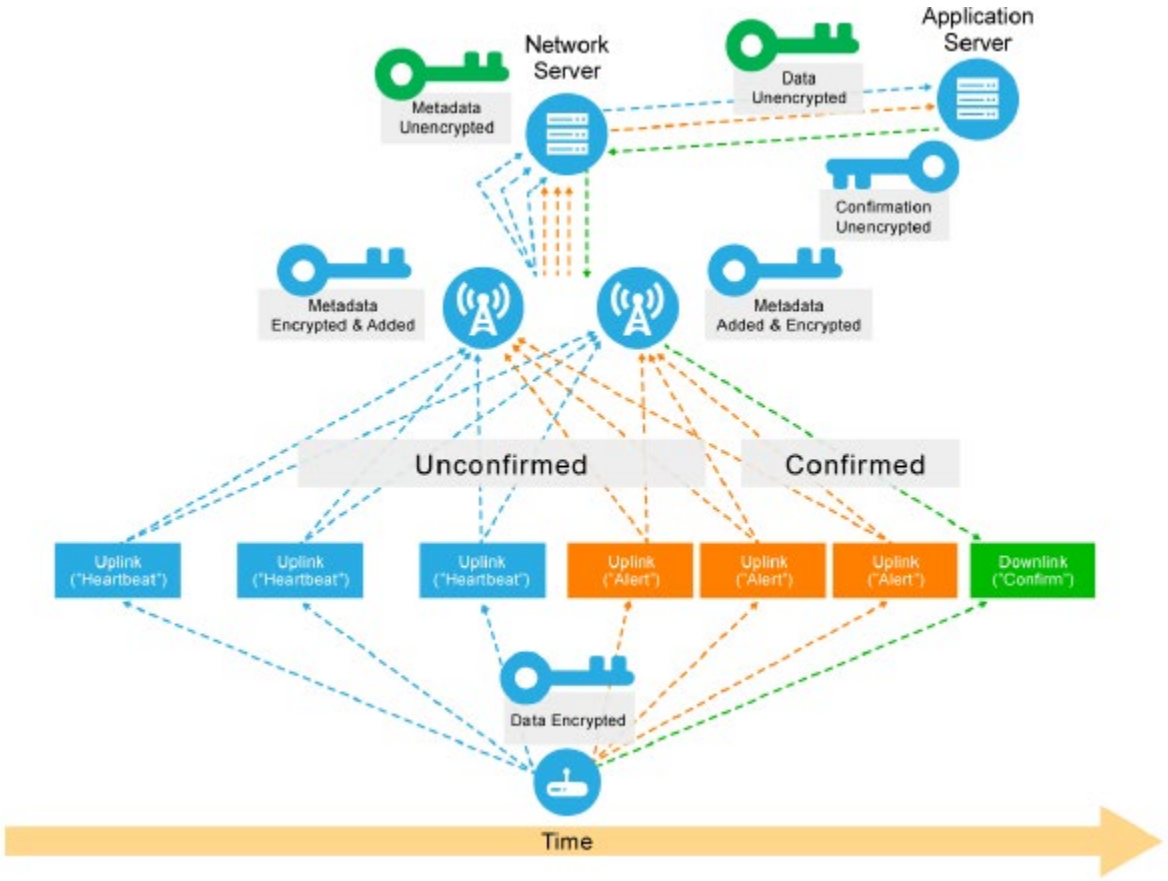

Figure 2.10: **Confirmed and unconfirmed LoRaWAN Class A messaging**

(Semtech Corporation, 2019)

Owing to the detector (end device) being a Class A device, data transmitted to it by the detector application server is delayed because the smoke detector must first wake up before the application server can deliver the data. This is not a true smoke-detection event, but rather a periodic communication (such as cycle of 8 hours) communicating system status—battery information—through the database server. The end device's receipt of this communication might be confirmed or unconfirmed. Figure 2.10 is a good example. The smoke detector is asleep, but the database server acquires information to relay to endpoint. The endpoint must send an uplink to the server before data can be transferred and the server transmits the downlink immediately after the uplink has been received and the device returns to sleep afterwards if it received an unconfirmed message.

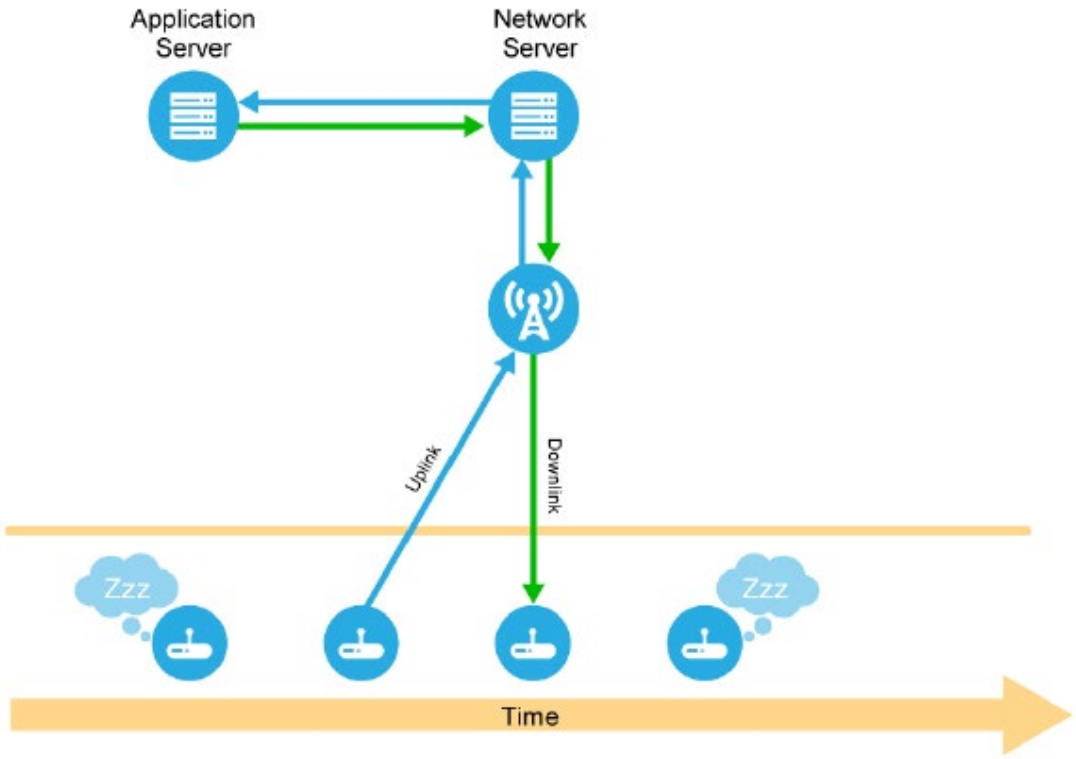

Figure 2.11: Application server's downlink

(Semtech Corporation, 2019)

Class B devices, on the other hand, provide for predictable downlink times from the network server. Class B gadgets are less energy efficient than Class A devices, hence their battery life is lower (Semtech, 2019).

In addition to those that open when a Class A-style uplink is transmitted to the server, end devices in Class B mode offer regularly scheduled receive windows. To make this work, the network broadcasts a time-synchronized beacon across gateways on a regular basis, as seen in Figure 2.11. To synchronize its internal clock well with network, the end device must receive these kind of network signals on a regular basis.

End devices may open receive windows (ping slots) at regular intervals based on the beacon time reference. The network infrastructure can start a downlink communication using any of these ping slots (Semtech, 2019).

An application server sends a downlink message to a Class B device.

1. A downlink message (DL) is queued by the application server (AS) in the network server (NS)

2. The next ping slot lineup is computed by the network server.

3. Based on the device's most recent uplink and the current gateway's transmission schedule, the network server determines the optimal gateway to utilize.

4. The downlink is queued by the network server for delivery to the specified gateway.

5. The gateway sends the downlink when the chosen ping slot initiation time is reached.

6. The gadget turns on its receiver and gets the downlink at the same moment.

When there is no downlink to send (approximately 99 %), the network does not transmit at all transmit. However, the device continues to open its receiver at the commencement of the ping slot. When it does not identify a preamble, it returns to sleep as soon as feasible to preserve power (Semtech, 2019).

Class B operation's power overhead is determined by the following factors:

- the beacon's time-on-air, which varies by area
- The ping slot data rate and
- the ping slot periodicity (application driven) (which sets the minimum duration of each ping slot)
- The average periodicity of a Class B downlink

There are two types of downlinks: unicast and multicast. Multicast communications are transmitted to several end devices at once, whereas unicast messages are transferred to a single end device. The following requirements must be followed in order for a multicast signal to be successful:

A multicast group's devices must all use the same multicast address and encryption keys. All devices must be active simultaneously, within the same channel, and with the same data rate.

Receive windows are virtually always open on endpoints that operate on C mode. Only when the gadget is transmitting do these windows close. As a result, C endpoints consume the most energy compared to A and B endpoints. Nonetheless, they have the shortest connection delay between the server and the endpoint (Semtech, 2019).

It is possible to briefly enter C mode on a gadget. An electronic gadget that runs on batteries might have its firmware updated using this method. For short minutes of time, a battery-operated to accept a firmware update over-the-air (FUOTA) communication, a gadget can switch to C. The device can return itself to normal A mode low-power

method of action when the notification has been distributed. The identical 2 receive windows that mode A endpoints utilize are also used by C endpoints, however the RX2 window is not closed until the server receives the subsequent communication. As a result, essentially at any moment within the RX2 window, a downlink is transmitted. A brief window at the RX2 frequency and data rate will be initiated between the end of the transmission and the start of the RX1 receive window, as shown in Error! illustration referenced from LoRaWAN documents (Semtech, 2019).

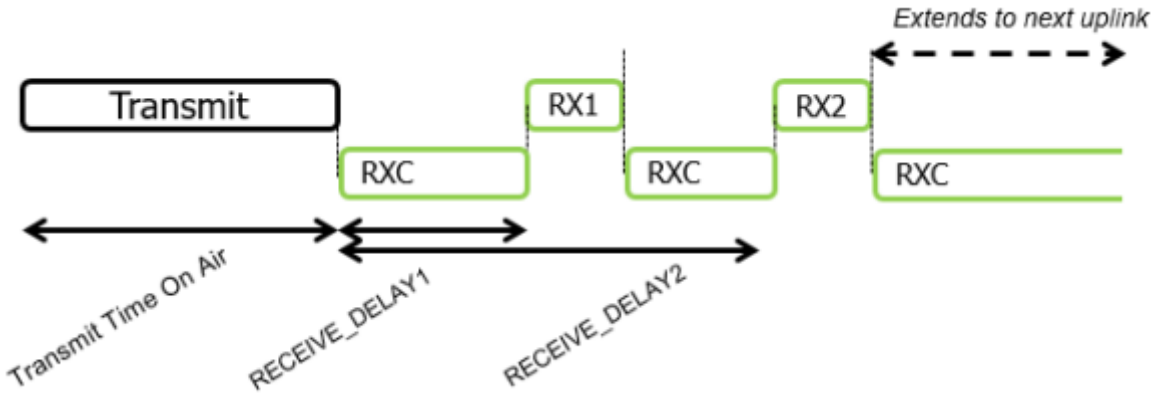

Figure 2.12: **Transmission and reception times for receivers**

(Semtech, 2019)

End devices in Class C mode can receive multicast downlink packets in the same way that Class B end devices can. The application layer must provide the multicast address, as well as the accompanying network and application session keys.

The FPending bit indicates that additional multicast data needs to be transmitted. The FPending bit will not cause any unique action on the end device because C endpoint has its receiver often in use (Semtech, 2019).

2.5. Summary

LoRaWAN, designed for broadcasting uplinks and provisioning downlinks, is well-suited for ubiquitous coverage in both indoor and outdoor environments. It is particularly ideal for data collection and monitoring applications in diverse industrial settings, often complementing RFID systems. Operating primarily in the 863-928 MHz frequency band, LoRaWAN leverages unregulated RF-based devices. Significant investments by cellular operators have substantially enhanced network coverage, with strategically placed gateways ensuring extensive communication reach.

Chapter 3: Energy harvesting

3.1. Kinetic energy

The technique of drawing power from motion or the mechanical deformation of a piezoelectric material is known as kinetic energy harvesting. Piezoelectric power conversion, electrostatic energy conversion, and magnetic induction are the three basic processes for turning kinetic energy into electrical energy.

The 1880 discovery of the piezoelectric effect is used in piezoelectric generators. Mechanical stress causes certain materials to develop an electric charge. This charge may be utilized to power gadgets with the right electrical circuitry. There are several different types of piezoelectric energy collecting circuits (Michele Magno, 2018).
Piezoelectric materials are frequently used in footwear heels for energy absorption. The basic idea behind electrostatic generators is that when a transducer moves counter to an electrical field, electricity is generated. The spacing between the two plates of a capacitor varies due to ambient vibrations. This process can generate energy when the voltage or charge are kept fixed since the basic capacitor formula states that the charge should be equivalent to capacitance multiplied by voltage (Magno, 2009) (Paradiso, 2001).

Faraday's law underpins magneto-inductive induction transducers. An electric field is created when the magnetic flux in an electrical circuit change. Using a mobile magnet whose flux is linked with a fixed coil or a constant magnet whose flux is linked with a changing magnetic field, this flux fluctuation may be achieved in practice. Magnetic flux across the coil area is connected to the energy gained from a single movement. As a result, larger transducers having larger coil surfaces could outperform diminutive transducers (Thielen M, 2017).

Over two decades ago, wristwatch makers demonstrated kinetic energy harvesting from human anatomy for wearables. Experimental results revealed how at most 1 mW could be obtained because of power conversion inefficiencies whenever the harvester was placed on the anatomy, contrary to previous studies that claimed 5–10 mW could be extracted from the human anatomy. Earliest record for harnessing kinetic energy from human anatomy dates from 1987, and since then, it was enhanced and included into several Seiko watches. The Kinetic brand of wristwatches had this self-winding mechanism. A revolving pendulum, a gear train (1:100), along with a tiny permanent magnet converter made up the design. A single swing from the pendulum generated hundred rotations on the converter because of wrist positioning. ETA, a Swiss firm, later released the Autoquartz in a new form. The pendulum mass in Autoquartz wound

a spring that was coupled to a tiny generator through a gearbox train. The generator rotated at 5-15 krpm for a brief period (50 ms) after the spring was fully wound, generating more than 15V and 6mA. (90mW). To operate with piezoelectric materials used in the soles of the shoes, the resonance frequency for kinetic walking energy must be steady and higher (about 40Hz) than human motion (approximately 1Hz). As a result, the piezoelectric material is used in very few works for human motions (Michele Magno, 2018).

Kinetron just announced a revolutionary micro generator system (MGS 26.4) that produces quantity of 3mW electricity. It produces alternating current (AC), which must be transformed before being stored inside a DC storage device (such as a supercapacitor or Li-Ion battery). The findings demonstrate encouraging outcomes that when the Kinetron is put on the human body, it can capture hundreds of microW. They offer an energy recovery circuitry that combines a passive AC diodes bridge rectifier and a Texas Instruments BQ25570 IC. While the approach is like that of the suggested technique, in this research a unique design based on a partially operative voltage converter that doubles as a highly efficient AC to DC rectifier. The NVC was created and tuned for use with Kinetron MGS as well as the DC-DC that follows. The entire system has a substantially greater conversion efficiency than earlier efforts due to the innovative architecture (Kinetron, n.d.) describes another recent study that used the MGS 26.4. The authors suggested an integrated circuit that archives up to 90% efficiency and is optimized for the MGS 26.4. A custom IC design is required because the recommended IC lacks a cold start feature.

3.2. Solar energy

Solar energy is by far the most common and plentiful source of electricity for the sensor node. Photons from the sun land on the photovoltaic cell's surface and create free charge carriers, releasing energy. Electrons and protons generate a potential difference from across PV junction solar cell, that in some situations it supplies direct power or alternatively charges the battery, extending its capacity (Chatterjee, 2015).

The three solar energy harvesting methods are:

Solar thermal collectors – the use of heat absorbing panels with a sequence of circulation tubes attached for electricity generation; concentrating solar power – the generation of power from a steam driven turbine by concentrating the sun’s ray using lenses or mirrors; photovoltaic technology – the use of light to generate electricity

through a material when the energy is pushes electrons to the outermost of an atom when hit by sunlight (Jones, n.d.).

An electrical tool which converts light energy to electric energy is a photovoltaic cell, also referred to as a solar cell. Photovoltaic effect is used to generate energy from photocells. The photovoltaic effect comprises of 1) charge carriers formed from light consumption, 2) charge carrier segregation, and 3) charge carrier collecting at the electrodes. The primary idea is to gather a numerous photons using photovoltaic elements including crystalline silicon, amorphous silicon, and cadmium telluride. To create electrical energy, the opto-electronic pool must be activated with a sufficient number of photons (al., 2016).

After the photons have been absorbed, the electrons inside the valance band are stimulated into the conduction band. A photon can be absorbed with as little as 1.12 eV of energy with a 1110 nm peak wavelength.

The quantity of energy gathered is determined by, The light's power, spectrum composition and incident angle. And the area, responsiveness and sort of photovoltaic (PV) cell utilized (al., 2016).

As far back as the 7th century B.C.E humans were already harnessing solar energy by concentrating sunlight using a magnifying glass material to set up fires. In the third century BCE, it was discovered that Greeks and Romans had utilized reflectors to collect solar energy to illuminate torches for sacraments. These reflectors were termed "fire mirrors". Chinese civilization also recorded similar usage of mirrors for this purpose about the year 20 CE. Researchers and scientists used sunlight to operate ovens for long trips in the late 17^{th} and early 18^{th} centuries. Steamboats powered by the sun were created. It's evident that collecting solar power was a widespread technique eons before the invention of solar panels (Richardson, 2018).

Photovoltaic mechanism was created iteratively with the assistance of many scientists. Consequently, a dispute has resulted regarding the accreditation of the invention. Others identify the French scientist Edmond Becquerel with pioneering the photovoltaic cells. He found how when two metal electrodes had been placed inside an electrolyte material, light helped promote energy production. The "photovoltaic effect," a breakthrough, influenced subsequent selenium-based PV technology (Richardson, 2018).

Selenium's photoconductive capability was recognized by Willoughby Smith in 1873, then William Grylls Adams and Richard Evans Day proved the metal's capacity to produce electricity whenever sunlight strikes it in 1876. Several scholars attribute the

innovation of solar cells to Charles Fritts since he designed the original solar cells made with selenium wafers in 1883 (Richardson, 2018).

Silicon is used to construct solar cells in today's industry instead of selenium. Nonetheless, many consider the innovation of the silicon PV cell by Gerald Pearson, Calvin Fuller, and Daryl Chapin at Bell Labs in 1954 as the actual originators of solar panels. Being the first successful PV system to operate an electric appliance incessantly all through the day, several researchers realize this moment to be the definite beginning of photovoltaic systems. The capacity factor of the pioneering silicon solar cell was merely 4%, below one-fourth of how much modern cells typically attain (Richardson, 2018).

The first implementation of photovoltaic panels was for powering spacecrafts in orbit. In 1958, a small one-watt panel supported the transmitters aboard the Vanguard I satellite. Thereafter in the same year, the Vanguard II, Explorer III, and Sputnik-3 were deployed utilizing solar technology. In 1964, NASA deployed its first Nimbus satellite which was completely operated with a 470-watt photovoltaic system. In 1966, the earliest Orbiting Astronomical Observatory was launched and functioned completely on a one-kilowatt panel.

In 1973, The University of Delaware constructed the first solar facility, dubbed "Solar One,". Solar thermal and photovoltaic energy were used to power the structure which was the origins of application of building integrated photovoltaics (BIPV) - solar panels were not utilized for the array rather embedded solar through roofing, comparable to Tesla's roof innovation (Richardson, 2018).

Between 1957 through 1960, Hoffman Electronics made great strides in advancing photovoltaic reliability, raising effectiveness standards from 8% to 14%. The next significant advancement followed in 1985, when the University of South Wales achieved 20% efficiency for silicon cells. The next significant advancement followed in 1985, when the University of South Wales achieved 20% capacity for silicon cells. In 1999, the National Renewable Energy Laboratory and SpectroLab Inc. collaborated to design a solar cell that has a 33.3% efficiency. The University of South Wales scholars obtained a new high of 34.5% efficiency in 2016 (Richardson, 2018).

In 1981, Paul MacCready built the first solar airplane, Solar Challenger, he piloted it across the English Channel from France to the United Kingdom. The autonomous photovoltaic airplane "Pathfinder" set an aviation milestone upon reaching 24.4-km in 1998. NASA set a new altitude milestone in 2001 of 29.3-km with a non-rocket aircraft.

Bertrand Piccard's Solar Impulse 2, the biggest and most advanced solar aircraft, accomplished the first solar flight around the globe in 2016 (Richardson, 2018).
Photovoltaic panel prices have declined dramatically in recent decades, resulting in a spike in consumer demand which has resulted in over one million installations within the United States as of early 2016. In 1956, the price of PV panels was around R5100/W. In 1975, the cost per watt had reduced to about R1700. A solar panel may now be purchased for as cheap as R8.50/W. From 1980, the cost of PV panels has decreased to less than 10% per year. Falling prices for PVs is primarily due to its increasing appeal and credibility as a viable power source for everyday use (Richardson, 2018).
The invention of photovoltaics innovated sun energy harvesting for power generation. However, due to its poor efficiency, the PV industry's growth is insufficient to meet market demand for solar panels. As a result, for the solar power sector, lower-cost, higher-efficiency solutions are required. These criteria prompted researchers to develop an alternative method based on the wave structure of light, replacing conventional solar cells using optical antennas incorporated into diodes to produce a rectifying antenna (rectenna) (Corkish R, 2002; B, 2003).

3.3. Optical antenna

The development of solar rectennas started with the discovery of wireless power transmission. At the time, all rectenna systems were built to operate at microwave frequencies and had efficiency of more than 80% at a single frequency (Al-Ani, n.d.). Most of the current research has focused on advancing solar rectenna’s conversion efficiency from visible electromagnetic spectrum to electrical energy while also harnessing the non-utilized fraction of solar energy (i.e., the electromagnetic radiation domain) (Biagoni P, 2012).

A solar rectennas is projected to be more efficient than conventional solar cells (mathematically 100 percent for monochromatic light) (Joshi S, 2013). Instead of being inefficient, solar rectennas eliminate PVs' additional drawbacks, such as reliance on band gap energy and narrowband function (solely for visible domain). However, various obstacles, such as substandard coupling connecting the optical antenna with the diode (Grover S, 2011) lead to the actual conversion efficiency being significantly lower than planned. To create electrical power, every photon in semiconductor solar cells generates an electron hole pairing. Only photons with energies higher compared to the band gap energy are absorbed by the gadget. In real-world devices, this reduces conversion efficiency to 44% or even lower. Traditional rectifiers, on the other hand,

accept electromagnetic energy which they then convert to DC energy at a conversion efficiency of 100 percent. The construction of solar rectennas follows the same approach for the purpose of achieving high efficiency over the electromagnetic spectrum. Because great efficiency is methodically achievable in addition to easily accessible and affordable components, the area of solar rectennas looks to be promising and appealing (Al-Ani, n.d.).

Early WPT experiments harken represent the work of Hertz and Tesla, who used a massive coil and 57-m high tower (from ground to top of cupola) with a 20-m-diameter copper hemisphere to transmit low-frequency electromagnetic waves between two different locations. Later, researchers created the concept of power transmission, particularly following considerable innovations in microwave technology (WC, 1984).

In 1963, the original rectenna was created by Raytheon Co., consisting of 28 half-wave dipole antennas that were all connected to a bridge rectifier. This design has a 40 percent total efficiency. The same institution later created the rectenna to be used for powering a microwave aircraft (Al-Ani, n.d.).

In 1972, Bailey proposed utilising rectennas to harvest solar energy. With the purpose of modifying a dipole utilizing two pyramids or cones, comparable to rod antennas. The pair and the load are connected utilizing a diode (half-wave rectifier) (Corkish R, 2002).

In 1984, Marks demonstrated matrices of crossed dipoles utilising an insulating sheet and instantaneous full-wave rectification (AM., 1984).

Bailey, on the other hand, developed a conventional broad side array antenna that absorbs the output signal upon traversing through multiple dipoles. The last-mentioned powers transmission lines which send waves to the rectifier. In such a strategy, combined signals are employed for in-phase amplification (Al-Ani, n.d.).

In 1996, Lin et al. reported the first simulation investigation on light transmittance by metallic reflective nanostructures and light frequency rectification. The device employs a dipole antenna matrix which is parallel-coupled and fabricated onto a silicon substrate. Half-wave rectification is achieved by using a p-n diode (Lin GH, 1996).

In 2003, Berland developed infrared (IR) rectenna framework metal-insulator-metal (MIM) diodes. It was created with dipoles and operates at a wavelength of 10 m. However, total inefficiency was quite high (>99%) (B, 2003). A helix solar nanoantenna was engineered in 2010 to collect energy in the mid-IR range (Kotter D, 2010). Kotter et al. proved significant advancement of such an approach.

Midrio et al. constructed a monopole antenna in 2011 that employed nickel as the primary material to manufacture the thermal radiation reception. The ground plane is overlapping with this antenna. MIM (nickel-nickel oxide-nickel diode) is employed to generate terahertz forces into electrical current. Other research papers (Midrio M,

2011) are also interested in investigating the effects of geometrical features on antenna performance.

Advantages of using solar rectennas are (Al-Ani, n.d.):

• Nanosheets, used for sun rectennas material, are readily accessible, and the production process is affordable in comparison to traditional solar cells.
• Solar rectennas can attain as high as or even higher efficiency than solar cells.
• The versatility of solar rectennas over PV devices allows for the collection of additional infrared wavelengths, including heat losses.

The disadvantages of solar rectennas are (Al-Ani, n.d.):

• With planar MIM diodes, it is challenging to attain the required time constant for converting visible light, that within the range of 0.1-fs.
• It is exceedingly difficult to achieve the required leakage current of 1-A for the diode.
• Adequate balancing of the diode and antenna impedances that enables optimal power transmission for improved efficiency is a challenge to achieve.

3.4. Radio frequency

The advantage of RF energy harvesting in comparison to solar, vibration and thermal harvesting is that it ordinarily has no downtime, which permits battery-less devices that operate on ambient low-energy RF harvesting. Additionally, it has the advantage of simply requiring an antenna to transduce, whereby all network devices already have; alternative energy collecting techniques, like photovoltaic cells, thermoelectric junctions, or mechanical generators, require non-standard materials and components, not just ordinary conductors and semiconductors.

Research into Wireless Power Transfer (WPT) was first conducted by Nikola Tesla when the 1800s were coming to an end. He would power the coil with 300-kW, and it would resonate at 150 kHz frequency, with the sphere's radio frequency peaking at 100 MV (Shinohara, 2021; Tesla, 1904). The transmitted power dispersed randomly employing radio waves of 150 kHz with 21 km wavelength which resulted in a failed experiment. Nonetheless, following Tesla's WPT trials radio waves made remote sensing and wireless communications possible, and the broadcasting system

employed today is like the WPT wide beam of Tesla's failed experiment (Shinohara, 2021; Tesla, 1904).

WPT is categorized as near-field or far-field WPT and its only recently that near-field WPT products have become commercialised based on inductive coupling using coils with a magnetic field with high-frequency such as a wireless charger for a cell phone and an inductive heater (Shinohara, 2021). Although considerable advancements were made in the 1960s on far-field WPT it was in 2006 that WPT research at the Massachusetts Institute of Technology (MIT) discovered resonance coupling can be used to increase the distance between two coils using a high Q-factor whilst maintain a high efficiency (A. Kurs, 2007). The MIT study reignited research into far-field WPT (A. Kurs, 2007).

In the nineteen forties an engineer at the Raytheon Company, named Percy L. Spencer discovered microwave heating (radio waves in the range of GHz) whilst he was developing a remote sensor using microwave radar during his invention of the first microwave oven (Shinohara, 2021). Ambient radio waves from the broadcasting system can be harvested for energy like the microwave oven. The Germanium radio popularly known as the crystal radio is the most notable utilization of energy harvesting of ambient radio waves its powered by the radio waves it receives for broadcasting, thus it does not require a battery to operate. In addition to ambient radio waves energy harvesting can be sourced from ambient ineffectual power from our surroundings like heat, electric light, and vibration (Shinohara, 2021).

A notable advocate of energy harvesting using radio frequency is the University of Washington that recommends the WISP (wireless identification and sensing platform) concept, which utilizes UHF RFID (uniform high frequency radio frequency identification) readers to provide power to and read a group of sensors (Shinohara, 2021; University of Washington , n.d.). They built a battery-less RF-powered mobile that was established on the WISP concept using a combination of digital and analogue applications requiring a low power of 3.48 μW (Shinohara, 2021; V. Talla, 2017). RF energy harvesting's greatest disadvantage is its low power output for instance in Japan the power density measured for mobile phones and television broadcasting waves is only a multitude of $\mu W/m^2$. On the other hand, RF energy harvesting does eliminate the requirement for a custom power transmitter. Nevertheless, it may be utilized for far-field WPT systems if user requires optimized power (S. Kitazawa, 2013).

Until recently in the 21st century did RFID seize to be the sole far-field WPT system. ISO (International Organization for Standardization) and IEC (International

Electrotechnical Commission) classifies traditional RFID systems applied for microwave and UHF as ISO/IEC 18000-6 between 860 and 960 MHz and ISO/IEC 18000-4 at 2.45-GHz (Shinohara, 2021). The permitted power is less than one Watts (W) and allowed antenna gain is less below six decibel-relative-to-isotrope (dBi). Backscatter communication and wireless power are utilised for passive-type RFID (Shinohara, 2021).

The development of wide-beam WPT technology is derived from RFID technology however wide-beam WPT is more versatile than RFID. Wide-beam WPT does not use geographical area target detection to provide wireless power to multiple users. The battery is charged with the energy sourced from ambient RF wireless power. Radio regulations leads RF information and RF power to depend on separate RF (Shinohara, 2021; Carvalho, 2019).

A field wireless charger was demonstrated from an airship for a mobile by Kyoto University In 2009, and in 2015 they demonstrated sensors boarded on to a drone that were wirelessly powered and in 2018 working alongside the Panasonic Corporation they developed RF powered vital sensors developed using the 920-MHz-band RFID system transmitting <1-W of power. Followed by the development of RF powered vital sensors that can transmit a wide-beam WPT system of <5-W in 2019. Recently a new concept named SWIFT (simultaneous wireless information and power transmission) supposedly has higher efficiency (Shinohara, 2020).

A rectifying antenna (rectenna) is an antenna with a rectification circuit that has a CMOS /diode that receives RF and converts RF to DC (direct current) electricity and is essential for wide-beam WPT systems and energy harnessing. Although the RF power density of the harnessing circuit cannot be controlled, it's possible to maximize the DC voltage output and DC power by increasing the rectenna RF-DC efficiency conversion (Shinohara, 2021). Using a SBD (Schottky barrier diode) an RF-DC conversion efficiency of >80% at 5.8 GHz band and >90% at 2.45% band can be achieved (J.O.L McSpadden, 1998). Even though this energy system has an exceptional efficiency it requires an RF power input higher than one watt for maximum efficiency to be actualized due to the diode's attributes. For input power greater than one watt the efficiency of RF-DC conversion is typically at 90%. For low input RF power less than -mW the efficiency is improved through employing a diode/CMOS with junction and low series impedance such as a superior Schottky barrier, and increased nonlinearity (Shinohara, 2021; X. Gu, 2019; X. Gu, 2014).

In 2019 a tunnel diode was developed at Eindhoven University of Technology, Netherlands which permits an input of 2.4 GHz of −25 to −10 dBm microwave power,

the tunnel diode showed an increased RF-DC conversion efficiency as against a conventional SBD (V. Manev, 2019). A high RF-DC conversion efficiency is also obtained through using an antenna with a high impedance (Q-matching circuit) as established by the Carnot limit (Shinohara, 2021). A low-power and wide-band rectenna with an impedance of >400-Ω was develop at the University of Liverpool and it accomplished a 75% RF-DC conversion efficiency between 0.9-1.1 GHz and 1.8-2.5 GHz (C. Song, 2017). In 2016, Kanazawa Institute of Technology, Japan, designed a 1.6-k Ω high-impedance rectenna to harvest digital television signals at 500-MHz, that can obtain 49% of RF-DC conversion efficiency at an inputted RF power of -15-dBm, and an 8.7% efficiency can be obtained for an -30-dBm input power (T. Furuta, 2016). Only a rectenna can increase wireless power when harvesting energy from ambient RF signals because the distribution of RF power cannot be controlled. However, in the consideration of a wide-beam WPT, there are greater options on increasing wireless power. In 2020 the Panasonic Corp. collaborated with Kyoto University to set out to increase received power and lower the density of transmitted power by developing a WPT system that's distributed (Y. Tanaka, 2020). The Ossia Corp. proposed a phased indoor WPT using a retro-directive array technique with target reference point (Fig.14) (Shinohara, 2021) (Zeine, 2016; Saghati, 2016). A target generates a guide signal, followed by a phased array and a power transmitter. From the resulting reference point signal, phase formation is established on every antenna in the phased array. Even in situations with various paths, the power beam develops towards the target due to phase formation. Even with two targets, the multipath condition allows for the viability of the retro-directive approach (Shinohara, 2018).

In 2016, ITU-R (International Telecommunication Union Radio) published the first "ITU-R report SM.2392 of WPT by radio waves" (Shinohara, 2021) (ITU-R Report SM.2392, 2016). Which includes all radio signal uses for WPT, wide- and narrow-beam WPT and SPS (Solar Power Satellite) (Shinohara, 2021). In 2019, the ITU-R accepted "Working Document Towards a Preliminary Draft New Report ITU-R SM. [WPT.WIDE-BEAM.IMPACTS] rev" (Shinohara, 2021; ITU-R Report SM.2392, 2016). Table 1 shows the WPT beam system specifications for commercialization and has received support from Japan and the United States, who approved the wide-beam WPT framework that venture companies specialise in "December 2017, June 2019, and October 2019" (Shinohara, 2021). The conversation regarding far-field WPT homegrown radio regulation (RR) begun with Japan in 2019 and is guided by WPT system future situation within 3-frequency bands, 920MHz, 2.4GHz, also, 5.7GHz, as displayed in Table 1. On the 14th of July 2020 an agreement was reached in Japan for

a new homegrown RR with wide-beam WPT (Ministry of Internal Affairs and Communications, 2020). In contrast with wired power transfer, the WPT narrow-beam method is described with a Fresnel region (radiative near-field) WPT method for maximizing beam effectiveness that would be is hypothetically near 100%. As a rule, narrow-beam WPT has a determined target detection that's focused on one target (Shinohara, 2018).

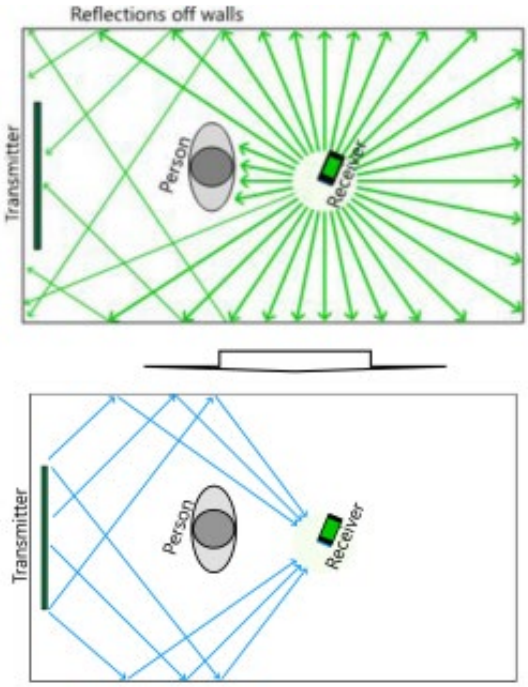

Figure 3.1: The Ossia system

(Shinohara, 2021)

Table 3.1: Wireless power transfer beam system specifications for commercialization

Method	S **Frequency**	P **Output Power**	e **Antenna Gain**	e **EIRP**	c **Modulation**	c **Location**
Method 1	920MHz bands (915-930MHz)	1W	6dBi	36dBm	To be determined	indoors
Method 2	2.45GHz bands (2.40-2.499GHz)	15W	24dBi	65dBm	To be determined	indoors
Method 3	5.7GHz bands (5.470-5.770GHz)	32W	30dBi	70dBm	To be determined	indoors

In 1964 and 1968 William C. Brown applied a narrow-beam WPT from a magnetron of 2.45 GHz to fly a drone. In Goldstone, US, in 1975 he successfully tested the longest distance WPT narrow-beam. In 1975, he likewise accomplished 54% DC-DC absolute system effectiveness with a magnetron of 1 kW–2.45 GHz in a lab trial and it remains the highest recorded total efficiency for WPT narrow-beam. The first injection-locked magnetron was developed by him (Brown, 1981) and so was the first rectenna. A microwave supply dependent on tubing remains the better option for narrow-beam WPT on account of its effective power. However, because a beam foaming framework is required the microwave tubing is inappropriate for beam foaming, because adaption for a narrow-beam WPT framework for a target that is in motion is difficult. To tackle the clashing prerequisites of high proficiency and pursuing a target, it is fundamental to have a phased array for beam forming. At Kyoto University, Japan, Hiroshi Matsumoto steered the research on narrow-beam WPT from the 1980s (Matsumoto, 2002). In 1992, Hiroshi successfully piloted a small airplane with the first narrow-beam WPT with a phased array of 2.411 GHz and fostered a number of retro-directive WPT frameworks from the 1980s to 1990s (Shinohara, 2021). In 1983, he executed the first WPT test with a magnetron from space and in 1993 the second WPT test using a phased array, his point was essentially an SPS (Solar Power Satellite). He additionally improved an SPS demonstrator using a 5.8 GHz at phased array. His innovations are connected to the SPS as well as the business uses of wide-shaft WPT in Kyoto University (Shinohara, 2021; Matsumoto, 2002).

In 2015 and 2019 due to their interest in the SPS and WPT by microwave the Japanese Ministry of Economy and Trade, and Industry (METI) led some WPT ground tests. Following the 2010s, many tests for narrow-beam WPT ground tests took place within Japan as well as in China and Korea. In 2020, Xing Chen, Sichuan University, developed and executed at 5.8 GHz a microwave power system. The test achieved 10 m transmission distance, and an 18.5% transmission efficiency for the transmission system of microwave wireless energy. In 2020, a transmission test over 300-m was conducted. The SPS is the major reason for the Chinese advancement of the narrow-beam WPT (Shinohara, 2021).

Beam shaping technique may overcome the conflicting prerequisite of pursuing a target and high efficiency regarding narrow-beam WPT. Wireless detection innovation as well as Multi-In/Multi-Out innovation used in wireless communication are the foundation of beam formation. Both being very similar to each other. Nonetheless, WPT necessitates increased microwave transmission effectiveness with exceptionally

high beam formation accuracy. Likewise, expense plus dimensions are significant (Shinohara, 2021).

Another phased array design incorporating advanced solid-state instruments has just been built in Japan targeting SPS operations. METI endorsed this initiative, then in 2015, Mitsubishi Electric Corp. designed innovative GaN HEMT semiconductors including narrow phased array systems with exceptional accuracy (S. Mihara, 2015). The project was managed by J-Space Systems. Most importantly, they advanced another 5.8GHz GaN HEMT with MMIC (monolithic microwave integrated circuit) high-power F-class speaker. Efficiency of 70% and power output of 7-W were reached. A high efficiency and size reduction of a phased array can be achieved with the new developed MMIC (S. Mihara, 2015).

In 2015, JAXA worked together with J-Space Systems. They completed an assessment trial to test the accuracy of the advanced phased array for beam forming accuracy by combining target detection and beam forming. The first approach uses a single pulse amplitude with a reference pulse point, whereas the second uses the technique of rotational electric field vectors. The accuracy is adequate considering the 36,000 km transmission distance for a >2-km diameter transmitting antenna requiring a beam forming accuracy of 0.0001 degree. The SPS configuration in Japan for a 36,000-km for a narrow-beam WPT has a beam efficiency of 96.2% with a transmitting antenna of 1.93-kmØ and a receiving antenna of 2.45-kmØ at 5.8-GHz without loss in ionosphere, air, and rain. Within the Japanese SPS the microwave power transmitted is above 1.3-GW from a phased array with >2-billion antenna elements. The Friis transmission formula is used to calculate the theoretical effectiveness for the beam connection of the transferring and the receiving antennas, also it's a beam efficiency limitation (K. Makino, 2015). The wide-angle antenna transmission tapers the amplitude to maximise beam effectiveness, like Gaussian tapering. Nonetheless, the tapered amplitude method is not the most efficient when WPT total efficiency is taken into consideration, inclusive of beam efficiency and the transmitting DC-RF and receiving RF-DC conversion efficiencies of the system because both the conversion efficiencies of the circuit are minimized due the tapering amplitude at both the receiving and sending antennas. Another tapering model was proposed by the Kyoto University to improve the beam efficiency and to maintain great DC-RF conversion efficiency for the transmitting antenna's microwave antenna (A. K. M. Baki, 2008; Shinohara, 2017). In consideration to the rectenna array's RF-DC energy transfer effectiveness an original level-top beam was proposed in the radiative near-field (N. Takabayashi, 2020; Shinohara, 2018). The microwave amplifier's DC-RF conversion efficiency below par

for this configuration. The both-sides retrodirective system was proposed in Japan to reduce leak energy (T. Matsumuro, 2019).

A phased array is a consequential technology for narrow-beam WPT. Nonetheless, regardless of whether exceptional phased array and beam forming designs are developed the Friis transmission equation hypothetically limits beam efficiency. The world has developed good rectennas that operate with W-band. In 2010, The National Central University in Taiwan designed a dual-band rectifier operating between 35-94GHz and CMOS 0.13μm (Chen, 2010). The measured efficiencies of the power conversion in free space were 53% and 37% for 35- and 94-GHz, respectively. A W-band rectifier of 75-110GHz in 65nm CMOS innovation with an efficiency of 2% was developed in Israel at the Tel Aviv University (N. Weissman, 2014). In 2015, Ecole Polytechnique Montréal, Canada, developed a rectenna of 94-GHz with GaAs SBD with a measured efficiency of 37.7-percent at 90GHz and 32.2-percent at 94GHz with an input power of 3dBm (S. Hemour, 2015). In 2018, a group in Tsukuba University, Japan, designed a 2.17% efficiency 303GHz rectenna for a DC output power of 17.1mW and a commercialised GaAs SBD. And a GaN SBD is still under development which is intended to improve the efficiency of sub-terahertz rectenna, commenced in 2019 (S. Mizojiri, 2019)

To increase beam effectivity for reduced antenna aperture the laser power transfer (LPT) technique is preferable. In May of 2019, the Naval Research Laboratory, US, was successful in LPT system between 325 m (NRL News Releases, 2019) where it transmitted 2-kW of laser power and received by a distinguishably designed photovoltaic receiver. The 400-W laser beamed from sender to receiver remained undetectable to the human eye. The project has ambitions of building an SPS noting the relaxed regulations in comparison to radio waves even for laser applications (Shinohara, 2021).

In November 2018, Japan founded the SIP (Cross-ministerial Strategic Innovation Promotion) Program to innovate the WPT system which involves fundamental research WPT research and its applications. The SIP recorded narrow-beam WPT to have higher power in comparison to wide-beam WPT and thus the Kyoto University R&D team is researching the harmonization technique for narrow-beam WPT (Shinohara, 2021). CDM (code division multiplexing), SDD (space division duplex), TDD (time division duplex) along with FDD (frequency division duplex) are techniques that can be utilized to minimize interference for a conventional wireless application. Although, it is difficult to execute it would be ideal to adopt FDD which would permit obtaining specific frequency for WPT. On the other hand, there is no modulation that

conventional WPT is established on therefore making it difficult to apply CDM (Shinohara, 2021).

As a matter of first importance, the impact of SDD and TDD for narrow-beam WPT is gauged. The pulse WPT is expected to maintain average wireless power and minimize time alongside high power in the TDD-WPT system. The Wi-Fi specifications of the WPT system are assumed to be 5.8GHz and 140ch according to IEEE802.11a W56, whereas the Wi-Fi victim matches the frequency band. The throughput of the harmonization condition is estimated to -10% which is maintained by the Wi-Fi upon the changes of the WPT duty ratio signal. The duty ratio and WPT power signal have reached a level of harmony. The pulse WPT can improve the effectiveness of RF-DC conversion (T. Hirakawa, 2019). One of the reassuring techniques is the pulse TDD-WPT in harmonizing conventional wireless system. Due to SDD technology suitability for narrow-beam WPT and specialised limited-distance connectivity for similar bands it has been considered as a follow-up competitor for similar bands (T. Hirakawa, 2019).

3.5. Summary

Energy harvesting offers a promising solution to power IoT devices without relying on traditional batteries. Kinetic energy harvesting converts mechanical energy into electrical energy through piezoelectric, electrostatic, or magnetic induction methods. Piezoelectric materials, for instance, generate electricity when subjected to mechanical stress, making them suitable for applications like wearable devices. Solar energy harvesting utilizes photovoltaic cells to convert sunlight into electricity, providing a renewable and abundant energy source. Radio Frequency (RF) energy harvesting captures ambient RF signals to generate power, making it suitable for low-power applications. While these techniques offer significant potential, challenges such as low power output and environmental factors need to be addressed. Efficient energy management systems are crucial to optimize the performance of IoT devices powered by energy harvesting.

Chapter 4: Space communication

4.1. Sir Arthur C. Clarke's Vision

The vision of satellite communication was first conceived and published by Sir Arthur C. Clarke. His first satellite publication was in February 1945 titled "Peacetime uses for V2" in the "Letters to the Editor" column of *Wireless World* where he suggested the use of a 24-hour orbit machined satellite in addition to three orbiting satellites at 120° separation. His second and more elaborate publication was on the 25th of May 1945, titled "The space station: It's radio applications" that received complete reception from the Interplanetary Society and his third and most famous early satellite paper was published in the British publication named Wireless World in October 1945 and is archived at the Smithsonian Institute in Washington DC (Barry G. Evans, 2011).

4.2. Technological Advancements and the Space Race

The transistor, solar cell, and traveling-wave-tube (TWT) amplifier inventions through the 1940s and 1950s, enabled the development of comparatively small, very dependable repeaters (Barry G. Evans, 2011) and the deployment of Russia's Sputnik satellite in October 1957 made history as the first satellite in space, and officially launched the "space race". Satellites can be used for espionage, and their launch vehicles can be employed to deliver intercontinental ballistic missiles throughout the world. Heavy military spending by the USA and Russia fuelled the creation of multiple early communications satellites (O'Neal, 1999).

4.3. Formation of Space Agencies and Early Satellite Launches

The United State of America formed NASA (National Aeronautics and Space Administration) in 1958 which is also the year they launched their first artificial satellite named Explorer 1. Thereafter a number of big international and transoceanic linked organizations were formed throughout the 1960s and the 1970s, namely INTELSAT in 1964, an intergovernmental association whose purpose was to manage a communications satellite network that provides intercontinental broadcast services. On the 30th of May 1975 ESA (European Space Agency) was founded when ESRO (European Space Research Organisation) and ELDO (European Launcher Development Organisation) merged. ESA later established EUTELSAT in 1977 an organization whose purpose is to manufacture, launch, and operate satellites. Between 1990 and 2001 it launched 11 satellites to cater to the growing digital satellite TV market for pay-TV platforms throughout Europe. INMARSAT was formally

established on the 16th of July 1979 which was originally a non-profit organization serving marine satellite communication but has gone on to be privately owned providing satellite communication for marine, military, airlines, and NGOs (Barry G. Evans, 2011).

Employing communication satellites to relay television signals over different zones started in 1963 with Telstar followed by INTELSAT 1 in 1965. Broadcasting from satellite to household began in the Northern territories of Canada in 1972 with the launch of ANIK-A1 a Canadian satellite after defining a practical direct link budget from satellite to home broadcasting to the Northern Territories which permitted access to live television although it was through a repeater network. Prior to ANIK-A1 the North had to depend on the broadcasting centers from the South to post them sports and news program tapes which resulted in them being a complete week behind broadcast (Barry G. Evans, 2011).

Broadcasting satellites are stationed at an altitude of 35 786 km above sea level this altitude is referred to as GSO orbit (Geosynchronous Orbit). There are different types of orbits which are named and briefly described as follows. GSO orbit is at an altitude of 35 786 km and orbits at a speed that ties with the Earth's rotation resulting in a constant location along a particular longitude. GSO is used for communicating to television networks, radio, backhaul, direct broadcast, in addition to some SBAS (Satellite-Based Augmentation System) satellites and a number of weather satellites. Geostationary Orbit (GEO) like GSO rotates at the speed of the Earth however it has an inclination of zero thus orbits directly above the equator only (Team, 2022). Highly Elliptical Orbit (HEO) orbit system is employed to enable satellites to be programmed to move at slow speeds at preferred latitudes which permits them to overcome the challenges of GEO orbit such as the coverage variance in the equator and polar regions and the increased probability of attaining a shaded path in low-elevation link instances (Barry G. Evans, 2011) they are suitable for communications, satellite radio and remote sensing (Team, 2022). Medium Earth Orbit (MEO) is at an altitude between 2000-km to 36000-km and is typically utilized for navigation systems such as the USA's GPS (Global Positioning System). Polar Orbit rotates between 30° of the planet's poles and is utilized to reconnaissance, track the weather, measure atmosphere conditions, and long-term planet observation. SSO (Sun-Synchronous Orbit) is a kind of polar orbit the difference is that SSO satellites are harmonized per the sun's orbit thus the satellites always pass over a particular region at the same local time. Low Earth Orbit (LEO) is at an altitude of 2000 km or less and is where the International Space Station (ISS) and Hubble Space Telescope are located. LEO is typically used for

communication and remote sensing systems and is where LoRaWAN satellites operate (Team, 2022).

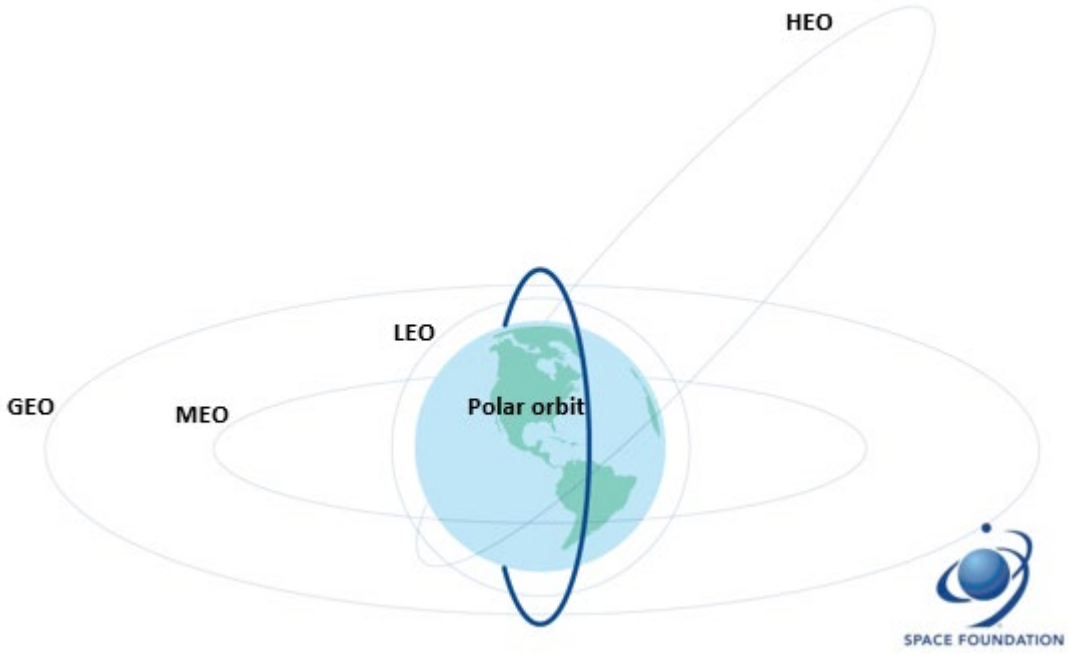

Figure 4.1: Different space orbits

(Team, 2022)

4.4. LoRaWAN Satellite Communication

The advancements in satellite orbits and applications have paved the way for innovative communication technologies, including the integration of LoRaWAN in satellite communication. This technology has revolutionized IoT by enabling long-range, low-power communication for remote sensing and monitoring applications providing global connectivity.

Inmarsat, in collaboration with Actility, became the first to incorporate LoRaWAN into their offerings in February 2017, providing global IoT connectivity through a hybrid approach (Inmarsat, 2017). Although Inmarsat did not have dedicated LoRa satellites at the time, their integration of LoRaWAN marked a significant step forward.

The first LoRaWAN satellite, FOSSASat-1, was launched by FOSSA Systems in December 2019 (FOSSA Systems, 2023), marking another milestone in satellite IoT communication. Swarm Technologies further advanced this field by deploying the first

commercial LoRa satellite constellation, achieving full global coverage with 72 satellites by early 2021 (Semtech, 2021).

Table 4.1 categorizes leading organizations pioneering LoRa satellite communication based on their satellite constellations, methods, primary focus, and key applications.

Table 4.1: Satellite organizations offering LoRaWAN communication

Organization	Satellite	Method	Focus	Key Applications
Inmarsat[1]	GEO: I-4 (ELERA Network)	Broad hybrid network	Comprehensive global IoT connectivity	Maritime, aviation, government, enterprise, energy, Aid & NGO
FOSSA Systems[2]	LEO: FossaSat-1	Dedicated & payload	Pioneering LoRa satellite connectivity	Demonstrating feasibility of LoRa for space communication
Swarm Technologies[3]	LEO: SpaceBEE	Dedicated	Specialized global IoT connectivity	Agriculture, energy, ground transportation
Lacuna Space[4]	LEO: LacunaSat series	Dedicated & payload	Specialized global IoT connectivity	Asset tracking, maritime, agriculture, environmental monitoring
Iridium[5]	LEO: Iridium NEXT	Hybrid gateways (Urb-IoT)	Comprehensive global IoT connectivity	Maritime, aviation, government, enterprise, media, energy, Aid & NGO

LoRaWAN satellite technology faces several hurdles, such as balancing low power usage with adequate range, data transfer speed, and message size. Although its low power consumption is perfect for devices with limited battery life, it restricts data transmission speed and payload capacity. Additionally, sustaining a reliable connection over long distances to satellites demands more energy. For success, LoRaWAN satellite technology must be engineered to meet diverse application requirements without depleting battery life, whilst maintaining compliance with communication regulations.

4.5. Summary

Seminal contributions of Sir Arthur C. Clarke laid the groundwork for geostationary satellite communication. Technological advancements, such as the transistor and solar cell, facilitated the creation of reliable satellite repeaters. The space race, spurred by the launch of Sputnik 1, accelerated satellite development and led to the formation of organizations like NASA, INTELSAT, and ESA. These international collaborations expanded satellite communication networks, making them integral to global connectivity. This historical perspective provides valuable insights into the evolution of space communication and its potential for future innovation.

Future research and development efforts in the satellite LoRaWAN community will focus on refining protocols for space environments, exploring new frequency bands, and enhancing the capabilities of satellite network. While these broader advancements are essential, this project specifically addresses the power consumption challenges associated with balancing transmission distance, data speed, and payload size. Additionally, ensuring compliance with regional and international communication regulations is a key focus. These aspects are further discussed in the following methodology chapter, which outlines the detailed approach and strategies employed in this research.

Chapter 5: Methodology

5.1. Introduction to Methodology

This section outlines the methodological approach undertaken to develop a software-based solution for optimizing energy harvesting in LoRaWAN networks, specifically tailored for space-based communication. The focus on software development, as opposed to hardware, allows for adaptable solutions that can be fine-tuned for various environmental conditions and application requirements.

The methodology is designed to address the core problem of efficiently managing energy resources within a LoRaWAN system to ensure reliable communication with satellite infrastructure. By developing a suite of software scripts in MATLAB that simulate the energy consumption and the parameters that affect it and the charging of a battery and of a supercapacitor using energy harvesting.

5.2. Research Design

The research conducted for this thesis is an experimental simulation study. This approach was chosen to develop and rigorously test a software algorithm designed for energy management in LoRaWAN networks, specifically for space-communication. The experimental simulations allow for a controlled environment to assess the algorithm's performance and its potential real-world application.

5.2.1. Experimental Framework

The experimental framework is centered around the creation of a software algorithm that optimizes energy harvesting, storage, and consumption within a LoRaWAN system. The goal is to ensure consistent communication with satellite infrastructure by maintaining efficient energy budget levels in real-time through energy harvesting.

5.2.2. Simulation Environment

The simulations were executed using MATLAB, with scripts specifically developed for LoRa transmission and reception. These scripts cover the full breadth of the communication sequence, including whitening, encoding, modulation, demodulation, and decoding. The LoRa transmission function meticulously calculates the energy required for transmission to assess whether the communication is feasible. This is contingent upon the energy available, which is evaluated by the battery charge

function. The latter simulates the charging of a supercapacitor with harvested energy and gauges the battery's charge level, ultimately determining the energy available for transmission.

5.2.3. Incorporation of Stochastic and Markov Models

To accurately represent the variability and unpredictability of energy availability, stochastic and Markov models were integrated into the energy harvesting simulations of each of the harvested energies. Stochastic models captured random fluctuations in energy due to environmental factors, while Markov models provided a probabilistic framework for predicting energy state transitions within the system.

Solar Energy Harvesting: The solar energy harvesting process is modeled by considering the solar irradiance, panel area, and efficiency. The harvested energy (E_h) at each hour (h) is given by:

Equation 5.1: Solar energy harvesting

$$E_h[h] = I_{actual}[h] \times A \times \eta$$

Where $(I_{actual}[h])$ is the actual solar irradiance after accounting for cloud cover variability, (A) is the solar panel area, and (η) is the panel efficiency.

The irradiance levels and cloud cover variability values for the simulation were derived from the classification developed by Govender and Sivakumar in Durban, from their investigation in diffuse irradiance variation under different cloud conditions in Durban, South Africa, using k-means clustering (Paulene Govender, 2019). Class I was chosen due to its relevance in providing a realistic representation of solar energy availability for most cloud cover, which is crucial for optimizing the performance of solar powered devices under worst case scenarios.

Thermoelectric Generator (TEG) Energy Harvesting: The TEG energy harvesting is described by the Seebeck effect, where the generated voltage (V_g) depends on the temperature difference across the device. The voltage at each hour (h) is calculated as:

Equation 5.2: ***Thermoelectric generator energy harvesting equation***

$$V_g[h] = \frac{S_c \times (\Delta T[h])}{1 + R_{th} \times (\Delta T[h])}$$

where (S_c) is the Seebeck coefficient, $(\Delta\, T[h])$ is the temperature difference, and (R_{th}) is the thermal resistance.

It is important to consider that outdoor temperature fluctuations can significantly affect the output power of TEGs. As highlighted by Wang et al. (Wang W, 2013), to account for these variations, a temperature variance of 10°C was chosen for the TEG simulation. This value represents a reasonable estimate for outdoor conditions, considering potential day/night and seasonal fluctuations. Such considerations ensure that the simulation remains relevant to real-world applications where temperature can vary widely.

Radio Frequency (RF) Energy Harvesting: RF energy harvesting is modeled by considering the power densities of different frequency bands and the efficiency of the rectenna. The harvested energy (E_{rf}) at each hour (h) is given by:

Equation 5.3: Radio frequency energy harvesting equation

$$E_{rf}[h] = \sum_{i=1}^{n} (P_{d,i} \times A_r \times \eta_r \times\ (1\ +\ V_f[h]))$$

where $(P_{d,i})$ is the power density for frequency band (i), (A_r) is the rectenna area, (η_r) is the rectenna efficiency, and $(V_f[h])$ is the variability factor due to environmental changes.

The values to simulate the rectenna systems were drawn from a recent study on RF energy harvesters for wireless sensors (Khan NU, 2024). The ambient power densities for GSM900, GSM1800 mobile transmitters and 2400Wi-Fi have been adopted as 0.45 nW/cm², 0.5 nW/cm² and 0.18 nW/cm^2, respectively, to reflect typical environmental conditions for urban energy harvesting.

5.2.4. Justification for the Design

This research design is justified by its ability to execute MATLAB scripts to analyze the dynamic interplay between energy consumption, energy harvesting, battery charge and supercapacitor charge over a 24-hour cycle. During message transmission, energy consumption impacts both the battery charge and supercapacitor charge. Energy harvesting sources replenish supercapacitor charge and battery charge. When battery charge drops, the supercapacitor acts as a buffer, providing quick energy top-ups to keep the battery at its maximum capacity. These interactions influence Signal-to-Noise (SNR) and Bit-Error-Rate (BER). Lower battery charge or supercapacitor charge may lead to degraded SNR and higher BER, affecting communication reliability. Additionally, the script evaluates:

- **Occupied Bandwidth (OBW):** Verifies that the OBW of the transmitted signals aligns with the chosen bandwidth (BW) and uses the spectrum efficiently and complies with LoRaWAN standards as set by the International Telecommunication Union (ITU) in the Radio Regulations, and specific bandwidth restrictions set by the Independent Communications Authority of South Africa (ICASA) for space-based LoRaWAN communication operation within the country of South Africa.
- **Power Spectral Density (PSD):** Verifies that the transmitted signal's power and frequency distribution is concentrated in alignment with the OBW and the allocated BW, to ensure there is no interference with neighbouring communication channels, and that the signal's peak power doesn't exceed the limits set by ICASA regulations at specific frequencies within the allocated bandwidth.

This approach emphasizes the efficiency of the simulation process and its alignment with industry standards, ensuring that the results are both accurate and relevant.

5.3. Algorithm Development

The development of the algorithm was a methodical process that spanned several stages, from initial conceptualization to the final implementation and testing. The steps taken in the development of the algorithm are detailed below.

5.3.1. Conceptualization

The first stage was to define the objectives of the algorithm, which aimed to enhance energy harvesting and consumption efficiency in LoRaWAN networks for space communication. The design was grounded in energy efficiency principles and sustainable communication protocols.

5.3.2. Programming Language and Tools

The entire algorithm was implemented in MATLAB, a choice driven by its powerful mathematical computing environment and its extensive toolboxes suitable for simulation and data analysis. MATLAB's ability to handle complex numerical problems and its built-in functions for signal processing made it the ideal choice for this project.

5.3.3. MATLAB Toolboxes and Functions

The development process leveraged specific MATLAB toolboxes and functions:

- The **Communications System Toolbox** was utilized for simulating the LoRa transmission and reception processes, providing built-in functions for various communication system components.
- Custom scripts were written to simulate the energy harvesting process, incorporating stochastic and Markov models to realistically represent energy availability and system behaviour.

5.3.4. Implementation

During the implementation phase, the following core functions were coded within MATLAB:

- A LoRa transmission function (B. Al Homssi, 2021) that includes a check for energy required before transmission based on time on air of a LoRaWAN packet. The OBW of the constructed LoRaWAN packet can be extracted from the generated signal, based on the spreading factor (SF) settings.
- A LoRa reception function is utilized to extract relevant signal characteristics, including the Bit-Error-Rate (BER), Signal-Noise-Rate (SNR) and spectrogram of the system (B. Al Homssi, 2021).

- A battery charge function that models the intricate energy flow within the system. It simulates the charging and discharging cycles of the supercapacitor, utilizing the harvested energy. Additionally, it accounts for the charging and discharging of the battery, which is governed by the surplus charge transferred from the supercapacitor and the energy expended during operation and includes the collection and processing power consumption by the microprocessor. This function provides a realistic depiction of the energy dynamics, essential for understanding the system's energy management.
- An Energy Required for Transmission function that checks for energy required for transmission based on the message size, transmit power and time on air for message transmission.

5.3.5. Theoretical Models

The algorithm's design was informed by theoretical models that were critical to its functionality:

- Stochastic models simulated the unpredictable nature of energy availability.
- Markov models provided the framework for predicting energy state transitions within the system.

These models, essential to the algorithm's design, were integrated into the MATLAB environment to ensure a realistic simulation of the energy management system for harvested energy.

Stochastic Models: Stochastic models capture the randomness and unpredictability in the system. For the solar energy harvesting simulation, the stochastic element is introduced by the variability in solar irradiance due to cloud cover, represented by a random variation (R):

Equation 5.4: Stochastic equation for solar irradiance

$$R = (rand() - 0.5) \times 2 \times C_v$$

where (C_v) is the cloud cover variability factor. This random variation affects the actual irradiance (I_{actual}), which in turn influences the harvested energy (E_h).

Markov Models: Markov models are used to predict state transitions based on probabilities. In the context of the thermoelectric generator (TEG) energy harvesting simulation, the Markov model is represented by a state transition matrix (P) that governs the changes in temperature states:

Equation 5.5: Markov matrix for the thermoelectric generator energy harvesting.

$$P = \begin{bmatrix} p_{11} & p_{12} \\ p_{21} & p_{22} \end{bmatrix}$$

where (p_{ij}) represents the probability of transitioning from state (i) to state (j). The current state (S_t) at time (t) is updated based on this matrix:

Equation 5.6: Markov equation for the thermoelectric generator energy harvesting.

$$S_{t+1} = StateTransitionS_tP$$

The temperature difference (ΔT), which is crucial for calculating the TEG voltage, depends on the current state determined by the Markov chain.

For the radio frequency (RF) energy harvesting simulation, the stochastic model is represented by a random walk (V_f) that simulates the variability in RF energy availability:

Equation 5.5: Markov step model for radio frequency energy harvesting

$$V_f[t] = V_f[t-1] + RandomStep()$$

This variability factor (V_f) affects the harvested energy (E_{rf}) for each frequency band.

5.3.6. Testing and Refinement

The algorithm underwent a detailed testing process within MATLAB, which was essential for validating its performance. This involved:

- **Function Testing**: Each function was tested individually before integration to ensure that they operated correctly in isolation. This step was crucial for identifying and rectifying any issues early in the development process.
- **Environmental Simulation:** The energy harvesting environment was simulated using stochastic and Markov models to replicate the variability of energy availability. This approach negated the need for iterative simulations, as the models themselves accounted for the range of possible environmental conditions.
- **Randomization of Message Sizes and Content:** To mimic the real-world application, the message sizes were randomized within specified intervals during the simulation runs. This variability was the primary factor altered between script executions, providing insights into the algorithm's handling of different data payloads.
- **Meaningful Content:** The script was further refined to transmit useful data instead of meaningless bit sizes containing:

    - **Sensor Data:** Temperature readings generated by the formula *20 + rand * 5* to simulate real-world temperature sensor data are transmitted every hour.
    - **Battery level:** The battery charge level reading at the time of transmission is transmitted every hour.
    - **Date & Time stamp:** The date and time stamp of the message is transmitted every hour.
    - **Message:** Additionally, the "Hello World!" message was occasionally included in some hourly transmissions to vary the payload size to simulate different communication scenarios. This approach provides more valuable insights into the system's performance under realistic conditions.

Time-on-Air (TOA): For each data transmission, the duration of the transmission (time-on-air) is recorded. This TOA value is crucial for calculating the duty cycle, which refers to the percentage of time the system is actively transmitting compared to the time it spends in a low-power state. Duty cycle is a critical parameter for energy management in LoRaWAN communication

Battery Level Reading: The current battery level of the device. Including this information allows the script to monitor the system's energy status and adapt its transmission behavior accordingly

Compliant Signal Characteristic Analysis: The testing process confirmed that the script successfully analyzes the OBW, PSD and spectrograms of the transmitted signals as described in the justification section. This analysis ensures the chosen

parameter settings generate signals that are compliant with ITU and ICASA regulations, particularly the frequency band, channel bandwidth, data rate and duty cycle as prescribed by the ICASA regulations.

- **Graphical Analysis:** The performance of the algorithm was observed and analyzed through graph plots, which provided a clear visual representation of its behavior over a simulated 24-hour cycle.

While the stochastic and Markov models sufficiently simulated the energy harvesting environment, and the spreading factor (SF) and bandwidth (BW) for space communication were predetermined, the testing focused on the algorithm's response to the simulated conditions rather than varying these set parameters.

5.3.7. Documentation

Comprehensive documentation of all function and simulation scripts was maintained throughout the development process, ensuring that each step was well-documented for reproducibility and future research reference.

5.4. Simulation Details

This section delves into the specifics of the simulation environment and the unique conditions under which the algorithm was tested. While the previous sections outlined the overall design and development of the algorithm, the focus here is on the operational aspects of the simulations.

5.4.1. Simulation Environment

The simulation environment was constructed using a combination of MATLAB to create a virtual representation of a LoRaWAN network engaged in space communication. This environment provided a platform for executing the algorithm and observing its behavior under various simulated conditions.

5.4.2. Testing Conditions

The algorithm was evaluated through a series of simulations designed to assess its performance under various energy availability conditions. These simulations were not just tests but also served as observations of system behavior, with the results visualized through graph plots. The specific scenarios included:

- **Energy Availability**: The simulations incorporated stochastic and Markov models to represent a range of energy harvesting conditions, from optimal to suboptimal. This approach simulated the real-world variability of energy availability without the need for separate scenarios for energy scarcity and abundance.
- **Time Cycle Simulation with Time-on-Air:** A 24-hour transmission cycle was simulated to represent a full day, with each hour coded to introduce variable temperature sensor readings and a 'Hello World!' message occasionally transmitted with the sensor readings to introduce variable message sizes. This helped in assessing the algorithm's adaptability and energy management over time. The time-on-air (TOA) of each transmission was recorded for duty cycle calculations. The chosen message sizes resulted in a dynamic duty cycle throughout the simulation, reflecting the impact of varying data loads on energy consumption.
- **Duty Cycle and Transmission Power**: The simulations focused on scenarios with typical or limited energy availability with the purpose of investigating the interplay between energy availability and communication effectiveness. An adaptable duty cycle and transmission power configuration were chosen to reflect realistic operating conditions and ensure adherence to ITU and ICASA regulations. The chosen configuration balanced communication effectiveness with energy consumption, staying within the allowable limits for LoRaWAN transmissions in South Africa.

Leveraging Harvested Energy for Dynamic Duty Cycle Management:

The inclusion of on-board energy harvesting mechanisms aimed to supplement the conventional battery and enable a **dynamic approach to duty cycle management**. By strategically utilizing harvested energy, the system could:

- **Accommodate variable data loads:** Increased energy availability from harvesting could potentially allow for transmitting larger data packets (e.g., sensor readings with higher resolution) without compromising communication effectiveness. This dynamic adaptation to data volume optimizes energy consumption while maintaining the desired level of information detail.
- **Enhance transmission frequency:** In scenarios with abundant harvested energy, the system could potentially increase the transmission frequency without relying solely on the conventional battery. This could be particularly beneficial for

applications requiring near-real-time data delivery from remote or hard-to-reach locations, reducing the need for human intervention for battery replacement.

- **Regulatory Compliance Analysis**: While the primary focus of the simulations was on energy management, the script also monitored key parameters relevant to regulatory compliance with ITU and ICASA regulations. This included analyzing the:

Occupied Bandwidth (OBW): The script verified that the OBW of transmitted signals fell within the designated bandwidth allocation for LoRaWAN satellite communication as outlined by the ITU and any narrower restrictions set by ICASA.

Power Spectral Density (PSD): The script analyzed the PSD to ensure the peak power of the signal adhered to the maximum power levels set by ICASA at specific frequencies within the allocated bandwidth. Additionally, it verified that the signal's power remained concentrated within the allocated bandwidth, minimizing interference with neighboring communication channels.

Graph plots, particularly those with two y-axes, were instrumental in comparing key performance indicators like BER and SNR_dB across the 24-hour cycle. These plots provided a clear visual representation of the algorithm’s performance and were a primary method for analyzing the simulation data.

5.4.3. Parameters and Variables

Key parameters and variables within the simulations included:

- **Energy-required-for-transmission**: A dynamic function that calculates the minimum energy necessary for a successful transmission, based on the message size and the time on air.
- **Energy Availability:** Stochastic and Markov models were employed to represent a range of energy harvesting conditions, reflecting real-world variability.
- **Supercapacitor and battery states**: Variables that track the charge levels, providing insights into the system’s capacity for data transmission.
- **Duty Cycle Calculation:** The duty cycle for each time interval (e.g., hour) was calculated by leveraging the pre-populated time-On-Air-Array. This array stores the time-on-air (TOA) values for each data transmission within the specific interval. Utilizing this pre-calculated data avoids redundant calculations and streamlines the

duty cycle determination process for each time step in the simulation and to ensure adherence to ITU and ICASA regulations for LoRaWAN in South Africa.

- **Time Cycle:** A 24-hour cycle was simulated, with each hour introducing variables of temperature reading and timestamps.
- **Signal characteristics**:
    - **Temperature Sensor Reading:** The script transmitted sensor data representing temperature readings. The temperature value was generated using the formula *20 + rand * 5*. This formula simulates real-world sensor monitoring data with a range of possible temperatures between 15°C and 25°C. In addition to transmitting the battery level and timestamp of each transmission
    - **Spreading Factor (SF):** The SF value of 9 was selected. This parameter influences the trade-off between transmission range, data rate, and energy consumption. A higher SF increases range and reduces data rate, while a lower SF offers faster data rates but with a shorter range. The chosen SF value aimed to balance these factors for the targeted communication scenario.
    - **Bandwidth (BW):** A bandwidth of 125-kHz was used. This parameter defines the frequency range occupied by the transmitted signal. The chosen BW adhered to the designated LoRaWAN satellite communication allocation as outlined by ITU and any narrower restrictions set by ICASA.
    - **Transmission Power:** The transmission power was set to **20 dBm** to ensure reliable communication for earth-to-satellite transmission within the context of our application. This increased power level compared to terrestrial LoRaWAN communication is necessary due to the significantly larger distance involved in satellite communication (jkadbear, 2020).
- **Message Size and Limit:** The size of transmitted messages was randomized within specified intervals throughout the simulation day. However, the maximum message size was capped at 256-bit limit. This limit reflects the standard maximum payload size for LoRaWAN communication.

5.4.4. Scenarios

The simulations were designed to evaluate the algorithm under a variety of conditions that reflect potential real-world applications. The scenarios were not just tests but also served as demonstrations of how the algorithm would perform under different energy availability conditions. The following outlines the key scenarios:

- **Energy Availability**: Utilizing stochastic and Markov models, the simulations depicted a realistic range of energy harvesting conditions. These models provided a spectrum of scenarios from low to high energy availability, allowing the algorithm to be assessed under conditions that mimic real-world unpredictability.
- **Communication Performance**: The primary focus was on the algorithm's ability to maintain communication integrity and regulatory compliance. This was evaluated by analyzing the relationship between Bit Error Rate (BER) and Signal-to-Noise Ratio (SNR_dB) and OBW over the course of a simulated 24-hour cycle for each transmission. Graph plots were crucial in this analysis, offering a visual representation of the algorithm's performance metrics over time.

5.5. Data Collection and Analysis

In this research, 'data collection' denotes the automated capture of simulation outcomes, which are crucial for assessing the LoRaWAN communication system's efficacy in direct-to-satellite applications. The simulation outcomes were primarily analyzed through graphical representations, offering an immediate and lucid insight into the system's performance. The following key performance indicators (KPIs) were systematically recorded and visualized:

KPIs that evaluate the overall performance and effectiveness of the communication system in terms of energy management and data transmission:

- **Energy Consumption**: This metric reflects the total energy used by the system during the simulated time.
- **Packet Delivery Ratio (PDR):** This KPI measures the percentage of transmitted messages successfully received by the intended recipient. It reflects the effectiveness of communication under different conditions.

- **Signal-to-Noise Ratio (SNR):** This metric indicates the strength of the desired signal compared to the background noise level. Higher SNR generally leads to lower BER.
- **Bit Error Rate (BER):** This KPI represents the percentage of bits incorrectly received during transmission. It reflects the quality of the received data and is influenced by factors like SNR and chosen SF/BW combination

Compliance KPI:

Occupied Bandwidth OBW: serves as a KPI specific to regulatory compliance and spectral efficiency. It ensures the system operates within the allowed boundaries and minimizes interference with other communication systems.

These KPIs were not manually recorded but were automatically logged by the simulation environment to ensure precision and consistency. The data was then visualized through a series of graphs, providing a clear and immediate understanding of the system's performance over a simulated 24-hour cycle. The plotted graphs include:

5.5.1. Visual Technique

- **Energy Consumption vs. Battery Charge Over Time**: Illustrating the relationship between energy used and the remaining battery charge.
- **BER vs. Time on Air**: Showing the correlation between the BER and the time taken for each transmission.
- **Energy Harvested vs. Energy Used**: Comparing the energy harvested through the supercapacitor with the energy consumed during transmissions.
- **Power Spectral Density (PSD)**: Analysing the power distribution of the signal across frequencies to ensure the peak power complies with ICASA's limits and the signal's power remains concentrated within the allocated bandwidth, minimizing interference.
- **Supercapacitor Charge vs. Time on Air**: Demonstrating the supercapacitor's charge in relation to the time on air for transmissions.
- **Battery Charge vs. Harvested Energy**: Highlighting the battery's state of charge against the harvested energy.
- **Time on Air vs. Energy Consumption**: Depicting the trade-off between the duration of transmissions and the associated energy consumption.

- **BER vs. SNR**: Comparing the BER with the SNR_dB to evaluate communication reliability.
- **BER vs. Supercapacitor Charge**: Examining the impact of the supercapacitor's charge on the BER.
- **Occupied Bandwidth (OBW)**: Examining the transmitted signal's bandwidth is within the designated allocation for LoRaWAN satellite communication, preventing interference with other systems.
- **Spectrogram:** Visualize signal's frequency content changes over time. It can reveal potential transient phenomena or interference not readily apparent in OBW or PSD. This can help identify and address issues like sudden spikes in power or unexpected frequency shifts.

Each graph serves as a visual analysis tool, enabling the identification of trends and the extraction of insights regarding the system's behavior under simulated conditions.

5.5.2. Ensuring Accuracy and Consistency

The integrity of the simulation data is paramount to the credibility of the research findings. To uphold the accuracy and consistency of the data, the following strategies were employed:

- **Automated Recording**: The simulation environment was meticulously programmed to automatically capture all relevant data points. This automation played a crucial role in minimizing human error and ensuring that each simulation's outcomes were accurately logged.
- **Parameter Standardization**: The simulations were conducted with a set of predefined, standardized parameters, such as the spreading factor (SF), bandwidth (BW), and power settings. This standardization ensured uniformity across all simulation runs, making the data collected directly comparable and consistent.
- **Code Validation**: While traditional repetitive testing to account for variability was not a component of this research, the simulation code underwent a thorough validation process during development. Each function was tested individually for correctness before being integrated into the main script, serving as a form of reliability check to ensure the code performed as intended.

These measures collectively contributed to the reliability of the simulation results, providing confidence in the robustness of the data analysis and the conclusions drawn from the research.

5.5.3. Justification for Visualization

The choice of visualization over traditional data storage was driven by the need for:

- **Clarity**: Graphs offer a clear and immediate understanding of complex relationships within the data.
- **Insight**: Visual trends and patterns are more readily discernible, allowing for quick identification of areas of interest or concern.
- **Communication**: Graphical representations are accessible to a wide audience, facilitating the sharing of findings with both technical and non-technical stakeholders.

By focusing on visualization, the research leverages the strengths of graphical analysis to present a dynamic and comprehensive view of the algorithm's performance.

5.6. Ethical Considerations

This research did not involve human subjects, personal data, or any activities that typically raise ethical concerns. As the project focused on the simulation of a LoRaWAN system for direct-to-satellite communication, the primary considerations were related to the responsible use of simulation tools, the accurate representation of results and ITU and ICASA regulations. All simulations were conducted in a controlled environment, and the data generated was purely synthetic, ensuring no real-world ethical implications.

5.7. Algorithm Efficiency

The efficiency of a low-power sensor node hinges on optimizing energy consumption, storage, and data transmission. This section delves into the strategies employed to balance data precision, message size, and energy efficiency, ensuring the device's longevity and reliable operation in resource-constrained environments.

- **Energy Harvesting Efficiency:** The proposed system employs a tri-harvesting approach, utilizing solar, thermal (TEG), and RF energy sources. This diversified approach enhances energy availability across various environmental conditions.

Solar harvesters are highly effective in direct sunlight, while thermal harvesters can supplement energy in low-light conditions or indoor environments with significant temperature gradients. RF harvesters provide a reliable energy source in both indoor and outdoor settings, particularly in areas with abundant radio frequency or Wi-Fi signals. By combining these technologies, the system can efficiently harvest energy across diverse environments, ensuring a robust and sustainable power supply.

- **Storage Efficiency:** The system incorporates a hybrid energy storage system, combining a supercapacitor and a battery. The supercapacitor, with its rapid charge and discharge capabilities, is ideal for buffering energy spikes from the harvesters. This ensures that even small amounts of harvested energy are effectively utilized. The battery, on the other hand, provides a stable and long-lasting energy source for powering the device. A threshold-based charging strategy is employed to optimize the charging of both the supercapacitor and battery.

- **Power Management:** The algorithm employs a simple yet effective energy management strategy. A baseline power consumption is assumed (This supports the temperature sensor node and micro-controller but also accommodates potential future expansions and additional functionalities), with additional power consumption during data transmission. Before each transmission, the algorithm checks for sufficient energy to prevent premature battery depletion. To balance data delivery and energy conservation, transmissions are scheduled hourly. The current algorithm, designed for continuous power supply, is compatible with all LoRaWAN modes (A, B and` C). However, future research will investigate strategies to optimize power consumption by leveraging the specific power-saving features of these modes, especially Mode A, to maximize battery life.

- **Data Transmission Efficiency:**

  To optimize the balance between data precision and energy efficiency, the algorithm employs a combination of high-precision data representation and efficient message formatting. Temperature readings are represented using a 32-bit float format to ensure accurate measurement, while timestamps are encoded in a 40-bit format for precise time recording. To minimize message size, shortened string representations (e.g., "temp" instead of "temperature") are used for sensor types, and optional message components are included to dynamically adjust data

size based on specific requirements. This approach results in a compact message size, reducing transmission energy requirements while maintaining high data quality.

By employing these strategies, the algorithm effectively balances data precision, energy efficiency, and transmission reliability. This approach is particularly well-suited for resource-constrained sensor nodes operating in energy-limited environments.

5.8. Limitations

While the methodology employed in this research was designed to be robust and comprehensive, there are inherent limitations to consider:

- **Modelling Constraints**: The use of stochastic and Markov models, while effective, may not capture all the nuances of real-world energy harvesting scenarios.
- **Simulation Scope**: The simulations were limited to a 24-hour cycle, which may not encompass the full range of conditions experienced in longer-term deployments.
- **Parameter Fixation**: Certain parameters, such as SF and BW, were kept constant, which may limit the understanding of the algorithm's performance under varying communication settings.

These limitations should be considered when interpreting the findings, as they may affect the generalizability of the results to real-world applications.

5.9. Summary

In summary, the methodology section has detailed a systematic approach to developing and testing a software algorithm for energy management in LoRaWAN networks. The process involved the use of MATLAB for simulation, automated data collection, and graphical analysis to assess the algorithm's performance. The research was conducted with a clear focus on accuracy, consistency, and the effective visualization of data. Despite the limitations acknowledged, the methods employed were appropriate for the research objectives and provide valuable insights into the potential of software-based solutions for energy optimization in direct-to-satellite communication.

Chapter 6: Results and Analysis

6.1. Results

This chapter presents the results obtained from a series of simulations designed to evaluate the performance of an energy-management algorithm for LoRaWAN communication in a space-based deployment scenario. The primary focus of the research was to investigate how the algorithm manages energy consumption while ensuring reliable data transmission under varying energy availability conditions.

To achieve this objective, the simulations addressed the following specific research questions:

1. **Energy Management under Variable Energy Availability:** How effectively does the algorithm manage the system's energy consumption and maintain communication functionality for space communication under **varying** energy harvesting conditions simulated using stochastic and Markov models? (This question focuses on the algorithm's ability to adapt to uncertain energy availability)
2. **Impact of Dynamic Duty Cycle on Energy Management and System Performance:** How does the algorithm manage energy consumption and maintain communication functionality under different transmission loads (resulting in dynamic duty cycle) simulated using stochastic and Markov models? This question explores the interplay between the dynamic duty cycle, energy consumption, and broader system performance metrics like BER and SNR.
3. **Impact of SF, BW, and Message Size on Energy Efficiency:** How does the chosen Spreading Factor (SF), Bandwidth (BW), and message size influence the system's energy consumption under the control of the algorithm? This question explored the role of these configuration parameters in the algorithm's decision-making process regarding energy management.

By investigating these research questions, the simulations aimed to assess the effectiveness of the proposed energy-management algorithm for LoRaWAN communication in a space-based environment. The following sections will present the detailed results of the simulations, focusing on key performance indicators (KPIs) such

as energy consumption, packet delivery ratio (PDR), signal-to-noise ratio (SNR), bit error rate (BER) and OBW.

6.1.1 Methodology Summary

This section provides a brief overview of the key aspects of the simulation setup used to evaluate the performance of the energy-management algorithm for LoRaWAN communication. A more detailed description of the methodology can be found in Chapter 5.

The simulations focused on a space-based LoRaWAN communication system and employed the following key elements:

- **Energy Harvesting Model:** An energy harvesting function was implemented to simulate the process of energy harvesting, considering factors like sunlight exposure and overcast cycles.
- **Energy Consumption Model:** An energy consumption parameter was extracted from the battery to account for the transmission power of when data is transmitted.
- **Energy-Management Algorithm:** The implemented energy-management algorithm monitored the available energy and dynamically adjusted system parameters (e.g., transmission power, data rate) to optimize energy consumption while maintaining communication functionality.
- **Performance Evaluation Metrics:** The simulations measured various performance indicators (KPIs) to assess the effectiveness of the algorithm. These KPIs included (energy consumption, packet delivery ratio, signal-to-noise ratio, and bit error rate).

6.1.2. Data Presentation

This section presents the key findings obtained from the simulations conducted to evaluate the performance of the proposed energy management algorithm for LoRaWAN space communication under varying energy availability and transmission loads. The simulations utilized stochastic and Markov models to simulate realistic scenarios. The results are organized into three thematic groups:

1. **Energy Management:** This group focuses on the algorithm's effectiveness in managing the battery and supercapacitor charge levels, energy consumption and harvested energy under dynamic conditions.
2. **System Performance:** This group explores how the algorithm balances energy management with maintaining communication functionality, as reflected by metrics like time on air, duty cycle, Bit Error Rate (BER) and Signal-to-Noise Ratio (SNR).
3. **Signal Characteristics:** This group presents findings related to the specific characteristics of the transmitted signal, such as spectrograms, bandwidth and power spectral density.

The core message format transmitted by the algorithm included essential sensor data and system information. Each message comprised of four key elements: 1) sensor type identifier (e.g., "temp"), 2), sensor reading (e.g., temperature value as a 32-bit float), 3) timestamp indicating the date and time of transmission, and 4) current battery level reading which amounts to 112 bits. To investigate the algorithm's adaptability to message size variations, a secondary message type, "Hello World!", was introduced to a subset (n = 7, at hours 3:00 am, 5:00 am, 6:00 am, 10:00 am, 12:00 pm, 19:00 pm, 22:00 pm) of the 24-hourly messages. This message equals a fixed payload size of 208 bits to the core message format (sensor type, sensor reading, timestamp, and battery level reading).

6.1.3. Thematic group 1: Energy management

This thematic group explores the effectiveness of the proposed energy-management algorithm in managing energy resources under dynamic conditions for a LoRaWAN space communication system. Results focusing on battery and supercapacitor charge levels, energy consumption patterns, and harvested energy over a 24-hour cycle are presented.

The first graph illustrates the correlation between the supercapacitor charge and the harvested energy. The harvested energy is responsible for charging the supercapacitor.

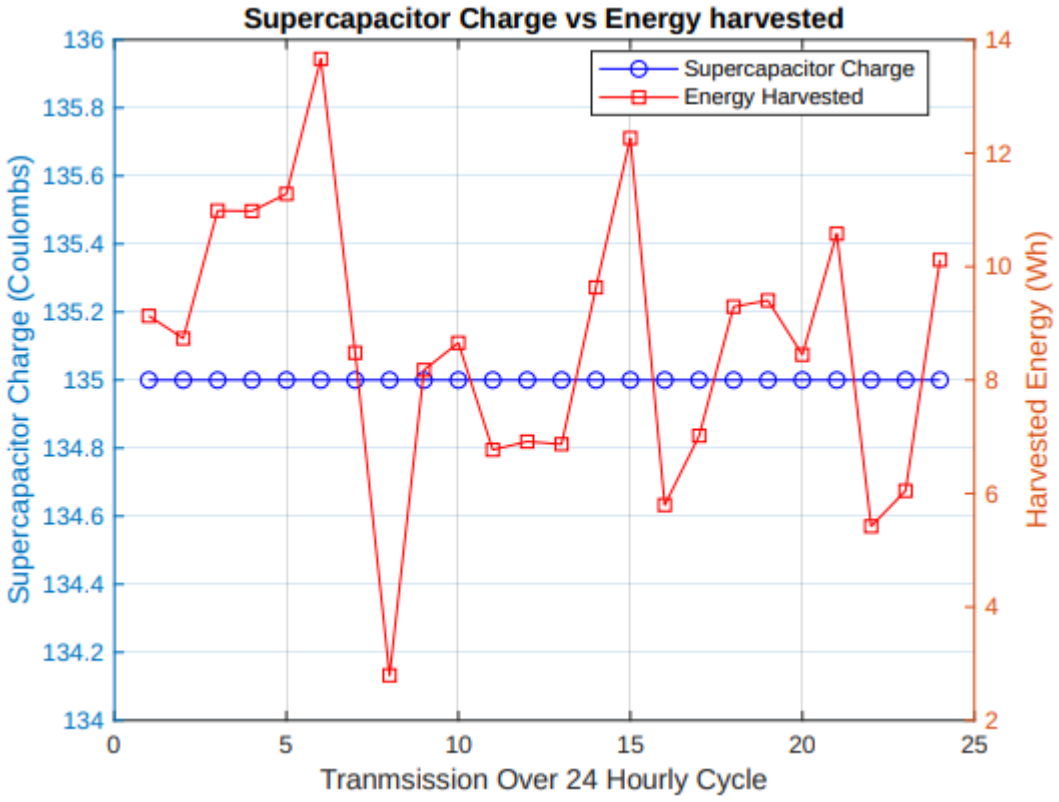

Figure 6.1: **Energy harvested vs supercapacitor charge over 24-hourly transmission cycle.**

Observations:

- The harvested energy (right Y-axis) fluctuates throughout the cycle, with the highest recorded value being 14-Wh and the lowest value at ~3.0-Wh. These variations reflect the stochastic and Markov models simulating the unpredictable nature of energy availability in the environment.
- Regardless of the fluctuations of the harvested energy the **supercapacitor charge level (left Y-axis) remains constant throughout the 24-hour cycle,** at 135 Coulombs.
- This **stable charge profile** suggests the supercapacitor's ability to effectively **accumulate and hold energy** regardless of the fluctuations in harvested energy.

In the next graph the correlation between the supercapacitor charge and the battery charge is illustrated and observed. The supercapacitor is responsible for charging the battery.

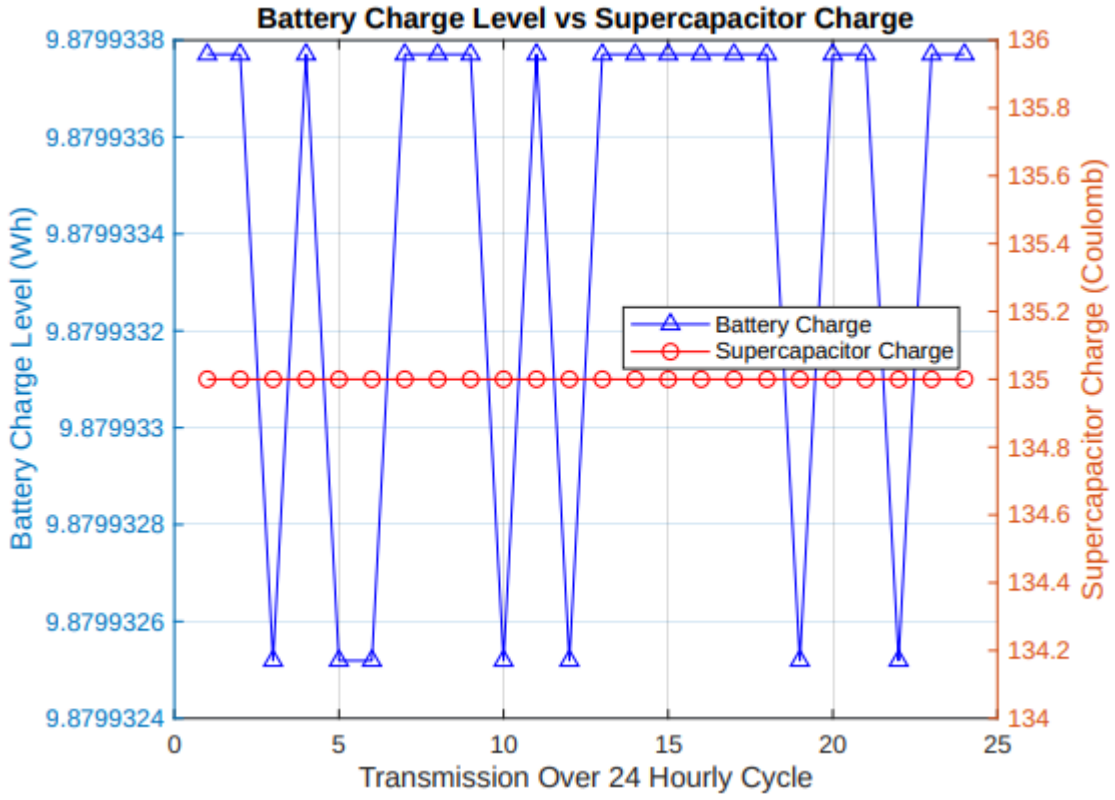

Figure 6.2: Supercapacitor charge vs battery charge level over 24-hourly transmission cycle

Observations:

- The supercapacitor charge level (Left Y-axis) exhibits a stable level of 135 Coulomb throughout the 24-hourly the cycle.
- In contrast, the battery charge level (right Y-axis) exhibits variations in its charge level with the highest charge level observed at ~9.8799338-Wh and the lowest charge levels observed at ~9.8799325-Wh.
- The battery charge level correlates with the message size being transmitted. The time of the transmission of the smaller message size of 112-bits correlates with the higher battery charge of ~9.8799338-Wh, and the time of the transmission of the bigger message size of 208-bits correlates with the lower battery charge level of ~9.8799325-Wh.
- Whenever the battery charge level briefly decreases due to an increase in message size it quickly returns to the higher battery charge level.

The next graph illustrates the correlation between energy consumption and battery charge.

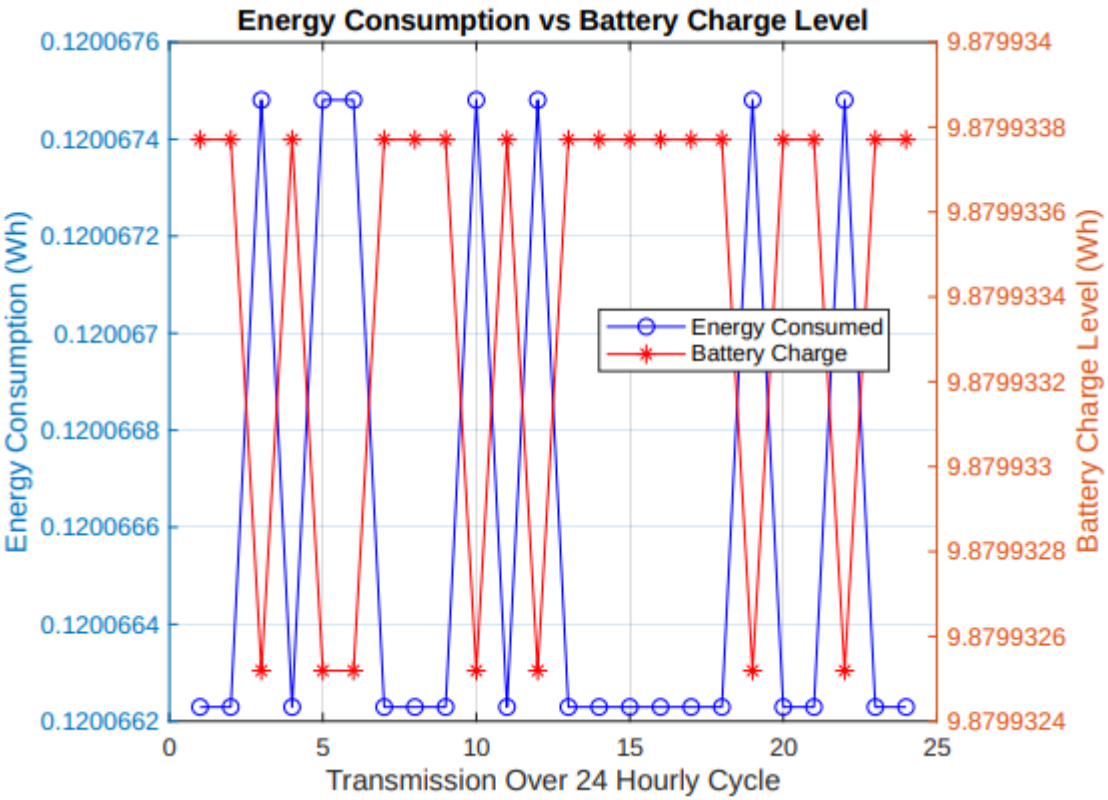

Figure 6.3: **Energy Consumption vs Battery Charge level over 24-hourly cycle**

Observation

- The energy consumption (Right Y-Axis) is at its lowest at 0.1200662-Wh which correlates with the time of transmission of the smaller message size of 112-bits, and the highest energy consumption is observed at ~0.1200675-Wh which coincides with the time of transmission of the higher message size of 208-bits.
- The battery charge level (Left Y-axis) is at ~9.8799338-Wh for the transmissions that correlate with the smaller message size of 112-bits and records its lowest battery charge level at ~9.8799325-Wh which correlates with the times of transmissions of the bigger message size of 208-bits.

The next graph illustrates the relationship between harvested energy and energy consumption.

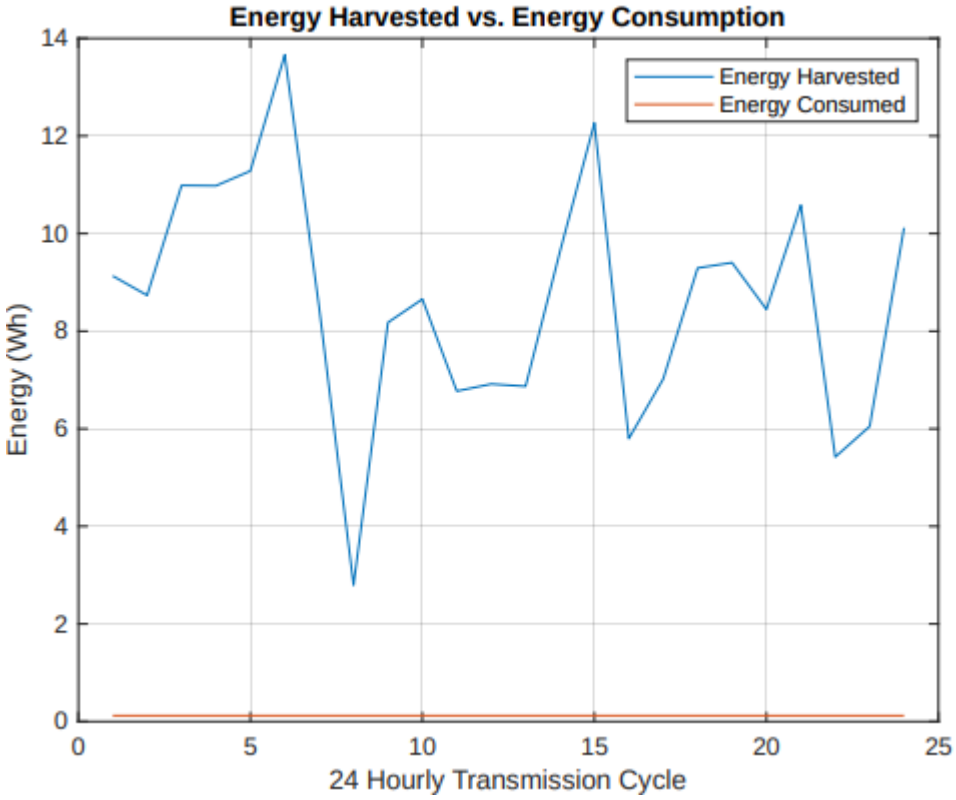

Figure 6.4: **Energy harvesting vs energy consumption over 24-hourly cycle**

Observation:

- The harvested energy (right Y-axis) fluctuates randomly throughout the cycle, with the highest recorded value being 14-Wh and the lowest value at ~3.0-Wh. These variations reflect the stochastic and Markov models simulating the unpredictable nature of energy availability in the environment.
- In contrast, the energy consumption remains stable and relatively low, close to 0-Wh throughout the 24-hour cycle.
- The energy consumed by the system has no correlation with the harvested energy behaviour.

Having investigated the proposed energy-management algorithm's efficacy in optimizing energy resources within a dynamic earth-based sensor network for space LoRaWAN communication. The subsequent section explores the algorithm’s ability to sustain reliable and effective communication while balancing energy consumption. The section explores the algorithm’s performance metrics in maintaining data transmission integrity and timeliness.

6.1.4. Thematic group 2: System Performance

This thematic group explores how the algorithm balances energy management whilst maintaining communication functionality. Key performance indicators including, duty cycle, time-on-air, Bit Error Rate (BER) and Signal-to-Noise Ratio (SNR) are presented to investigate the algorithm's performance under varying energy availability and varying payloads.

The first graph illustrates the correlation between the data payload size and the transmission time (time-on-air), showcasing how the energy consumption of the system is impacted by the size of the data payload.

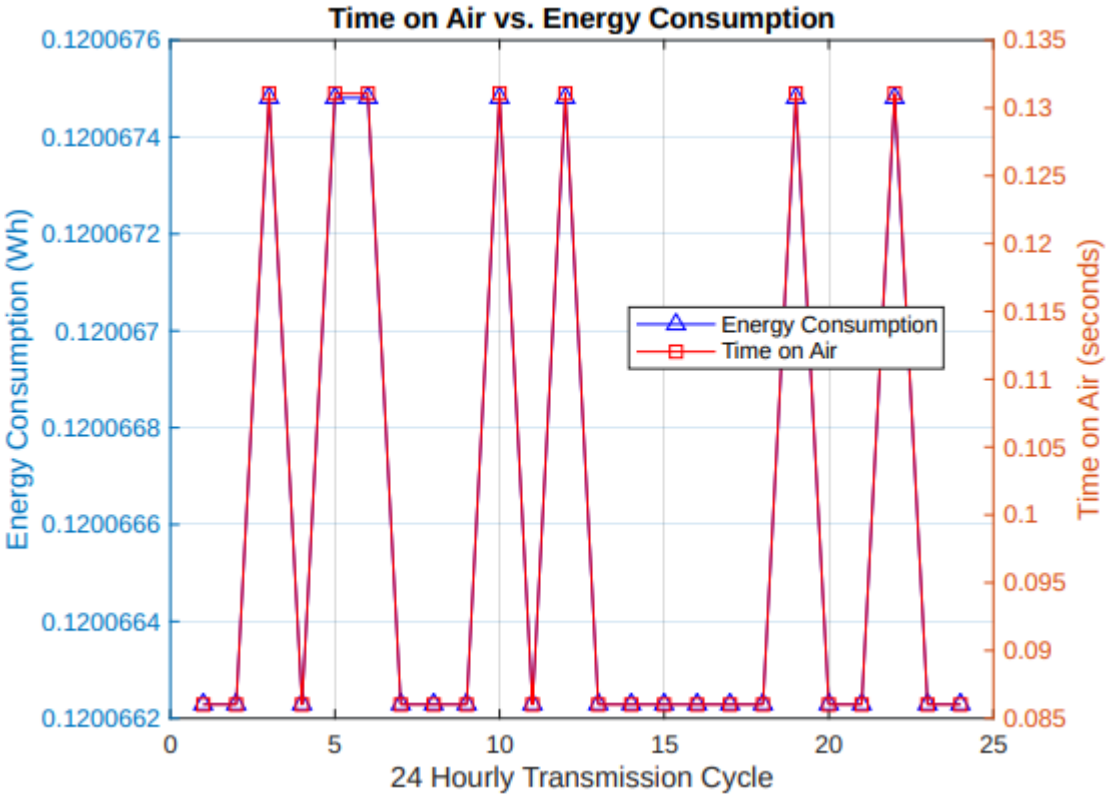

Figure 6.5: Time on air vs energy consumption of data payload

Observation:

- The transmission time (time-on-air) (right Y-axis) reveals a direct correlation with data payload size. Bigger payloads of 208-bits generate longer transmission times of approximately ~0.13 seconds, whereas smaller payloads of 112-bits result in shorter transmission times of approximately ~0.085 seconds.

- The energy consumption (left X-axis) of the system records its highest value at ~0.1200675-Wh which correlates with when the bigger message size is transmitted, and the lowest energy consumption value is recorded at ~0.1200662-Wh which coincides with when the smaller message size is transmitted.
- The plot of the transmission time and the plot of the system's energy consumption have parallel trends which suggests that the size of the data payload being transmitted affects both system performance metrics.

The next graph illustrates the algorithm's adaptability in managing energy consumption by observing the duty cycle which is generated by the system's active time of transmission. This graph reveals the system's **efficiency to adapt to energy demand and optimize energy utilization**. By dynamically adjusting the duty cycle, the system adapts to varying energy requirements.

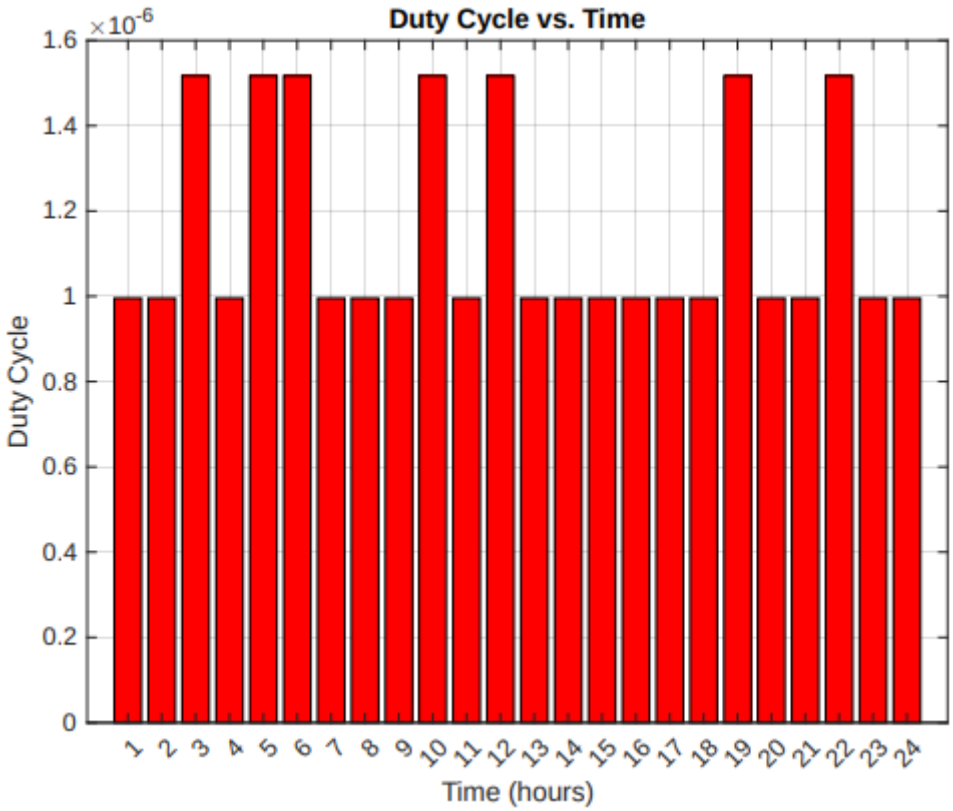

Figure 6.6: Duty Cycle graph

Observation:

- The two distinct duty cycle levels observed coincide with the two different message size transmissions. The bigger message sizes of 208-bits generate a higher duty cycle ~0.00015% and the smaller message size of 112-bits generates a smaller duty cycle 0.00010%. The duty cycles of both data payloads are well below the 1% duty cycle limit set by ICASA.
- The duty cycle level which dictates the system's active time coincides with the size of the time-on-air for the respective data payload. This suggests the algorithm's **adaptive control mechanism**, efficiently regulating energy expenditure by adjusting the duty cycle based on message payload.

Having examined the system's duty cycle – a crucial factor for adapting to varying energy demands especially influenced by data payload size. The subsequent graph presents two pivotal metrics: the Signal-to-Noise (SNR) and the Bit Error Rate (BER). These metrics provide insights into communication quality and robustness against noise, ensuring both energy efficiency and reliable data transmission.

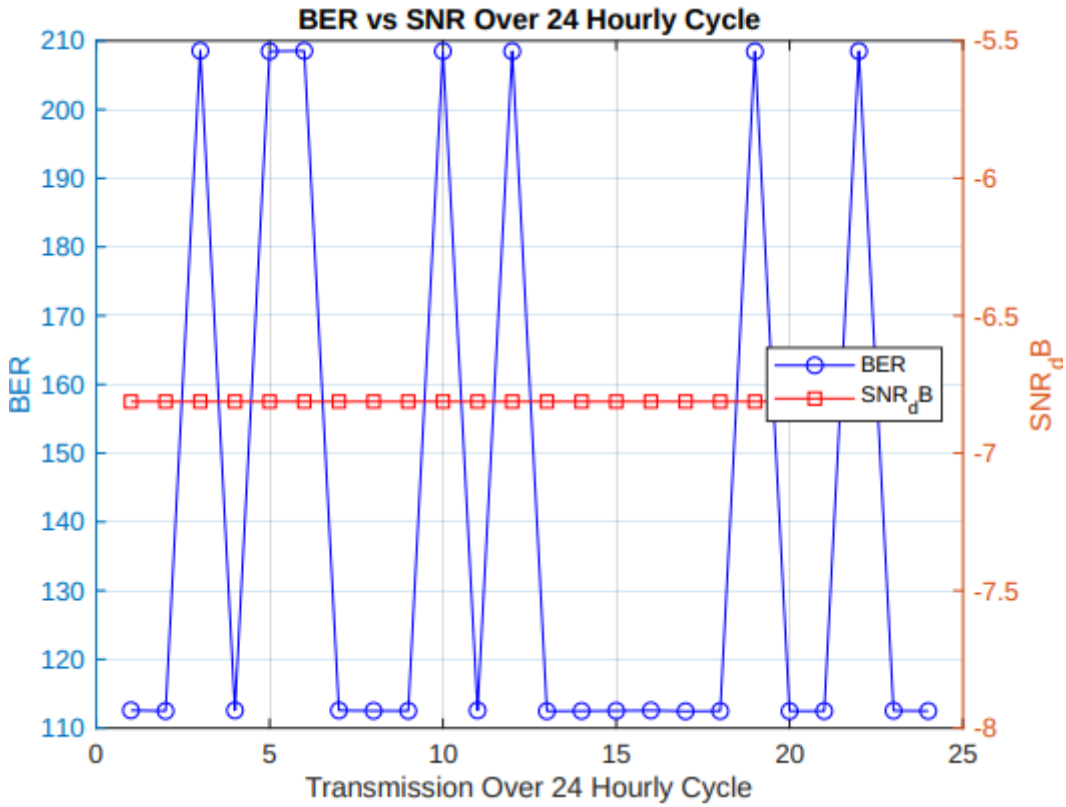

Figure 6.7: BER vs SNR_dB over 24-hour cycle

Observation

- The BER (left Y-axis) value corresponds with data payload size. The highest BER value recorded 210 which correlates with the larger payload of 208-bits and the lowest BER rate is approximately ~ 110 which correlates with 112-bits. An increase in data payload size results in an increase of BER.
- The SNR_dB plot (right Y-axis) remains constant at a value of ~-6.77 dB. The negative value indicates that the noise power is greater than the signal power. This value is within the typical LoRa SNR values range of -20 dB to +10 dB.

Having evaluated the system's performance in terms of energy efficiency and data transmission reliability, the next section delves into the underlying signal characteristics that influence system performance's metrics. The following section examines the spectral properties of the transmitted signal through analyses of the signal's occupied bandwidth (OBW), spectrogram, and power spectral density (PSD).

6.1.5. Thematic group 3: Signal Characteristics

This thematic group delves into the spectral properties of the transmitted signal, examining its characteristics through spectrograms, power spectral density (PSD), and occupied bandwidth (OBW). These analyses provide insights into the signal's frequency content, bandwidth efficiency, and potential for interference. While each message generates unique spectral patterns, this section focuses on a single representative message to illustrate the signal's fundamental characteristics. Spectrograms, PSDs, and OBWs of the remaining messages are provided in the appendices for reference

To gain deeper insights into the signal's frequency content and its evolution over time, a spectrogram is employed. This visual representation provides a time-frequency analysis, displaying the signal's spectral components as they change over the observation period. An observation window of 120 milli-seconds was generated for all the spectrograms. By examining the spectrogram, we can identify dominant frequency bands, frequency hopping, and other spectral characteristics relevant to the system's performance.

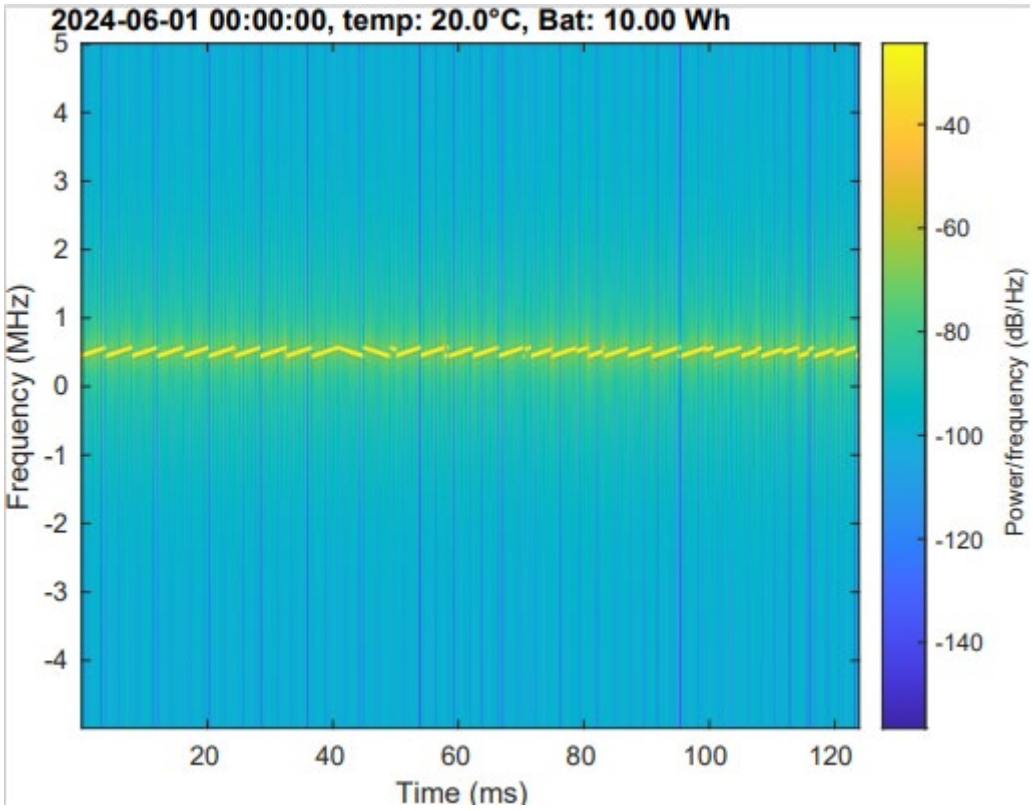

Figure 6.8: **Spectrogram of the first message, at 00:00 am.**

Observation:

- The data being transmitted is indicated by the title of the spectrogram and the ~120ms is the observation window of the signal. The yellow symbols represent the LoRa signal and are known as chirps.
- The centre axis of the chirps represents the centre frequency of the LoRa signal which is 868 MHz and the vertical frequency range (the width) that the chirps occupy represents the bandwidth 125 kHz of the signal.
- The sequence of the chirps is correct with the first 10 upward chirps representing the preamble and the two downward chirps representing the time synchronisation, and the quarter downward chirp, thereafter it is the data payload that is being transmitted.
- The first 10 unmodulated upchirps take 40ms to pass which indicates that the symbol duration T_s is 1ms this translates to a wide sweep rate. The width of the chirps is narrow which coincides with the lowest bandwidth allowed for LoRa and the number of chirps in the preamble corresponds with the stipulated frequency band 868-Mhz as per ICASA regulations. 868-MHz should have 8 symbols and the preamble time is calculated as follows $T_{preamble} = (n_{preamble} + 4.25)T_s$ where $n_{preamble}$

= 8 symbols, corresponds to the number of chirps that are observed 8 + 4.25 = 12.25. The 12.25 corresponds with the 10 unmodulated upward chirps to detect the start of a packet, the 2 downward chirps for time synchronization and the quarter chirp.

- The colour of the chirps is yellow which corresponds with a ~-20dB/Hz power spectral density of the signal.

The next subplots are the Occupied Bandwidth and the Power Spectral Density graphs. The OBW graph was generated using the *obw* function in MATLAB which directly calculates the OBW based on the signal's power spectral density and the PSD graph was generated by using the pwelch function in MATLAB which calculates the PSD by dividing the signal into overlapping segments, applying a window function, computing the periodogram of each segment, and averaging the periodograms. This process can introduce some spectral leakage and smearing, especially at the edges of the spectrum.

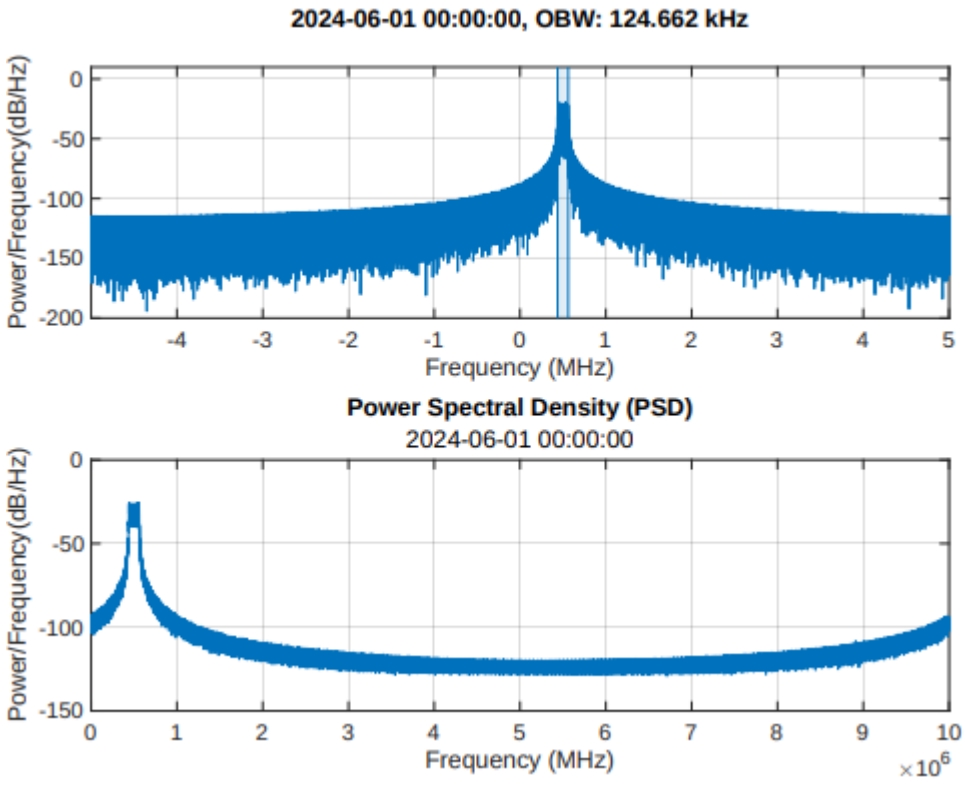

Figure 6.9: OBW and PSD subplots of message 1

Observation:

- The OBW for the first message observed outputs a narrow bandwidth peak corresponding to 124.662 kHz, which is close to the set 125 kHz.
- The power spectral density peaks at ~-20dB/Hz.
- The OBW graph has a flat line on both sides of the peak between -5 and -3Hz and 3 and 5Hz at ~-120dB/Hz power spectral density indicating a presence of white floor noise.
- The PSD graph has a similar narrow bandwidth where it peaks at ~-25dB/Hz power spectral density. The PSD graph peaks at the same frequency and power spectral density peak.
- However, the PSD graph has a noticeable extended flat slope which indicates that the signal has a significant noise power density. Between 3 and 8Hz the slope is flat which indicates white noise at ~-120dB/Hz and between 8 and 10Hz the steep indicates blue noise. The PSD graph does not have any other peaks besides the peak that corresponds to the OBW graph.
- The OBW graph was generated using the *obw* function in MATLAB which directly calculates the OBW based on the signal's power spectral density and the PSD graph was generated by using the *pwelch* function in MATLAB which calculates the PSD by dividing the signal into overlapping segments, applying a window function, computing the periodogram of each segment, and averaging the periodograms. This process can introduce some spectral leakage and smearing, especially at the edges of the spectrum which could explain the skewed PSD graph in comparison to the OBW graph, given that they peak at the same frequency.

The next section will delve deeper in analysing the observed results of all three key aspects of the energy management algorithm for LoRaWAN space communication under variable energy availability, focusing on three key aspects: energy management, system performance, and signal characteristics. These findings provide valuable data, but the analysis section delves deeper into their implications. It examines the effectiveness of the algorithm's adaptation strategies, exploring how it prioritized communication functionality during variable energy availability. Additionally, the analysis investigates the interplay between duty cycle and the algorithm's decisions, assessing how it adjusted transmission frequency to match energy availability and energy demand while maintaining acceptable BER and SNR. Finally, it explores the impact of configuration parameters like Spreading Factor (SF), Bandwidth (BW), and message size on energy efficiency, revealing the reasons behind the observed energy consumption.

6.2. Results Analysis

The analysis section aims to delve deeper into the findings presented in the results section. By interpreting the data, connections are drawn, and the implications of the research on the energy management algorithm for space communication under variable availability are explained.

Summary of Key Findings

The results section presented the findings from the research, focusing on three key aspects:

4. **Energy Management:** The algorithm's effectiveness in managing battery and supercapacitor charge levels, energy consumption and harvested energy under dynamic conditions.
5. **System Performance:** The algorithm's ability to balance energy management with maintaining communication functionality, as reflected by metrics like time on air, duty cycle, Bit Error Rate (BER) and Signal-to-Noise Ratio (SNR).
6. **Signal Characteristics:** The specific characteristics of the transmitted signal, such as spectrograms, bandwidth and power spectral density under the algorithm's control.

These findings provide valuable data, but the analysis section goes a step further. It delves deeper into the meaning of these results, drawing connections between them and explaining their implications.

Interpretation and Discussion of Results

6.2.1. Research Question 1: Energy Management under Variable Energy Availability

Results presented: The algorithm's effectiveness in managing energy consumption and maintaining communication functionality under varying energy harvesting conditions was evaluated.

Analysis: Examines the effectiveness of the algorithm's adaptation strategies. Specifically, investigate whether the algorithm maintained communication functionality during both periods of high and low energy availability. This analysis seeks to reveal how the system's design impacted overall energy consumption and communication reliability.

The observations from the algorithm simulation demonstrate its effectiveness in managing energy and maintaining communication under varying energy harvesting conditions. Here's a breakdown of the key findings:

1. Supercapacitor Performance:

- The supercapacitor charge level remained remarkably stable at 135 Coulombs throughout the 24-hour cycle, regardless of fluctuations in harvested energy (3-Wh – 14-Wh). This indicates the algorithm's ability to effectively accumulate and hold energy within the supercapacitor, acting as a buffer against the unpredictable energy availability.

2. Battery Management:

- The battery charge level exhibited minimal variations between 9.8799338 Wh and 9.8799325 Wh. This suggests the algorithm efficiently utilizes the supercapacitor to manage short-term spikes in energy consumption during message transmission (112-bit vs 208-bit messages).
- Importantly, the battery charge level quickly recovered after brief dips associated with larger message transmissions. This highlights the algorithm's capability to maintain a stable battery level for consistent communication functionality.

3. Energy Consumption:

- Energy consumption followed the message size, with slightly higher consumption observed during transmissions of larger messages (208-bit). However, the overall consumption remained very low, ranging from 0.1200662-Wh to 0.1200675-Wh.
- Notably, energy consumption showed no correlation with the fluctuations in harvested energy. This signifies the algorithm's success in decoupling communication functionality from the unpredictable environmental energy source.

Overall, the observations strongly suggest that the algorithm effectively manages energy consumption while maintaining communication functionality. The supercapacitor acts as a reliable buffer, and the algorithm efficiently utilizes it to maintain stable battery levels even under varying energy harvesting conditions.

6.2.2. Research Question 2: Impact of Dynamic Duty Cycle on Energy Management and System Performance

Results presented: The algorithm's management of energy based on different transmission loads (dynamic duty cycle) and its impact on BER and SNR were investigated.

Analysis: Delves into the interplay between duty cycle and the algorithm's decisions. Assesses whether the algorithm adjusted transmission frequency (duty cycle) to match energy availability and demand while maintaining acceptable BER and SNR. This investigation will highlight the trade-offs made and their effects on overall system performance.

1. **Energy Consumption and Transmission Efficiency:**

- The observations confirm a direct correlation between data payload size and both transmission time and energy consumption. Larger payloads (208-bits) resulted in longer transmission times (~0.13 seconds) and higher energy consumption (~0.1200675-Wh) compared to smaller payloads (112-bits) with shorter transmission times (~0.085 seconds) and lower energy consumption (~0.1200662-Wh).
- The relationship between time-on-air and energy consumption from the graph can be used to calculate the average power transmission of each message.

2. **Dynamic Duty Cycle and Energy Management:**

- The algorithm effectively utilizes a dynamic duty cycle to adapt to varying energy demands based on data payload size. Two distinct duty cycle levels were observed: a higher level (~0.00015%) for transmitting larger payloads and a lower level (~0.00010%) for smaller payloads. This directly correlates with the respective transmission times, indicating the algorithm's ability to adjust active transmission time based on energy requirements.

- ICASA regulation stipulates that the duty cycle should not exceed 1% per hour for unlicensed ISM band devices 1% in the 868 MHz band. This confirms that the observed duty cycle levels in the simulations (0.00015% and 0.00010% per hour) fall well within the ICASA regulatory limits.

- The observed correlation between data payload size and duty cycle demonstrates the algorithm's ability to dynamically adjust transmission time while adhering to

regulations. This efficient management ensures extended system operation without violating duty cycle limitations.

3. **Trade-offs Between Energy Efficiency and Communication Performance:**

- While the dynamic duty cycle optimizes energy consumption for different message sizes, the analysis reveals a trade-off with BER. Larger payloads (208-bits) experienced a higher BER (210) compared to smaller payloads (112-bits) with a lower BER (~110). This suggests a potential decrease in data transmission reliability with increasing message size.
- Notably, the SNR_dB remained relatively constant at ~-6.77 dB throughout the experiment which indicates that the signal operates beneath the noise floor. While negative, this value falls within the typical LoRa range which is between -20 dB and +10 dB and signals below the noise floor (-7.5 dB to -20 dB) can be demodulated by LoRa (B, 2019).

Overall, the results demonstrate the algorithm's effectiveness in managing energy consumption through a dynamic duty cycle. However, a trade-off exists between energy efficiency and data transmission reliability, with larger payloads experiencing higher BER. This finding highlights the importance of considering application-specific requirements when optimizing communication strategies.

6.2.3. Research Question 3: Impact of SF, BW, and Message Size on Energy Efficiency

Results presented: The influence of the chosen Spreading Factor (SF), Bandwidth (BW), and message size on the system's energy consumption was analyzed.

Analysis: The impact of these configuration parameters on energy efficiency is investigated. The analysis will investigate whether the algorithm adjusted SF, BW, or message size to optimize energy usage and the specific reasons for the observed energy consumption patterns. The impact of these configuration parameters on energy efficiency is investigated.

1. **Signal characteristic and communication quality**

- The wide sweep rate of 1ms observed in the spectrogram is a result of a spreading factor of 9 and a code rate of 4. The wide sweep rate indicates enhanced error

correction capabilities and increased processing gain, this configuration prioritizes robust data transmission particularly beneficial in noisy environments.

- On the other hand, a wide sweep rate indicates slower data transmission time due to the longer symbol duration. This creates a trade-off between error correction and communication speed.
- The observed narrow bandwidth in the spectrogram, OBW and PSD graphs, and the confirmed output OBW of 124.662-kHz from the OBW graph indicates that the signal operates at the intended data rate of DR3 based on LoRa classification. DR3 uses 125kHz channel bandwidth and can transmit data over longer distances whilst still maintaining decent data rate speed. It may not be the fastest speed but it is also not the slowest speed. This allows a balance of long-range communication at reasonable fast transmission speeds with enhanced error correction capabilities.
- The noise floor observed in the PSD graph represents the baseline level of the noise present in the system. It is the sum of all unwanted signals and background noise and not interference. Interference presents itself as spikes in the plot which were absent in the observed frequency band plot. This indicates that the signal is resilient against interference even though LoRa is sensitive and can detect weak signals and operates in an unlicensed ISM (Industrial, Scientific and Medical) band which is crowded. The signal remains resilient against external factors.
- The observed signal characteristics indicate a configuration which prioritizes robust communication over maximizing speed. While this aligns with ICASA regulations and ensures reliable data transmission, it suggests a trade-off between energy efficiency and message size due to an emphasis on error correction and low data rate. This is favourable for small message sizes, the advantages of robust communication (due to error correction) are meaningful because the energy cost of transmitting these smaller messages is relatively low, making the trade-off favourable. On the other hand, the low data rate when transmitting larger messages may require the message to be broken into multiple transmissions which increases the total energy consumption because each transmission requires power. Subsequently the energy consumption may be higher compared to a system that prioritizes speed.

6.2.4. Compare and contrast with existing literature

This study investigated the potential of energy harvesting to enable LoRaWAN transmission for space communication for the benefit of regions with limited electrical

and/or telecommunication infrastructure, with a focus of three key areas: energy management, system performance, and signal characteristics.

Energy Management:

Similarities: Findings of this study align with existing literature (Kenzi, 2022) by demonstrating the benefits of energy harvesting for wireless sensor networks. Harvested energy replenishes battery reserves, extending system operation compared to battery-powered devices.

Differences: Unlike some studies that model energy harvesting or focus on specific harvesting techniques primarily for terrestrial communication, this paper's analysis explores how a system leverages harvested energy to manage duty cycle and transmission demands for space communication whilst designing within the communication regulations of the region.

Future Exploration: Further investigation is needed to quantify the impact of harvested energy on extending the battery life, supercapacitor efficiency and enabling higher transmission frequencies for space communication compared to existing literature. Additionally, analyzing the specific energy harvesting algorithm and its efficiency in field testing would be valuable.

System Performance:

Similarities: This study's observation on the dynamic adaption of the duty cycle based on data payload size, aligns with existing research (Norhane Benkahla, 2018) on LoRaWAN duty cycle management for energy efficiency. Additionally, adhering to ICASA regulations regarding duty cycle limits, reflects responsible communication practices observed in similar studies.

Differences: The specific duty cycle limit (1% per hour) and the potential SF/BW settings observed in this study's analysis are unique to the simulated scenario and relevant regulations. Existing literature might explore different regulatory limits and communication strategies based on application requirements.

Future Explorations: Comparing the developed dynamic duty cycle and signal configuration adjustments with existing literature on energy management strategies for LoRaWAN deployments in remote areas for space communication would be beneficial. This could involve analyzing how other systems handle varying data payloads and environmental conditions.

Signal Characteristics:

Similarities: The observed trade-off between communication quality (error correction, robustness) and energy efficiency (data rate) aligns with existing literature on LoRaWAN communication (Ulysse Coutaud, 2020). The chosen signal characteristics prioritize reliable data transmission, which is crucial for many remote communication applications.

Differences: The specific SF and BW settings observed in this paper's analysis depend on the chosen communication range, noise conditions, and desired level or error correction. Existing literature might explore different signal configurations based on their specific application requirements.

Future exploration: Further investigation is needed to analyze the impact of different signal configurations (SF, BW) on energy consumption for various data payload sizes in the context of remote communication applications.

Overall: This study contributes to the understanding of how energy harvesting can enable LoRaWAN communication for space communication in regions with limited infrastructure. While the analysis aligns with existing literature on core LoRaWAN principles, the specific regulatory framework (ICASA) and focus on energy management using harvested energy add unique aspects to the research. Further exploration is recommended to compare the developed system with existing deployments in remote areas and quantify the impact of energy harvesting on various performance metrics.

6.3. Summary

The Results and Analysis chapter present the outcomes of simulations evaluating an energy-management algorithm for LoRaWAN communication in a space-based deployment scenario. The research demonstrated that the Ambient Energy Management (AEM) system effectively optimized energy harvesting, significantly improving the energy efficiency of LoRaWAN IoT devices in a Direct-to-Satellite (DtS) communication environment. The study found that dynamic duty cycling, and signal design adjustments enhanced the overall system performance, extending the operational lifespan of IoT devices. Analysis showed that specific configurations of spreading factor (SF), bandwidth (BW), and message size directly impacted energy efficiency and signal reliability. The findings suggest that implementing the AEM

system can lead to more sustainable and cost-effective IoT deployments, particularly in remote and infrastructure-limited areas. The proposed solutions offer benefits such as reduced operational costs and extended device lifespans. However, challenges include the initial setup complexity and the need for precise calibration of energy harvesting components. This research contributes to the advancement of energy-autonomous IoT systems, highlighting the potential for widespread adoption in various industries, including environmental monitoring and asset tracking. The study introduces novel algorithms and insights into energy management for satellite communication, paving the way for future innovations in IoT and space communication technologies.

Chapter 7: Conclusion

This study investigated the feasibility of using energy harvesting to support LoRaWAN for space communication in regions with limited infrastructure. The analysis focused on three key areas: energy management, system performance, and signal characteristics. The findings demonstrate that energy harvesting can enable continuous system operation and support dynamic adjustments to meet the energy demands of transmissions. The system adapts its duty cycle based on data payload size, adhering to relevant regulations while prioritizing reliable data transmission.

Future research should delve deeper into quantifying the impact of energy harvesting on extending battery life and/or enabling transmission frequencies. Additionally, comparing the developed system with existing deployments and analyzing the influence of different signal configurations on energy consumption in remote areas would provide valuable insights for optimizing LoRaWAN communication in resource-constrained environments.

By building upon this research, future developments can leverage energy harvesting to create robust and sustainable LoRaWAN networks for space communication in remote areas.

Bibliography

- A. K. M. Baki, K. H. N. S. T. M. a. H. M., 2008. Isosceles-trapezoidal-distribution edge tapered array antenna with unequal element spacing for solar power satellite. *IEICE Trans. Commun.,* E91-B(2), pp. 527-535.
- A. Kurs, A. K. R. M. J. J. P. F. a. M. S., 2007. Wireless power transfer via strongly coupled magnetic resonance. *Science,* Volume 317, pp. 83-86.
- al., S. K. e., 2014. Ambient rf energy-harvesting technologies for self-sustainable standalone wireless sensor platforms. *Proc. IEEE,* 102(11), p. 1649–1666.
- al., S. S. e., 2016. An assessment on performance of DC-DC Converters for Renewable Energy Applications. *Renewable and Sustainable Energy Reviews,* 58(Elsevier), pp. 1475-1485.
- Al-Ani, A. M. S. a. O. A., n.d. Solar Rectennas: Analysis and design. In: *Recent Wireless Power Transfer Technologies.* s.l.:InTechOpen.
- AM., M., 1984. *Device for conversion of light power to electric power.* United States, Patent No. 4,445,050.
- B. Al Homssi, K. D. S. M. H. W. S. K. a. A. A.-H., 2021. IoT Network Design using Open-Source LoRa Coverage Emulator. *IEEE Access.*
- Barry G. Evans, P. T. T. G. E. C. A. V.-C. E. A. C., 2011. 1945-2010: 65 Years of satellite history from early visions to latest missions. *Proceedings of the IEEE,* 99(11), pp. 1840 - 1857.
- B, B., 2003. *Photovoltaic technologies beyond the horizon: Optical rectenna solar cell,* s.l.: National Renewable Energy Laboratory.
- B, B., 2003. Photovoltaic Technologies beyond the Horizon: Optical Rectenna Solar Cell.. *National Renewable Energy Laboratory.*
- B, E., 2019. *LoRa Documentation.* [Online]
  Available at: https://readthedocs.org/projects/lora/downloads/pdf/latest/
  [Accessed 19 July 2024].
- Biagoni P, H. J. H. B., 2012. Nanoantennas for visible and infrared radiation. *Reports on Progress in Physics,* Volume 75, pp. 1- 76.
- Bionic Power, n.d. *Bionic Power.* [Online]
  Available at: https://www.bionic-power.com/
  [Accessed 20 May 2022].
- Brown, W. C., 1981. Status of the microwave power transmission components for solar power satellite. *IEEE Trans. Microw. Theory Techn,* 29(12), pp. 1319-1327.
- C. Song, a. e., 2017. Matching network elimination in broadband rectennas for high-efficiency wireless power transfer and energy harvesting. *IEEE Trans. Ind. Electron.,* 64(5), pp. 3950-3961.
- Carmen Delgado, J. M. S. C. B. J. F., 2021. Batteryless LoRaWAN Communications Using Energy Harvesting: Modeling and Characterization. *IEEE INTERNET OF THINGS JOURNAL,* 8(4), pp. 2694-2711.

- Carmen Delgado, J. M. S. J. F. I., 2019. On the Feasibility of Battery-Less LoRaWAN Communications using Energy Harvesting. *IEEE,* 6(19).
- Carvalho, R. C. a. N. B., 2019. *Backscatter solutions for SWIPT systems.* s.l., IEEE Asia-Pacific Microw.
- Chatterjee, G. C. a. S., 2015. A 300-nW Sensitive, 50-nA DC-DC Converter for Energy Harvesting Applications. *IEEE Transactions on circuits and systems,* 62(11), pp. 2674-2684.
- Chen, H. K. C. a. I.-S., 2010. High-efficiency dual-band on-chip rectenna for 35-and 94-GHz wireless power transmission in 0.13-µm CMOS technology. *IEEE Trans. Microw. Theory Techn,* 58(1), p. 3598–3606.
- Corkish R, G. M. P. T., 2002. Solar energy collection by antennas. *Solar ,* 73(6), pp. 395-401.
- EnOceon, 2022. *EnOceon Self powered IoT.* [Online]
  Available at: https://www.enocean.com/en/technology/energy-harvesting/
  [Accessed 20 May 2022].
- F. Fraternali, B. B. Y. A. L. B. a. R. G., 2018. Pible: Battery-free mote for perpetual indoor ble applications: Demo abstract. *Proc. 5th Conf. Syst. Built Environ. (BuildSys),* p. 184–185.
- F. Orfei, C. B. M. a. F. C., 2016. Vibrations powered lora sensor: An electromechanical energy harvester working on a real bridge.. *Proc. IEEE Sensors,* pp. 1-3.
- G. Dalpiaz, A. L. M. N. R. P. a. D. B., 2018. A battery-free non-intrusive power meter for low-cost energy monitoring. *Proc. IEEE Ind. Cyber Phys. Syst. (ICPS),* p. 653–658.
- G. Loubet, A. T. E. G. A. D. L. F. U. a. D. D., 2019. Lorawan battery-free wireless sensors network designed for structural health monitoring in the construction domain. *Sensors,* 19(7), p. 1510.
- Graczyk, R., 2017. *Energy harvesters for space,* Luxembourg: University of Luxembourg.
- Grover S, M. G., 2011. Applicability of metal/insulator/metal (MIM) diodes to solar rectennas.. *IEEE Journal of Photovoltaics.,* 1(1), pp. 78-83.
- Hafiz Husnain Raza Sherazi, L. A. G. M. A. I. G. B., 2021. Energy-Efficient LoRaWAN for Industry 4.0 Applications. *IEEE TRANSACTIONS ON INDUSTRIAL INFORMATICS,* 17(2), pp. 891-902.
- InStep Nano Power, 2016. *InStep Nano Power.* [Online]
  Available at: http://www.instepnanopower.com/
  [Accessed 20 May 2022].
- ITU-R Report SM.2392, 2016. *Applications of wireless power transmission via radio frequency beam.* [Online]
  Available at: https://www.itu.int/pub/R-REP-SM.2392
  [Accessed 10 October 2021].
- J.O.L McSpadden, F. a. K. C., 1998. Design and experiments of a high-conversion-efficiency 5.8-GHz rectenna. *IEEE Trans. Microwave Theory Technology,* 12(46), pp. 2053-2060.

- jkadbear, 2020. *Github.* [Online]
  Available at: https://github.com/jkadbear/LoRaPHY/blob/master/LoRaPHY.m
  [Accessed 10 March 2024].
- Jones, K., n.d. *Harvesting energy from the sun solar photovoltaics,* Colorado: Colorado State University Extension.
- Joshi S, M. G., 2013. Efficiency limits of rectenna solar cells: Theory of broadband photon-assisted tunneling.. *Applied Physics Letters,* 102(083901).
- K. Makino, e. a., 2015. Development and demonstration of the high precision beam steering controller for microwave power transmission which takes account of applying to SSPS (space solar power systems). *IEICE Space Aeronaut. Navigat. Electron,* 115(91), pp. 37-42.
- K. Takahashi, K. K. Y. N. a. H. M., 2019. "Battery-less shoe-type wearable location sensor system for monitoring people with dementia. *n Proc. 13th Int. Conf. Sens. Technol. (ICST),* Issue 13, pp. 1-4.
- Kenzi, F. Y. a. A., 2022. *Energy Harvesting in wireless communication: A survey.* E3S Web of Conferences, E3S Web of Conferences.
- Khan NU, K. F. F. M. M. A., 2024. RF energy harvesters for wireless sensors, state of the art, future prospects and challenges: a review.. *Physical and Engineering Sciences in Medicine,* 47(2), pp. 385-401.
- Kinetron, n.d. *MICRO GENERATORS.* [Online]
  Available at: https://www.kinetron.eu/technology/generator-technology
  [Accessed 28 April 2022].
- Kotter D, N. S. S. W. P. P., 2010. Theory and manufacturing processes of solar nanoantenna electromagnetic collectors.. *Journal of Solar Energy Engineering.,* 132(1).
- Lin GH, A. R. B. J., 1996. Investigation of resonance light absorption and rectification by sub nanostructures.. Issue 80, p. 565.
- Lorawan, n.d. *Lorawan specification version 1.1.* [Online]
  Available at: https://lora-alliance.org/resource_hub/lorawan-specification-v1-1/
  [Accessed 13 03 2022].
- Magno, M. B. D. T. L. a. B. L., 2009. Adaptive power control for the solar harvesting multimodal wireless smart camera. *In Distributed Smart Cameras,* Third (ACM/IEEE), pp. 1-7.
- Matrix, 2022. *Matrix.* [Online]
  Available at: https://www.matrixindustries.com/
  [Accessed 20 May 2022].
- Matsumoto, H., 2002. Research on solar power station and microwave power transmission in Japan. *IEEE Microw. Mag,* 3(4), pp. 36-45.
- Michele Magno, D. K. P. M. a. L. B., 2018. Micro Kinetic Energy Harvesting for Autonomous Wearable Devices. *International Symposium on Power Electronics, Electrical Drives, Automation and Motion,* pp. 105-110.

- Midrio M, R. M. B. S. D. A. C. L. A. M. D. e. a., 2011. Flared monopole antennas for 10-µm radiation.. *IEEE Journal of Quantum Electronics.,* 47(1), pp. 84-91.
- Ministry of Internal Affairs and Communications, 2020. *Technical condition of in-room far-field wireless power transfer.* [Online]
  Available at: https://www.soumu.go.jp/main_content/000697268.pdf
  [Accessed 12 October 2021].
- N. Takabayashi, N. S. T. M. M. F. a. T. F., 2020. Rectification improvement with flat-topped beams on 2.45-GHz rectenna arrays. *IEEE Trans. Microw. Theory Techn,* 68(3), pp. 1151-1163.
- N. Weissman, S. J. a. E. S., 2014. W-band CMOS on-chip energy harvester and rectenna. *IEEE MTT-S Int. Microw. Sym*.
- Norhane Benkahla, H. T. Y.-Q. S. M. F., 2018. Enhanced Dynamic Duty Cycle in LoRaWAN Network. *Ad-hoc, Mobile, and Wireless Networks,* 11104(978-3-030-00246-6), pp. 147-162.
- NRL News Releases, 2019. NRL News Releases. *NRL News Release*, October, pp. https://www.nrl.navy.mil/news/releases/researchers-transmit-energy-laser-power-beaming-demonstration.
- O'Neal, D. M., 1999. COMMERCIAL COMMUNICATIONS SATELLITES: HISTORY AND HIGHLIGHTS. *IEEE MTT-S Digest,* 99(5), pp. 1919 - 1921.
- P. Spanik, M. F. a. A. K., 2014. Life time of the electrolytic capacitors in power applications. *ELEKTRO,,* pp. 233-238.
- P. Spanik, M. F. a. A. K., 2014. Life time of the electrolytic capacitors in power applications. *ELEKTRO*, May, p. 233–238.
- Paradiso, N. S. a. J., 2001. Energy scavenging with shoe-mounted piezoelectrics. *IEEE micro,* Volume 3, pp. 30-42.
- Paulene Govender, V. S., 2019. Investigating diffuse irradiance variation under different cloud conditions in Durban, using k-means clustering. *Journal of Energy in Southern Africa,* 30(3), pp. 22-32.
- R. Dekimpe, P. X. M. S. P. G. D. F. a. D. B., 2019. A battery-less ble smart sensor for room occupancy tracking supplied by 2.45-ghz wireless power transfer. *Integration,* Volume 67, pp. 8-18.
- R. Sanchez-Iborra, J. S.-G. J. B.-V. M.-D. C. a. A. F. S., 2018. Performance evaluation of lora considering scenario conditions. *Sensors,* 18(3), p. 772.
- Richardson, L., 2018. *The history of solar tech,* s.l.: Solar Tech.
- S. Hemour, C. H. L. a. K. W., 2015. Small-footprint wideband 94GHz rectifier for swarm micro-robotics. *IEEE MTT-S Int. Microw. Symp.*.
- S. Kitazawa, M. H. S. A. H. K. H. B. a. K. K., 2013. Field test results of RF energy harvesting from cellular. *Global Symp. Millimeter-Waves,* 6(1569736061).

- S. Mihara, e. a., 2015. The result of ground experiment of microwave wireless power transmission. *Int. Astronaut. Congr,* IAC-2015-C3.2.1(66).
- S. Mizojiri, e. a., 2019. GaN Schottky barrier diode for sub-terahertz rectenna. *IEEE Wireless Power Week*.
- Saghati, H. Z. a. A., 2016. Remote wireless power transmission system. *Frontiers of Research and Development of Wireless Power Transfer*, pp. 185-196.
- Semtech Corporation, 2019. *An In-depth look at LoRaWAN® Class A devices.* [Online] Available at: https://lora-developers.semtech.com/uploads/documents/files/LoRaWAN_Class_A_Devices_In_Depth_Downloadable.pdf [Accessed 9 03 2022].
- Semtech, 2019. *An In-depth Look at LoRaWAN® Class B Devices.* [Online] Available at: https://lora-developers.semtech.com/uploads/documents/files/LoRaWAN_Class_B_Devices_In_Depth_Downloadable.pdf [Accessed 26 March 2022].
- Semtech, 2019. *An In-depth Look at LoRaWAN®Class C Devices.* [Online] Available at: https://lora-developers.semtech.com/uploads/documents/files/LoRaWAN_Class_C_Devices_In_Depth_Downloadable.pdf [Accessed 29 March 2022].
- Semtech, 2020. *Coexistence of LoRaWAN and UHF RFID.* [Online] Available at: https://lora-developers.semtech.com/uploads/documents/files/Coexistence_of_LoRaWAN_and_UHF_RFID_Final_v3.pdf [Accessed 20 March 2020].
- SemTech, 2020. *Wireless RF: The Ins and Outs of LPWAN Technologies.* [Online] Available at: https://lora-developers.semtech.com/uploads/documents/files/Wireless_RF_Matchbox_Approved_Final.pdf [Accessed 20 March 2022].
- SemTech, n.d. *TRIO mXTEND™ Antenna.* [Online] Available at: https://lora-developers.semtech.com/documentation/tech-papers-and-guides/an-evaluation-of-multi-band-antennas-for-use-with-lora-edge-part-one/trio-mxtend-antenna/#trio-mxtendtm-conclusion [Accessed 22 March 2022].
- Sequent, 2022. *Sequent.* [Online] Available at: https://sequentworld.com/ [Accessed 20 May 2022].
- Shinohara, N., 2020. Wireless power transfer in Japan: Regulations and activities. *14th Eur. Conf. Antenna Propag,* Volume 14.

- Shinohara, N., 2021. History and Innovation of Wireless Power Transfer via Microwaves. *IEEE Journals of Microwaves,* 1(1), p. 11.
- Shinohara, N. H. a. N., 2017. C-band active antenna design for effective integration with a GaN amplifier. *IEEE Trans. Microw. Theory Techn,* 65(12), p. 4976–4983.
- Shinohara, S. K. a. N., 2018. Investigation of effective range of focused Gaussian beam compared to focused uniform beam in Fresnel region. *12th Eur. Conf. Antennas Propag,* CS09.3(12).
- Shinohara, T. S. a. N., 2018. Study on multipath retrodirective for microwave power transmission. *IEEE Wireless Power Week*.
- SolePower, n.d. *SolePower.* [Online]
  Available at: http://www.solepowertech.com/#smartbootsgraphic
  [Accessed 20 May 2022].
- Sorber, J. H. a. J., 2017. *The future of sensing is batteryless intermittent, and awesome.* New York, ACM.
- Sorbet, J. H. a. J., 2017. *The future of sensing is batteryless, intermittent, and awesome.* Delft, s.n., pp. 1-6.
- T. Furuta, M. I. N. N. K. I. K. N. a. J. I., 2016. *The 500 MHz band low power rectenna for DTV in the Tokyo area.* s.l., IEEE Wireless Power Transfer.
- T. Hirakawa, C. W. a. N. S., 2019. RF-DC conversion efficiency improvement for microwave transmission with pulse modulation. *Cambridge J. Wireless Power Transfer*, March.
- T. Matsumuro, Y. I. a. N. S., 2019. Basic study of both sides retrodirective system for minimizing the leak energy in microwave power transmission. *IEICE Trans. Electron,* E102-C(10), pp. 659-665.
- Team, S. F. E., 2022. *Space briefing book.* [Online]
  Available at: https://www.spacefoundation.org/space_brief/types-of-orbits/#:~:text=Types%20of%20Orbits%201%20Low%20Earth%20Orbit%20%28LEO%29,Sun-Synchronous%20Orbit%20%28SSO%29%206%20Highly%20Elliptical%20Orbit%20%28HEO%29
  [Accessed 14 September 2022].
- Tesla, N., 1904. The transmission of electric energy without wires. *Proc. 13th Anniversary Number Elect. World Eng.,* Issue 13.
- Thielen M, S. L. M. M. H. C. B. L., 2017. Human body heat for powering wearable devices: From thermal energy to application. *Energy Conversion and Management,* Volume 131, pp. 44-54.
- Tingwen Ruan, Z. J. C. M. Z., 2017. Energy-Aware Approaches for Energy Harvesting Powered Wireless Sensor Nodes. *IEEE sensors journal,* 17(7), pp. 2165-2173.
- U. Raza, P. K. a. M. S., 2017. Low power wide area networks: An overview. *IEEE Commun. Surveys Tuts,* 19(2), pp. 855-873.

- Ulysse Coutaud, M. H. B. T., 2020. *Fragmentation and Forward Error Correction for LoRaWAN small MTU networks.* France, International Conference on Embedded Wireless Systems and Networks.
- University of Washington , n.d. *Wireless Identification Sensing Platform (WISP.* [Online] Available at: https://sensor.cs.washington.edu/WISP.html [Accessed 14 10 2021].
- V. Manev, H. V. P. B. a. H. G., 2019. *A comparison of tunnel diode and Schottky diode in rectifier at 2.4 GHz for low input power region,* IEEE Wireless Power Week: s.n.
- V. Talla, B. K. S. G. a. J. S., 2017. Battery-free cellphone. *Proc. ACM Interact,Mobile, Wearable Ubiquitous Technology,* Issue 25.
- Wang W, C. V. W. N. H. M. O. B. O. C., 2013. Thermoelectric Energy Harvesting for Building Energy Management Wireless Sensor Networks.. *Elsie: International Journal of Distributed Sensor Networks,* 9(6), p. 232438.
- WC, B., 1984. The history of power transmission by radio waves.. *IEEE Transactions on Microwave Theory and Techniques,* 32(1), pp. 1230-1242.
- Wearable, 2022. *Wearable.* [Online] Available at: https://www.wareable.com/hybrid-smartwatches/lunar-solar-powered-smartwatch-review [Accessed 20 May 2022].
- X. Gu, E. V. G. A. T. P. V. K. W. a. S. H., 2014. Towards low-power high-efficiency RF and microwave energy harvesting. *IEEE Trans. Microw. Theory Techn,* 62(4), pp. 965-976.
- X. Gu, E. V. G. A. T. V. K. W. a. S. H., 2019. *Environment-aware adaptive energy harvesters for IoT applications.* s.l., IEEE Wireless Power School.
- Y. Tanaka, e. a., 2020. A study of received power in distributed wireless power transfer system. *IEEE AP-S/URSI,* Issue THA5.3P.2.
- Yonatan Shiferaw, A. A. F. K., n.d. *LoRaWAN Class B Multicast Scalability,* Delft: Delft University of Technology.
- Zeine, H., 2016. *Method & apparatus for focused data communications.* United States of America, Patent No. 9,351,281.

[1] (Inmarsat, 2017)
[2] (FOSSA Systems, 2023)
[3] (Semtech, 2021)
[4] (Lacuna Space, 2022)
[5] (Iridium, 2017)